Use of electric fields for cell manipulation in a microfluidic environment

Dipl. Ing. Florian A. J. F. L'Hostis, BSc (Hons),

A thesis submitted in partial fulfillment of the requirements for the degree of

Master of Engineering

in

Electrical and Electronic Engineering

at the

University of Canterbury, New Zealand, 3rd January 2008

Abstract

Lab-On-a-Chip (LOC) or Micro Total Analysis System (µTAS) technology requires precise control of minute amounts of liquid. Moving liquids in small capillaries requires bulky expensive external pumps that defy the purpose of microfabrication. By integrating a micropump into the device, it allows the system to be transportable, reliable, energy efficient and inexpensive. Such a microsystem built on a chip has been designed to study separation by dielectrophoretic chromatography. Nanobeads were successfully separated and used separately to measure fluid velocity and study the electroosmosis effect. Cell or beads of different type can be trapped in this system.

This system encompasses a solid-state AC electroosmotic pump for the manipulation of liquid-containing cells or molecules. AC Electroosmosis is the movement of induced charges over polarised electrodes created by a non-uniform electric field. The charges undergo Coulomb forces and drag the fluid with their motion. This results in bulk flow over the electrodes. This micro pump is used in a LOC. by fabricating the pump on two sides of a microfluidic channel.

The transport of material from what can be an analyte to a cell is of critical interest. The described system in the second part of this thesis presents the advantage of having a defined number of droplets, each of which is a lab on chip. The paradigm is the droplet and therefore the vessel that carries the information. Surfaces are then the place of interaction with the vessel which carries the second aspect of this thesis.

Several approaches have been investigated, in particular by enclosing the droplet between two slides in order to increase the change of contact angle under the presence of polarised electrodes. This system is known as EWOD (ElectroWetting On Dielectric). It follows the approach of modified Lippmann laws and the modification of the apparent contact angle and therefore the motion of the droplet. The lid is somewhat a problem and the possibility of using liquid dielectrophoresis to create a multitude of droplets of calibrated volume is an advantage, as it is harder to create fixed-volume droplets with an open geometry by EWOD due to contact angle hysteresis.

Aspects of this work has been published as follow :

"*Solid state AC electroosmosis micro pump on a chip*" L'Hostis, F.; Green, N.G.; Morgan, H.; Alkaisi, M.; Nanoscience and Nanotechnology, 2006. ICONN '06. International Conference on,3-7 July 2006 .Brisbane, Australia

*"AC dielectrophoresis of spherical particles using 2-D interdigitated microelectrode array structures",*J. Muys M. M. Alkaisi, F. L'Hostis, J. J. Evans and M. L. Chang, *Proc. ENZCON '04* (2004).

"Liquid Dielectrophoresis and ElectroWetting on Dielectric Substrates for Particle Transport", Florian L'Hostis, Richard J. Blaikie, Nicolas G Green, Hywel Morgan, and Thomas B. Jones, AMN-3 International Conference on Advanced Material and Nanotechnology (Oral presentation : O207), February 2007, Wellington, New Zealand.

"Integrated AC Electoosmosis micropumps for Dielectrophoretic Chromatography"
Florian L'Hostis, Nicolas G Green, Hywel Morgan, Maan Alkaisi, Nanotech 2005, Oxford, Poster Presentation.

The Authors is also the recipient with Shaun Hendy from Victoria University of the Dumont D'Urville grant for research collaboration between France and New-Zealand. The fund contributed to the organization of the 1st Microfluidic workshop symposium in New Zealand. Christchurch, New Zealand, 2007.

Acknowledgement

First and foremost I wish like to acknowledge the support and outstanding professional leadership of my supervisor Prof. Richard Blaikie which this thesis would had never seen the day without him. I would like here to thank the MacDiarmid Institute for the funding of my research and all the staff that keep this organization yielding world standard research.

I wish to acknowledge Prof. Hywel Morgan who provided the access to his lab and all the resources of Southampton University (U.K.). Within Hywel Morgan's group I would like to thank Dr Shady Gawad, Dr Mairi Sandison, Giuseppe Benazzi, Ferran Revilla, Dr Nicolas Green and especially David Holmes who showed me how to obtain good microfluidic systems and all the tip and tricks associated with it. Also I wish like to thanks Prof. T. B. Jones for introducing to me the electrowetting scheme and its 6 month mentoring without which no electrowetting scheme would have worked.

I would like to thank Prof. Alison Downard and Dr Paula Brooksby for sharing their time and knowledge on electrochemical studies. I would like to thank Helen Devereux and Gary Turner for their constant work in the lab and to keep it going smooth despite the general trend of hardware to break down just before deadlines…

I wish also to thank Volker Knock, Leo Schuler, Euan Boyd, Erwin Berthier, Jim Partridge, Alan Dunbar and James Muys which in disorder provided regular supplies of cheese cake, political discussion on how to put the world to right, climbing activities, New Zealand outdoor unique knowledge, vast amount of caffeine, microfabrication tips, kiwi knowhow and in general a plethora of occasion to procrastinate.

Finally I would like to thank Mum, Dad, Annabelle, Christophe for their support through the hardship we faced in the last four years. I am finally coming home…!

Since I spent the last 4 month listening to a lot of music and my mind drifted occasionally to vertical limestone cliffs I want to dedicate this thesis to Rock n' Roll and Thai Climbing.

Table of contents

Chapter I :

1. Introduction

1.1. General thoughts

In a world that changes at a speed that we cannot observe it is often difficult to see obvious technological revolutions. We can fail to consider that the most simple advances into applied areas can modify for instance our ways of communicating but also our ways of operating our most common tasks (e.g. computing, medical diagnostic, transport).

Richard Feynman in 1959 declared “There is plenty of room at the bottom” in a meeting at the American physical society at Caltech. It was in 1953 that Crick, Watson and Wilkins offered the first double helix DNA structure and were rewarded by a Nobel prize in 1962. Incredibly we were very quick on filling up the gap at the bottom which saw to advent of microelectronics and its scale reducing acronyms such as VLSI and ULSI.

The famous Moore’s law [1] states that transistor integration doubles every year, which so far as been respected. Nevertheless this is only possible due to the advanced possibilities of optical lithography, and today its relative of electron beam lithography. That allows us to create 2D structures to create a pattern on a substrate with the desired material to be etched or deposited down to the nanometer scale. This is at the heart of the microelectronic revolution.

Although these techniques are very useful in microelectronics they have inherent drawbacks especially since using light it is limited to its diffraction aperture. In the realm of mechanics, micromechanics lagged behind microelectronics and if the first micromechanical system was a pressure sensor it is hardly a complex mechanical system. Other micro mechanical systems followed with a diverse range of success, nevertheless the industry was slow to adopt this micromechanical system later on called MEMS (Micro Electro Mechanical Systems). It is only in the last 20 years that this industry emerged as a major player and an offshoot of the semiconductor industry. It is from this industry that most of today’s systems derive. Thus most of the products are based on silicon material and its technology as a well understood and cheap material.

Since the use optical lithography is based on 2D patterning, 3D mechanical systems are still a challenge to produce. The heavy use of fast etching techniques and intelligent manipulation of resist and sacrificial layers allows the construction of complex structures. Although major developments occurred earlier on in mechanical systems as previously mentioned, it is only in 1975 that the first microfabricated device using liquid was reported by S.C. Terry - Stanford University [2]; also, later on, the first manipulation of droplets for inkjet printing was the accumulated use of electronic and mechanical integration in conjunction for the precise manipulation of liquids [3].

The micromanipulation of liquid was thus born, and within its core the potential for using this technique in conjunction with the life sciences. These preliminary systems are the proof of feasibility for integrating several stages on a chip of what is normally achieved at a lab scale. Tissue pre-treatment, integrated fluid treatment, cleaning and chemical monitoring downscale to a chip size. The BioMEMs is born. There are two main types of such devices, one in vivo and the other in vitro. Although the in vivo system offers some fantastic opportunity we will limit out discussion to in vitro system.

The progress made in genomics lead to the human genome project [4, 5] which in turn created a demand for new tools to perform routine analysis faster and more accurately. It is within this scope that instruments such as capillary electrophoresis and DNA micro arrays were developed. This is also a turn into a more biological approach to Lab On Chip (LOC) applications [4-7], where tools are developed with only one aim-to perform better what is already available at the lab scale. Nevertheless, BioMEMs like this do not take advantage of scaling the LOC approach in order to achieve the desired results. This is where the manipulation of single cells is an asset.

The study of a population of cells is an average of the behaviour of millions of cells in general. For instance, pituitary cell are made of 6 different cells that contribute to the female hormonal cycle. Each of these cell types have an influence on the hormone cycle but are difficult to tell apart. Therefore isolating the population and the cell presents an obvious advantage for the biologist [8].

The isolation and manipulation of cells can also be applied for diagnostic and purification purposes, especially in blood or bone marrow for the detection of cancer cell but also with pathogen disease (malaria, dengue fever, HIV). In the case of rare cells

isolation this can lead to the diagnosis of malign cells very early into the development of a disease such as cancer or malaria [9-11].

The manipulation of cells was for long time the domain of micro clamps and pipette [12]. Direct mechanical contact has consequences on the cell surface which can result in damaging the surface and perturbation of the interaction of the cell surface with its environment. Alternative cell manipulation techniques would therefore be desirable, and if these could also facilitate cell sorting and diagnosis a powerful tool would result.

Electric fields are easy to produce thanks to the coplanar fabrication of electrodes. Electric fields can interact with fluid but also with particles. They are also scalable and can fit the diversity of sizes encountered in the life science domain. The use of such for fluid and cells movement in a LOC environment is the topic of this thesis.

The University of Canterbury developed a Biochip dedicated to the trapping of cells on its surface[13]. It uses intense electrical fields to attract and a trap cells on prefabricated pits. The aim is to obtain a surface to be inspected by an AFM and also fabricating a tool to discriminate cells at its surface. Nevertheless the system is simple and no advanced microfluidic apparatus exist to displace the cells closer to the electrodes in charge of trapping them.

1.2. Statement of aims

The Biochip developed at the University of Canterbury is an illustration of such techniques mentioned earlier [14]. Its aim is to isolate particular cells as well as rare cells (less than 1%) from heterogeneous cell suspensions on a textured or microfabricated surfaces. It is useful for a variety of clinical and biological applications. The majority of them can be therefore subdivided into two main categories: (1) the positive selection of a particular cell type for analysis or clinical use. e.g. isolation and detection of cancer cell (2) the depletion of undesired cells from population of desired cells e.g. the removal of bacteria from blood products. In one particular case the Biochip is being used to study and isolate a particular cell type, namely gonadotroph for the study of FSH and LSH (Follicle Stimulating Hormone and Luteinizing Stimulating Hormone) [13, 15].

The current protocol for manipulating the cells and displacing them onto the surface is crude and lacks control. Namely, the cells in suspension are brought to the

surface by dropping the liquid onto the surface with a pipette. The dielectrophoresis forces (DEP) forces used for the trapping are of short distance they are proportional to the gradient of the square of electrical field. These forces decrease rapidly with distance and are only effective on sizeable objects [16, 17].

This thesis proposed to investigate technological means to improve the control of cells or particles in colloids for integration into future generation of the Biochip. It has the aim to manipulate precisely the liquid that contains the colloid to move the targets to particular locations at the surface of the chip. The optimal goal is to isolate from a colloid population one individual and transport it to a predestined location on the chip. In order to achieve these goals two strategies have been investigated: (1) AC electroosmosis pumping; (2) electrowetting using a droplet as the vessel that contains the colloids.

1.3. Thesis outline

This thesis describes the design, microfabrication and simulation of LOC devices for the purpose of manipulating precise amounts of fluid and/or particles suspended in a liquid media. The systems investigated are microfabricated using the relevant techniques described later on. Chapter One introduces the historical background and the reason for this research. Chapter Two introduces cells and offers an overview of existing separation and isolation of colloids. Chapter Three describes forces applied on liquid for the purpose of fluid motion and also pondemorotive force resulting from the polarisation of insulators. Chapter Four describes the materials and methods used, and also describes the devices created and the technique. Chapter Five describes the preliminary simulations necessary to evaluate the devices. Chapter Six describes the fluidic results for AC electoosmosis and chapter Seven discusses of the results for digital microfluidic and Chapter Eight concludes and provides directions for future work.

Chapter II :

2. Introduction to labs on chips and biological systems

Eighteen years ago, the book known as **The Cell** by Alberts and Co [18] widely acclaimed as an overview of actual knowledge on biological cell started with these words : “There is a paradox in the growth of scientific knowledge. As information accumulates in ever more intimidating quantities, disconnected facts and impenetrable mysteries give way to rational explanations, and simplicity emerges from chaos”.

This book now has 1500 pages and is on its 4th edition; its only goal is to describe to the reader the inner mechanism of cells. It is daunting to appreciate the wide knowledge necessary in order to cross the border of different science realms. It is here that we try to understand the basics of cell biology for us to identify cell characteristics to use on microfabricated devices and/or the characteristics that may assist us to electrically manipulate the cells in these devices.

2.1. Cells features

They are between 10 and 100 million living species on Earth today. They all reproduce faithfully and spawn progeny that are largely identical to their parents. The parent organisms transmit the information and specify in extraordinary detail the characteristics that their offspring should have. This phenomenon of hereditary transmission is a central part of the definition of life. This central process to life takes place, the simplest form of which is mitosis, the simple replication observed in prokaryotic organisms but also in eukaryotic systems for growth and repair of multi-cellular organisms. These two different organism types have different structure and response to electromagnetic fields, and are described briefly here.

2.1.1. Prokaryotes

These are defined by not having a nucleus, therefore their hereditary material is contained within the cell membrane. They are also the most biochemically diverse organisms as they obtain all their energy and nutrients from inorganic chemical sources. They are also characterised by holding only one chromosome which contains 1000 to 4000 genes. Bacteria fall under this definition together with archaea. Many of the genes within a single organism show strong resemblance implying that they originated from the same ancestral gene through gene duplication and divergence. Homologie are also clear when compared between different species. Some of these genes can be observe amongst the three domains of the living world (bacteria, archea, and eukaryote). The simplicity of their lack of internal structure, in bacteria such as E-coli, make them prime candidates for single-cell study and cell manipulations. It is also, as we will see later, ideal to organize research based on the complexity of the cell (Electric field response varies with the frequency and the internal component of a cell).

2.1.2. Eukaryotes

By definition and contrary to prokaryotic cells, these conserve their DNA material contained in the nucleus separated from the cytoplasm by the nuclear envelope. Eukaryotes cells are in general 10 times larger in linear length and 1000 times in volume than prokaryotes but they have complex features like cytoskeletons – systems of girders, ropes and motors that gives the cell mechanical strength and in particular allows it control its shape. This has several consequences for this research: most important the interaction with an electric field will surely be more complex than a simple bacteria yet yeast cells are robust and readily available and could be of use. As we will see later (in Chapter 2) the dielectric response of a multiple-shell depends on its size and the electrical characteristics of its internal components [19-21].

2.2. Some Relevant Cells.

Cells of most interest for clinical study are those in the human body responsible for diseases. Blood cells are readily available since we carry pints of it. A single finger prick provides us with both white and red blood cells. Blood cells and cancer cells are two very common classes and their broad characteristics are reviewed here.

2.2.1. Cell type in Blood

Blood contains a variety of cell types, each with a different physiological role. The three major species are red blood cells (RBCs), white blood cells (WBCs) and platelets, which are all suspended in a protein rich fluid call plasma. Plasma is 90% water and constitute55 % of the volume of blood. Plasma contains various proteins like albumin, fibrinogen and other clotting protein.

Red blood cells (erythorcytes)

These are perharps the most recognizable component of whole blood. They have bi-concave disc morphology and contain haemoglobins an iron containing protein that carries oxygen. They are manufactured in the bone marrow and have a spherical shape and a nucleus on their unmature stage. They live approximately 120 days in the circulatory system before being removed by the spleen.

White blood cells (Leukocytes)

These are part of the immune system and protect the body from foreign substances like pathogen bacteria, fungui and viruses. Most of the WBCs are also produced in the bone marrow where they outnumber RBCs, however in whole blood they are outnumbered by a factor 1 to 600. The immune system is complex and they are several WBCs with specialist task.

Platelets

These are small cells of about 1 µm and are essential to blood clotting. They live 9-10 days and are removed by the spleen. They are vital to life as they stitch wounds upon any trauma that results in blood loss.

Cancer Cells

The detection and measurement of rare cancer cells in blood or bone marrow is potentially very important for diagnostic and therapeutic purposes [9, 10, 22, 23]. These cells, if isolated, could be used to determine the likely prognosis and early decision making about the type and aggressiveness of treatment. High dose chemotherapy treatments destroy the haematopoietic system. It is generally followed by autologus bone marrow transplantation to restore the patient's blood cell production. In order to avoid the possibility of the re-infusion of the contaminated tumour cells back into the patient, thus, these tissues need to be purged of tumour cells. Ideally a detection system with a high threshold is therefore necessary.

This also identifies two type of detection on for diagnosis and prognosis and the other for treatment and depletion of large stock of cellular compound.

2.3. Cell separation and detection

We describe here the existing methods of cell separation, control and identification. This is to introduce method and apparatus commonly used but also some potential for miniaturisation. There are a plethora of cell separation techniques but only two exhibit some industrial needs mostly required by laboratories and medical profession. There are the Fluorescent Activated Cell Sorting (FACS) and the immuno magnetic technique Magnetically Activated Cell Sorting (MACS).

2.3.1. Flow Cytometry

There are two kind of flow cytometer: the analyser and the sorter. Sorters have not only the ability to acquire a range of data on sub cell populations, but also to segregate them based upon criterias (i.e. by particular fluorescent labelling technique and light scattering technique).

The Coulter technique

This allows the measurement of the number and size of colloids passing by one by one through an orifice (Figure 2-1). The change in impedance as the particles pass through the holes is dependent of the size of the particles this technique is used to count blood cells and bacterias.[24]. The pulses give therefore overall information on the particle distribution (Figure 2-1).

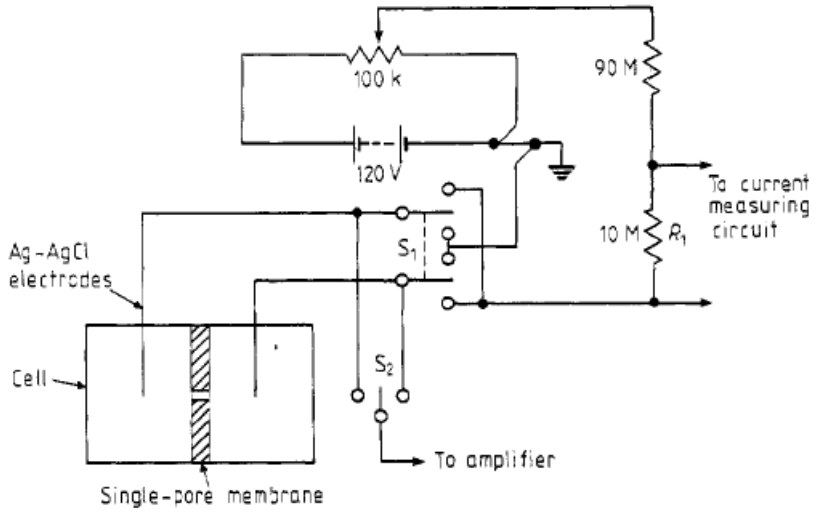

Figure 2-1: Coulter technique schematic

Fluorescence Activated Cell Sorter (FACS)

FACS describes an instrument that can measure physical as well as multicolour fluorescent properties of cells flowing in a stream. As stated earlier, these systems can be either sorters or analysers. The principle is shown in Figure 2-2 Antibodies tagged with a fluorochrome are attached to the cells; these fluorescent labels allow the identification of particular cell type. The particles in suspension are inserted into a pumping system that injects them into a jet formation for droplet generation. A fluid jet with periodic disturbance is yielded with droplets that contain the desired colloid (segregated by the optical stage) which is charged charge for later deviation. The cells are excited by a light source (laser or other) and the collection is made either directly opposite to light source (forward scatter FSC) or normal to the direction of the light source (side scatter SSC). FSC correlates mainly with cell size whereas SSC correlates with the internal content as much as size.

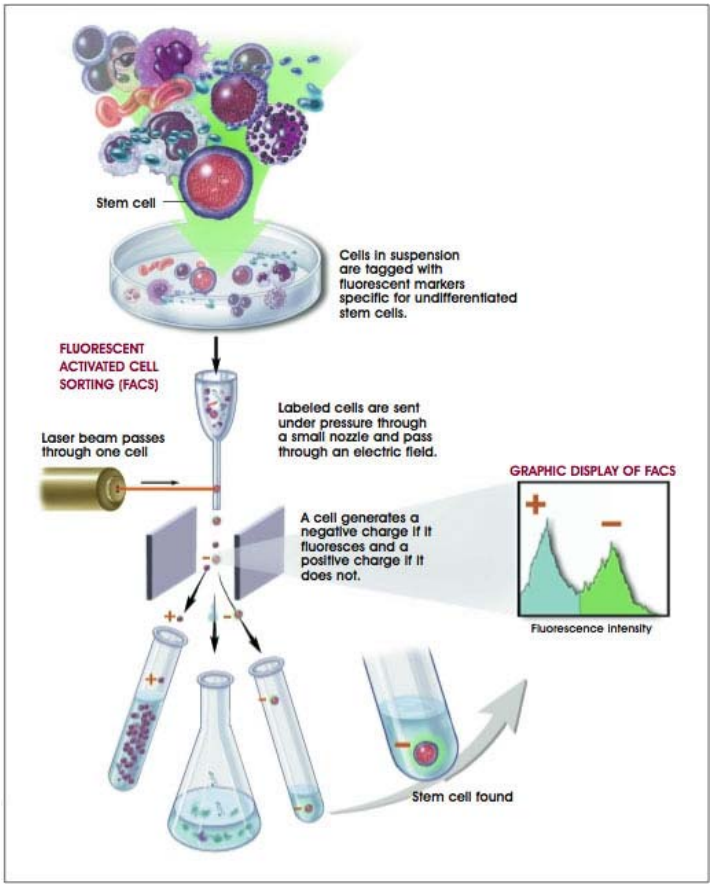

Figure 2-2 : Example of cell separation by FACS here in the case of stem cells [25]

Immuno magnetic technique

In principle MACS (Figure 2-3) is very similar to FACS. Cells are tagged by antibodies that carry magnetic matrices, generally nanoparticles. Again specific antibodies target the cell type of interest and after incubation the cells are passed through a separation column bathed in a strong magnetic field; the magnetically labeled particles are retained into the column whilst the non tagged cells carry on. After removal of the column the magnetically labeled cells can be eluted.

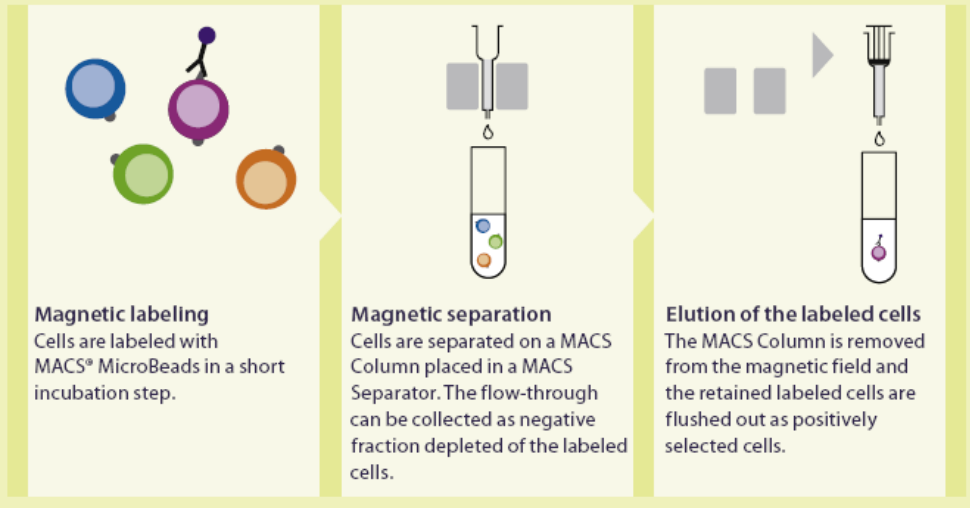

Figure 2-3 : MACS principle schematic

The very small size of magnetic nanoparticle reduces the mechanical stress on cells. Also their composition can be biocompatible (polysaccharide and iron oxide) and do not activate cells or other metabolism contrary to fluorescent and radioactive markers. Thus cells with their tags can be immediately used in other assays. MACS has been used for 1 to 10^8 separation. It is also possible to conjugate fluorescent markers as well as magnetic markers so that after separation further analysis can be obtained.

Conclusion

This flow cytometry technique has emerged as a major tool in the diagnosis of numerous immune system disorders including immunodficiencies and lymphoma/leukaemia [26-28]. Furthermore, the measurement of the levels of specific white blood cells via discriminatory markers is now routinely used in monitoring the success of drug therapy in several diseases including HIV/AIDS [29, 30]. Indeed, the measurement of CD4+ T lymphocyte counts by flow cytometry is presently the gold standard for the monitoring of patients receiving antiretroviral treatment [30].

These cell separation techniques represent the majority of both sorting and separating cells. FACS systems can use more parameters to segregate cell than MACS. Both methods used label techniques and markers which involve a costly and lengthy conjugating step. It does not all the time have 100 % efficiency. It is, although, limited to antibodies conjugating with the cells and smaller sized particles like virus cant be eluded by this method.

2.3.2. Other separation methods

Lysis

In the case of blood, 99 % of the cells are RBCs. They can be easily removed due to their susceptibility to hypotonic shock compared with that of leukocytes (WBCs) and other nucleated cells (Low salt concentration and lysis kit are available commercially). The ion concentration difference creates osmotic pressure shock that bursts the cell by the rapid flow of water inside the membrane - note here that similar method can be taken to 'inflate' the bi-concave erythrocyte to create spherical red blood cell with the membrane stressed to create ghost erythrocytes [31]. Density gradient separation can be used to separate dead cell (RBCs) from live (WBCs) which we used to prepare solution to trap (see Chapter 5).

Density Gradient

Different cell types differ in their densities in the case of blood for instance. Red blood cells are the densest where are plasma is the lightest, therefore in a fixed container red blood cells would sediment and leukocytes will float in the middle with the plasma above. Based on this all cells can be separated based on continuous gradient density. The commonly used is ficoll (high molecular weight sugar) which is used to adjust the density.

This is far from being exhaustive and other method exists with diverse results. Nevertheless these methods describe physical methods for separation but it is necessary to label these cells in many of those.

2.4. Other relevant issues

Today the separation and identification of rare cells is more crucial than ever. Not only because of what we already mentioned but because new treatment and new research have a high demand for such methods in developed countries, and is a method for rapid diagnosis in underdeveloped countries where the need for accurate inexpensive robust test method is paramount to derail pandemics like malaria (1-5 millions death a year according to the WHO) and AIDS (3 million death a year 65% of the 34 million people infected with AIDS leave in sub-Saharan Africa).

Flow cytometry is not a transportable tool, and far from robust; it also needs highly qualified and trained operators. The step of binding a marker to a target cell adds

to the complexity of the system and also the cost. For the point-of-care paradigm the existing systems of diagnosis are not performing as they should and reduced cost could be obtained by integrating these system onto a chip. Several options exist and in our case the already existing Biochip at the University of Canterbury was a starting point. This system use DEP cell separation as short distance force segregation system.

2.5. Dielectrophoretic separation and tag-free cell identification.

All matter when dipped into a electric field presents two major behaviours: one as a conductor and the other as a dielectric. The response of this material can be monitored by observing the force, field, current and potential resulting on this body. This concept is interesting for particles and fluid since an electric field will interact with them within a certain distance. We will see later in Chapter 3 how these fields interact with particles. Dielectrophoresis (DEP) was first applied to bioparticles by Pohl [32]. In brief, when a cell is suspended in an electrolyte solution and subjected to an external electric field it will polarise by the disturbance of the charge [23] distribution around the cell. As we will see later the non uniformity of the electric field translates by a ponderomotive force that varies in sign and intensity with the frequency of the applied field. It can also create a torque on particle producing rotation (know as electrorotation). The force and torque varies also according to intrinsic parameter such as internal conductivity and permittivity of the particle. These advantages can be used to segregate particles according to their core difference since no marker is used this is a label-free technique.

2.6. Conclusion

We have seen in this chapter cells and biological system that could be a target for LOC and BioMEMS. Also was presented diverse techniques currently in use in order to segregate colloids. These systems have all the characteristics necessary to be downsized using moden microfabrication technique and electric field as the micro manipulating tools. The next chapter will investigate the interaction of electric fields with colloids and liquids. We will use this theoretical approach to further investigate using simulation tools.

Chapter III

3. Forces in AC electrokinetics

3.1. Introduction

The application of electric fields to colloids in a fluid can both actuate the liquid as well as the colloids [32, 33]. In a system where colloids are suspended in a media where a controlled electric field exists, the system is subjected to a variety of deterministic forces which we can control as well as stochastic forces that we cannot influence.

The two major electrical forces that exist are electrophoresis (EP) and dielectrophoresis (DEP). EP occurs due to the action of the electric fields on the fixed net charge of the particles whilst DEP occurs when there are induced charges and only results in a motion in non uniform fields (DC or AC).

This chapter presents the theory behind the polarisation of dielectric materials, along with description of AC and DC electrokinetic phenomena arising from the interaction of an applied non uniform field and such polarisations. It also derives these forces for the particular case of the interaction with tri-line systems present in digital microfluidics. Finally, discussion and presentation of other forces pertinent to this work are presented.

3.2. Dielectrics

Dielectric materials polarize under the influence of an external applied electric field [34]. Polarization is the ability of a material to acquire a dipole through the action of this external electric field. Ideal dielectrics possess no free charge carriers, with all charges being strongly bound to the atoms or molecules of the dielectric material. Upon the application of an electric field these bound charges can only be forced to move slightly, with the positive charges moving one direction and the negative charges moving in the opposite direction. A dielectric in which this charge displacement has taken place is said to be polarized [17].

For the case of a homogeneous dielectric there are three polarisation processes: electronic α_e, atomic α_a and orientational α_o. In the case of a heterogeneous dielectric system, a further polarisation mechanism is present, interfacial polarisation α_i. The total polarisability of the material α_T is the sum of these processes, $\alpha_{T=}\alpha_\varepsilon+\alpha_\alpha+\alpha_o+\alpha_i$. Each of the polarisation processes posses a characteristic time constant, resulting in a dielectric relaxation or dispersion. With these definitions the polarisation P is expressed

$$\underline{P} = \alpha_T \underline{E} \tag{1}$$

where $\underline{E}$ is the applied electric field.

3.2.1. Debye relaxations

For a homogeneous dielectric the movement or formation of each dipole has a characteristic relaxation time. Due to the physical size of the dipole moment there is a limit to the speed with which it can orient within a time-varying electric field. If the applied field has a period much shorter than the relaxation time of the dipole, the dipole is unable to orient with the field and the polarisation no longer occurs.

3.2.2. Electronic polarisation

Electronic polarisation occurs in both polar and non-polar materials. An applied field causes the nucleus and electrons of an atom to experience oppositely directed forces. The electron orbitals are distorted in such a way that their average position no longer coincides with that of the nucleus. The electric fields generated by the microfabricated electrodes used in dielectrophoretic systems are typically of the order of $10^6 Vm^{-1}$, and considerably smaller than those within the atom of order $10^{11} Vm^{-1}$. The displacement of the charges is therefore only of the order of 10Å. The frequency region of this polarisation process is above 10^{14}Hz (UV regions and higher) and therefore of no consequence to this work since we are working at below GHz frequencies.

3.2.3. Atomic polarisation

Atomic polarisation occurs as a result of the displacement of differently charged ions within a material, and can contribute greatly to the total polarisation in inorganic compounds. This mechanism only makes a small contribution to the total polarization in organic solvents where there are no ions present. Atomic polarisation occurs in the frequency range above 10^{12}Hz again making it of little consequence to this work.

3.2.4. Orientational polarisation

Orientational polarisation only occurs in polar molecules, i.e. those molecules that contain permanent dipoles in their chemical structure. The permanent molecular dipoles in these materials are free to rotate about their axis of symmetry and to align with an applied electric field. Orientational polarisation is temperature dependent. As the temperature of the material is increased so the thermal agitation of the molecules within the material increases, this results in a reduction in the level of polarisation of the material. This reduction is due to the increased random movement and consequent disordering of the orientation of the molecules in the material.

As just described, dipole reorientation is typically the slowest polarisation mechanism in a homogeneous dielectric and is usually the first polarisation term to disappear as the frequency of the field is increased. The atomic and electronic polarisation processes have relaxation frequencies high enough such that their contribution to the total polarisation is unaffected by the angular frequency of the electric fields used in this work. As a consequence, the low frequency limit of polarisation for a homogeneous dielectric is given by the sum of the electronic, atomic and orientational polarisations, while the high frequency limit of polarisation is given by the sum of the electronic and atomic polarisations only (Figure 3-1).

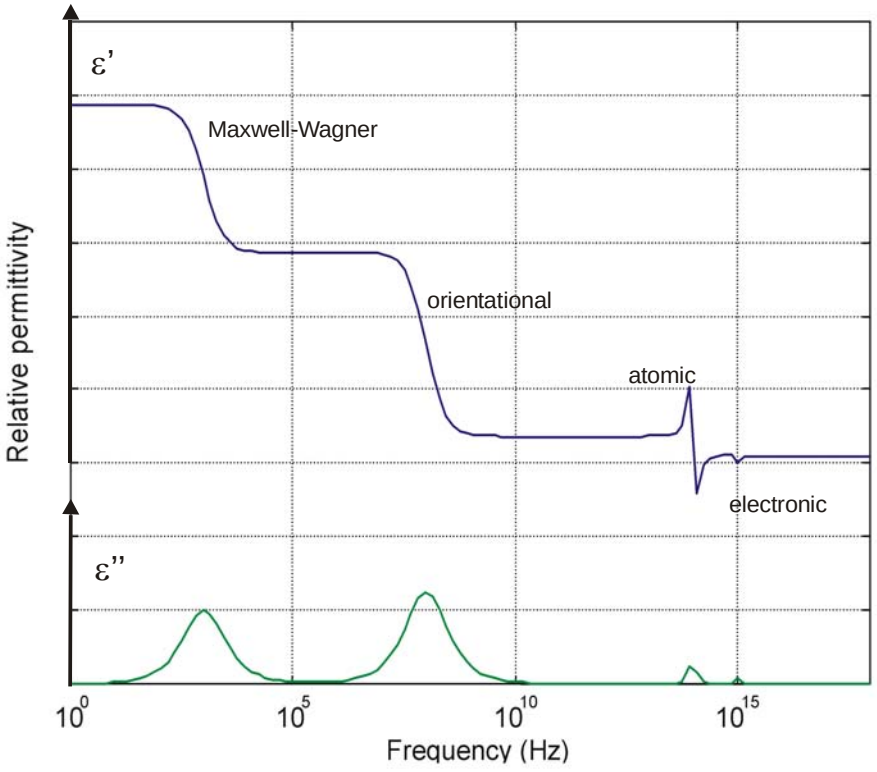

Figure 3-1 : Real and imaginary part of the permittivity through a dielectric relaxation

3.2.5. Interfacial polarisation: Maxwell-Wagner polarisation

When a heterogeneous system is subjected to an applied electric field it generally shows frequency dependent dielectric and conductive properties that are different to those of the constituent parts. Heterogeneous systems therefore exhibit further dispersions due to interfacial phenomenon; these are in addition to the above-mentioned polarisation processes and are known as Maxwell-Wagner interfacial polarizations. An accumulation of charges at the structural interface between the dissimilar materials gives rise to the formation of a charge layer at the boundary.

The simplest example of a Maxwell-Wagner interfacial polarization is that of a parallel plate capacitor comprised of two dielectrics of differing thickness (d_1, d_2), permittivities (ε_1 ,ε_2) and conductivites (σ_1 ,σ_2) and plate area A, as shown in Figure 3-3. Conductivity can be thought of as a measure of the ease with which current flows through a material, while permittivity is a measure of the energy storage in a system.

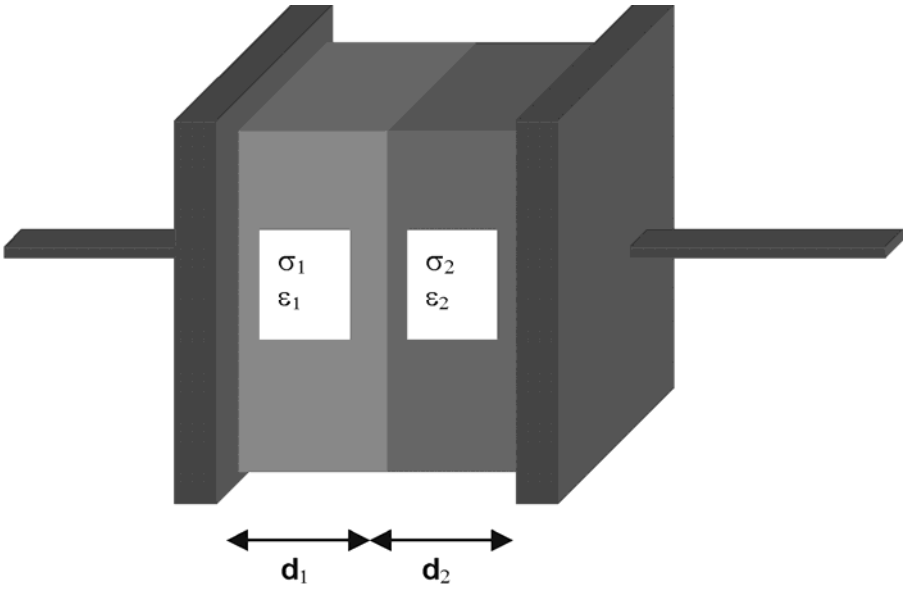

Figure 3-2: Parallel plate capacitor made of two generic materials of thicknesses d_1 and d_2.

The frequency, at which the relaxation due to the Maxwell-Wagner interfacial polarisation occurs, depends on the nature of the interface. Figure 3-2 shows the variation in the real ε' and imaginary ε'' parts of the complex permittivity (ε^* is the complex permittivity given by $\varepsilon^* = \varepsilon_0[\varepsilon' - j\varepsilon'']$), with frequency for a typical Maxwell-Wagner interfacial polarisation. Δε is the dielectric decrement.

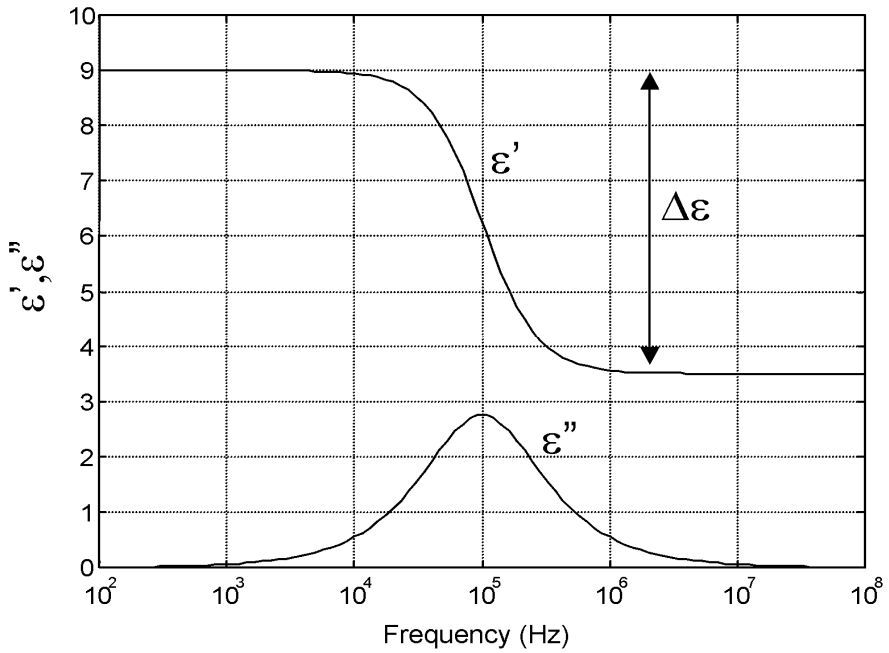

Figure 3-3 : Imaginary and real part Maxwel Wagner relaxation

The overall effect of each of these polarisation processes (electronic, atomic, orientational, interfacial) is to produce a number of dispersions and in the dielectric permittivity of the system.

As the applied field frequency is increased from the steady state, the permittivity changes from the static field value $\varepsilon_{\omega\to 0}$, to the high frequency value $\varepsilon_{\omega\to\infty}$ equal to 1. At the optical end of the frequency spectrum the electronic and atomic polarisations appear as resonances in the system, and the associated peaks in ε'' characterise the absorption of radiation by the material.

3.3. Two layer system: simple case

The variation of the permittivity of a mix of dielectrics can be approached by the two layer system. It is a preliminary to the shell model [17] and allows us to understand the relaxation shown in Figure 3-3.

The simple two layer system can be modelled as a pair of capacitors in series. Assuming that σ_2 is negligibly small (and that σ_1 is not), and that ε_1, ε_2 and σ_1 are frequency independent, a simplified expression is obtained for the behaviour of the dielectric system. The total capacitance of the two capacitors is given as

$$\frac{1}{C_{tot}} = \frac{1}{C_1} + \frac{1}{C_2}, \tag{2}$$

where

$$C_1 = \frac{A\varepsilon_o\left(\varepsilon_1 - \frac{j\sigma_1}{\omega}\right)}{d_1} \tag{3}$$

and

$$C_2 = \frac{A\varepsilon_o\varepsilon_2}{d_2}, \tag{4}$$

with $d=d_1+d_2$. Here ε_0=8.854 x 10^{-12} Fm^{-1} is the permittivity of free space, giving the total capacitance as

$$C_{tot} = \frac{A\varepsilon_o\varepsilon_2\left(\varepsilon_1 - \frac{j\sigma_1}{\omega}\right)}{d_2\left(\varepsilon_1 - \frac{j\sigma_1}{\omega}\right) + d_1\varepsilon_2}, \tag{5}$$

from which the low frequency limit ($\omega \to 0$) of the effective permittivity is given by

$$\varepsilon_{\omega \to 0} = \frac{\varepsilon_2 d}{d_2}, \tag{6}$$

and the high frequency limit ($\omega \to \infty$) of the effective permittivity is given by

$$\varepsilon_{\omega \to \infty} = \frac{\varepsilon_1 \varepsilon_2 d}{d_2 \varepsilon_1 + d_1 \varepsilon_2}. \tag{7}$$

If there is a difference between ε_1 and ε_2 the system will exhibit a dielectric dispersion.

3.3.1. Two layer system: complete analysis

A fuller analysis of the two-layer system [17] (i.e. not taking σ_2 to be negligibly small, and assuming that ε_1, ε_2 and σ_1 are frequency dependent) demonstrates that the dielectric dispersions can be described in terms of the Debye equations giving the following expressions for the dielectric parameters of a two-layer system,

$$\varepsilon' = \left(\varepsilon_{\omega \to \infty} + \frac{\varepsilon_{\omega \to o} - \varepsilon_{\omega \to \infty}}{1 + \omega \tau} \right) \varepsilon_0, \tag{8}$$

and

$$\varepsilon'' = \left(\frac{\left(\varepsilon_{\omega \to o} - \varepsilon_{\omega \to \infty} \right) \omega \tau}{1 + \omega^2 \tau^2} + \frac{\sigma}{\omega \varepsilon_0} \right) \varepsilon_0, \tag{9}$$

and

$$\varepsilon_{\omega \to o} = \frac{d\left(\varepsilon_1 d_1 \sigma_2^2 + \varepsilon_2 d_2 \sigma_1^2 \right)}{\left(d_2 \sigma_1 + d_1 \sigma_2 \right)^2}, \tag{10}$$

and

$$\varepsilon_{\omega \to \infty} = \frac{\varepsilon_1 \varepsilon_2 d}{d_2 \varepsilon_1 + d_1 \varepsilon_2}, \tag{11}$$

where

$$\tau = \frac{\varepsilon_o\left(\varepsilon_1 d_2 + \varepsilon_2 d_1\right)}{d_2\sigma_1 + d_1\sigma_2}. \quad (12)$$

The conductivity of the interfacial system as a whole is given by,

$$\sigma = \frac{d\sigma_1\sigma_2}{d_2\sigma_1 + d_1\sigma_2}. \quad (13)$$

This two layer system gives us the trend of a mix of materials for a range frequency, such as in a two shell model of a cell; we can derive the dielectric response of this sytem and therefore forcast its force. This force acting on the dielectric is a ponderomotive force the dielectrophoretic force.

3.4. Dielectrophoresis (DEP)

As described in section 3.2.5, when an electric field is applied, the interface between a particle and the medium in which it is suspended undergoes Maxwell-Wagner interfacial polarisation. The interaction of the charges (associated with the formation of the effective dipole moment) with the applied electric field results in a force, which acts upon the particle. For a uniform electric field the net force experienced by a neutral particle is zero. However, if the particle is placed in a non-uniform electric field the resulting force imbalance across the particle causes it to move. This movement arises due to the variation in the charge density over the particle. It is important to make the distinction between the phenomenon of dielectrophoresis and electrophoresis.

3.4.1. Electrophoresis

Electrophoresis is the motion of charged matter under the influence of an applied electric field. The direction of motion is always toward the electrode of opposite charge to that of the particle, and it is of no consequence whether the field is uniform or non-uniform. Due to the presence of the double layer (see section 3.5), a charged particle when suspended in aqueous solution appears electro-neutral. Despite this, movement of the particle still occurs due to the mobility of the ions in the double layer. The velocity of a charged particle due to the electric field is a function of the particle's size and charge as well as the viscosity and conductivity of the suspending liquid (i.e. the

thickness of the double layer surrounding the particle). The electrophoretic mobility of a charged particle suspended in solution is given by the function (see section 3.5.1)

$$\mu_E = \frac{2\varepsilon\zeta}{3\eta} f(\kappa a) \tag{14}$$

where η is the viscosity of the liquid, ε the absolute permittivity of the liquid, ζ the particle's zeta potential, and $f(\kappa a)$ is a function of the ratio of the particle radius a to the double layer thickness κ^{-1}. The function $f(\kappa a)$ varies between 1 and 1.5 as the value of κa varies between 0 and ∞ (see [35] and 3.5.1 for further details).

The main application of electrophoresis is in the separation of macromolecules such as DNA and proteins, with the different macromolecules moving with different velocities under the influence of the applied electric field. As the technique will work with any charged particle it is applicable to the separation of cells, which typically have a net negative surface charge at physiological pH [5-6].

3.4.2. The dielectrophoretic force

Dielectrophoresis is distinctly different in nature from electrophoresis. Dielectrophoresis (DEP) is the translational movement of neutral matter as a result of polarisation effects in non-uniform electric fields

Under the influence of a uniform DC electric field, a particle with charge q will experience a net force toward the electrode of opposite polarity to that of itself. A neutral particle will become polarised as a result of the electric field, depending on its polarizability relative to the background but will experience no net movement in the uniform field, as shown in Figure 3-4.

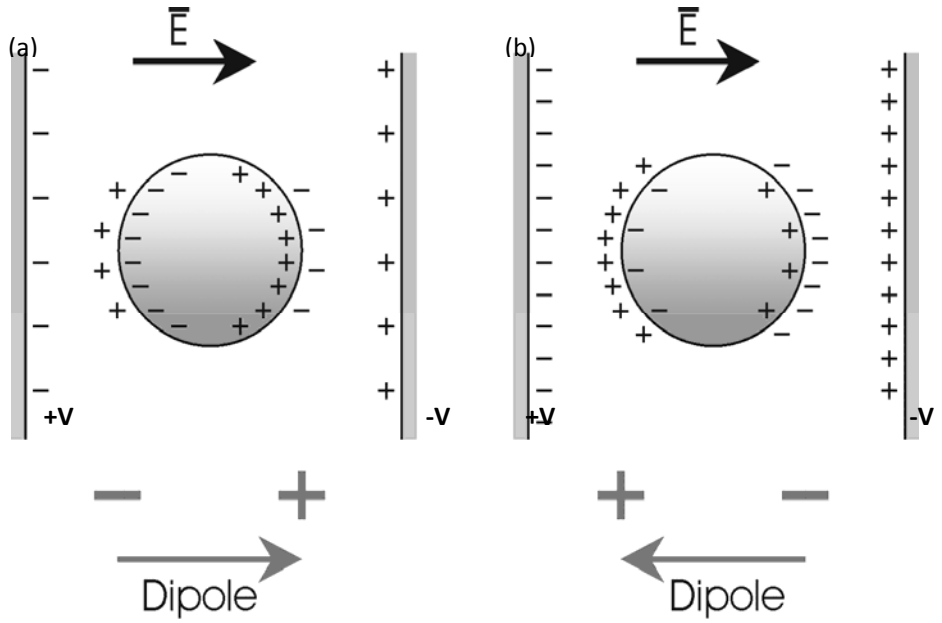

Figure 3-4 : Induced dipole depending on the polarisibility

If these particles are now placed in a non-uniform DC electric field the situation is somewhat different. The charged particle will still experience a net translational force towards the electrode of opposite polarity. However, the neutral particle will now experience a net translational force, moving it towards or away from the regions of high electric field intensity, depending upon the relative polarisability of the particle and the suspending medium, as shown in Figure 3-5.

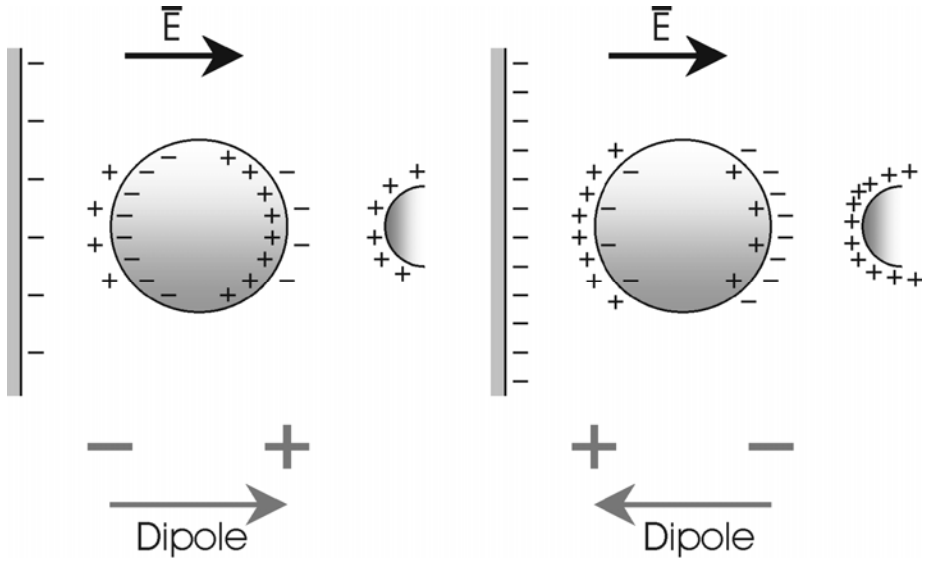

Figure 3-5 : Effect of a non-uniform field on uncharged particles depending on the polarisability

The charge redistribution in and around the particle due to the field results in equal amounts of oppositely charged ions facing the electrodes of opposite polarity. However, as the field is non-uniform, the forces experienced by opposite ends of the neutral particle have different magnitudes. The resultant net translational force in this case is therefore non-zero, giving rise to motion. If the neutral particle is more polarisable than the surrounding medium, the translational force is along the field line toward the region of higher electric field intensity. If the particle is less polarisable than the surrounding medium, the translational force is away from the region of higher electric field intensity.

For an AC electric fields, the neutral particle will always move towards the high or low field regions as described above, irrespective of the polarity of the electrodes. At low frequencies the charged particle will move toward the electrode of opposite polarity under the influence of electrophoresis, its direction oscillating with the field direction. At higher frequencies the DEP force will move the charged particle towards the region of high or low field strength depending upon the relative polarisabilities of the particle and the surrounding medium. The direction of the electrophoretic force is changing so rapidly that the particle has no time to move and the effect of electrophoresis is no longer observed.

3.4.3. Positive and negative dielectrophoresis

In the previous sections it was shown that the polarisation of a dielectric material is frequency dependent with characteristic dispersions of polarisation occurring at different frequencies. Materials therefore exhibit characteristic dielectrophoretic spectra due to differences in their dielectric properties. Particles may therefore experience a force towards a region of high field intensity at one frequency and may experience an oppositely directed force at a different frequency, all other things remaining the same. Figure 3-6 shows the normalised DEP force frequency spectra for a latex particle suspended in water (see section 3.4.5 for further details).

The movement of a neutral particle to a region of high field intensity is called positive dielectrophoresis (+DEP), and the movement of a neutral particle away from a region of high field intensity is called negative dielectrophoresis (-DEP). The frequency at which the polarisability of the particle is equal to that of the suspending medium is known as the crossover frequency f_x. At this frequency the particle experiences no DEP.

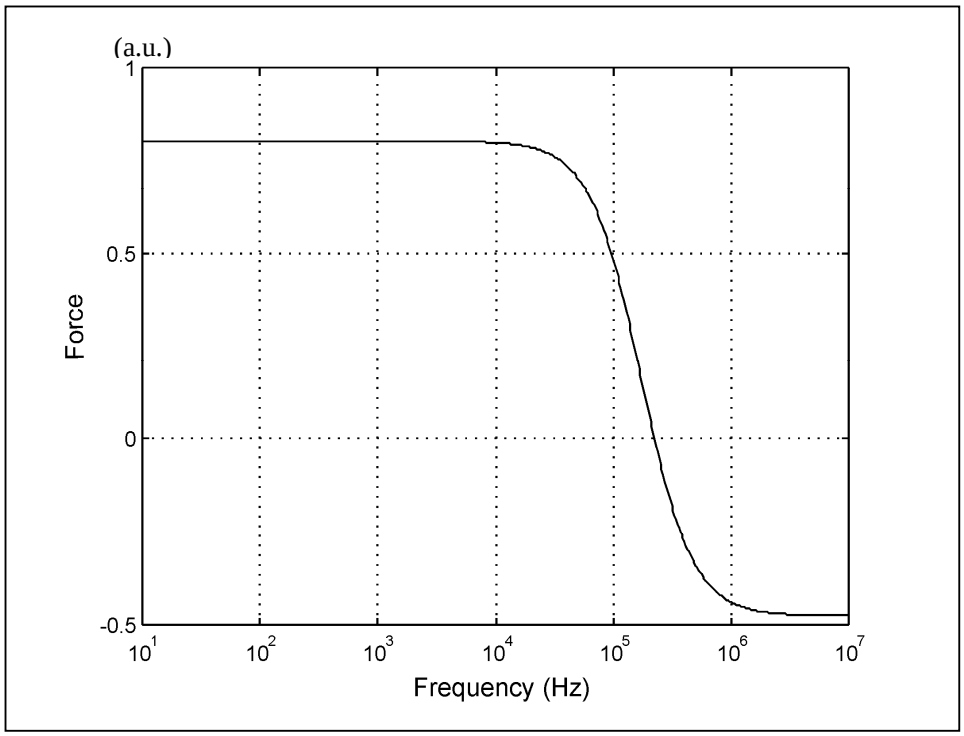

Figure 3-6 : normalised DEP force frequency spectra for a latex particle suspended in water

3.4.4. Derivation of the force on a dipole

The DEP force acting on a particle can be derived first by estimating the net force upon a small physical dipole, and then generalising to the force acting on a particle of effective dipole moment $\boldsymbol{p}_{eff}$ (see [17] and [35]).

A neutral particle within an externally applied electric field has an induced dipole moment, with centres of equal positive and negative charge separated by a distance $\boldsymbol{d}$, as shown in Figure 3-7. We assume that no field contributions arise from the dipole itself. For a dipole in a non-uniform field the positive and negative charges experience different electric field strengths. This gives rise to a total force on the particle of,

$$\boldsymbol{F} = q\boldsymbol{E}(\boldsymbol{r}+\boldsymbol{d}) - q\boldsymbol{E}(\boldsymbol{r}), \tag{15}$$

where $\boldsymbol{r}$ is the position vector of $-q$.

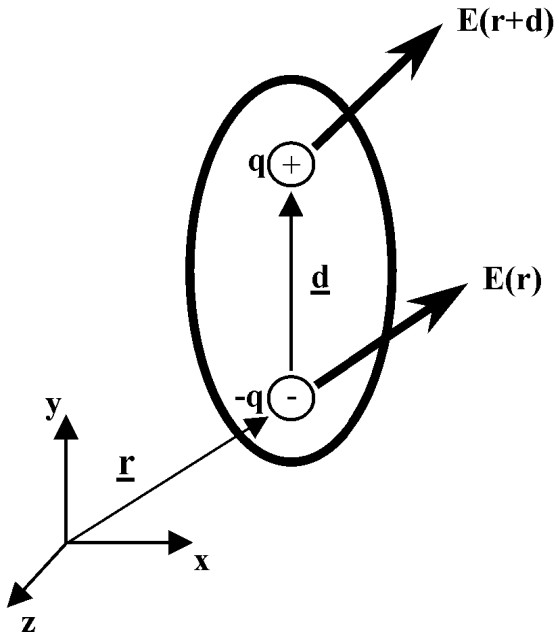

Figure 3-7 : **Field acting on dipole in space**

If the magnitude of $\boldsymbol{d}$ is small compared to the characteristic scale of the electric field non-uniformity, a simplified vector Taylor series can be used to describe the electric field about position $\boldsymbol{r}$, giving

$$F = \mathrm{q}d \cdot \nabla E \tag{16}$$

Where ∇E is the electric field gradient.

From this we obtain the force on a dipole due to an applied electric field,

$$\boldsymbol{F}_{dipole} = (\boldsymbol{p} \cdot \nabla)\boldsymbol{E} \tag{17}$$

The above equation is an approximation for the force exerted on any physical dipole. For a polarisable particle of finite size this gives good results if the electric field gradient non-uniformity can be neglected, when measured over a length scale similar to the size of the particle. This approximation generally leads to good results when applied to small micron or sub-micron sized particles interacting with the electric fields produced by the

electrodes of the size used in this work However, when calculating the forces experienced by particles very close to the electrode edge, or the fields generated by mutual particle-to-particle interactions (between closely spaced particles) the approximation can become significantly erroneous. Higher order linear multipolar terms must therefore be included in such situations.

3.4.5. The effective dipole moment

From the above discussion it is apparent that a dielectric particle suspended in a liquid will experience Maxwell-Wagner interfacial polarization at the particle/liquid interface, inducing a dipole moment in the particle. The concept of the effective dipole moment, $\boldsymbol{p}_{eff}$ of the particle, can then be defined as the moment of the equivalent point dipole immersed in the same fluid with its position the same as the centre of the original particle.

The electrostatic potential ϕ_{dipole} due to a point dipole of moment $\boldsymbol{p}_{eff}$ in a dielectric medium of permittivity ε_m is given by

$$\phi_{dipole} = \frac{\boldsymbol{p}_{eff} cos\theta}{4\pi\varepsilon_m r^2}, \tag{18}$$

where θ and *r* are polar coordinates for a spherical system.

The effective complex polarisability α of a homogeneous solid dielectric sphere can be written in terms of the complex dielectric properties of the sphere and the surrounding medium,

$$\alpha = 3\varepsilon_m \left(\frac{\varepsilon_p^* - \varepsilon_m^*}{\varepsilon_p^* + 2\varepsilon_m^*} \right) \tag{19}$$

where ε^* is the complex permittivity given by $\varepsilon^* = \varepsilon_0\varepsilon_r - j\frac{\sigma}{\omega}$ and the subscripts *m* and *p* refer to the medium and the particle respectively [16].

The effective dipole moment of a dielectric particle suspended in a liquid is therefore frequency dependent and can be expressed as

$$\boldsymbol{p}_{eff} = v\alpha \boldsymbol{E}\,, \tag{20}$$

where *v* is the particle volume. This can be written more explicitly as

$$\boldsymbol{p}_{eff} = 4\pi\varepsilon_m \left(\frac{\varepsilon_p^* - \varepsilon_m^*}{\varepsilon_p^* + 2\varepsilon_m^*} \right) a^3 \boldsymbol{E}\,. \tag{21}$$

The frequency dependence of the effective dipole moment is described by the term in brackets known as the *Clausius-Mossotti* factor,

$$f_{CM} = \frac{\varepsilon_p^* - \varepsilon_m^*}{\varepsilon_p^* + 2\varepsilon_m^*}\,. \tag{22}$$

This corrects for the fact that the field acting locally on the dipole is not the same as the external field applied to the system, due to the effect of the fields associated with the neighbouring dipoles.

The effective moment method described above simplifies the calculation of the force on a particle and avoids the need for complicated derivations based on the Maxwell stress tensor (see [17] for detail). It may be used to calculate the forces on particles as long as the dielectric loss in the suspending liquid is negligible (i.e. $\varepsilon_m'' << \varepsilon_m'$).

3.4.6. The time averaged dielectric force

The instantaneous force on a dipole in an electric field is given above. For the case of a time varying electric field ($\boldsymbol{E} = E_o e^{j\omega t}$) the dipole varies with the same angular velocity as the electric field, but with a phase lag ϑ. The time-averaged force is,

$$\langle F \rangle = \frac{1}{2} \mathrm{Re}\left[(p \cdot \nabla) \overline{E} \right] \tag{23}$$

where $\overline{E}$ is the complex conjugate of $\boldsymbol{E}$. After manipulation using suitable vector identities and inserting the expression for the effective dipole moment the time averaged DEP force becomes [17],

$$\langle \boldsymbol{F} \rangle = \pi \varepsilon_{\boldsymbol{m}} a^3 Re\{f_{CM}\} \nabla |\boldsymbol{E}|^2 \qquad (24)$$

where $\nabla |\boldsymbol{E}|^2$ is the gradient of the square of the electric field and $Re\{f_{CM}\}$ is the real part of the *Clausius-Mossotti* factor, which is defined by the limit $-0.5 < Re\{f_{CM}\} < 1$. The *Clausius-Mossotti* factor modulates the electric field responsible for the force. It allows us to have either repulsive or attractive forces. Since the force depends strongly on the size of the particle we can assume that there exists a size limit where drag and Brownian motion overpower the DEP force. Experimentally we observe that 500 nm beads are more influenced by viscous drag than DEP force. Beads over a micron are more susceptible to be attracted to the edge of an electrode (within the 5-40 micron electrodes size fabricated).

3.5. Electrokinetic effect and fluid movement

We briefly mentioned this in section 3.4.1 and expand the discussion here. For the interaction of fluids with a charged surface (induced or natural), we only mentioned the interaction with dielectrics is by the way of the dielectrophoretic force. The free charges in a liquid system also undergo a force. We develop here the concept of disturbed charge distribution and fluid characteristic at the interface of a solid and a liquid. But also we take advantage of these irregularities in charge distribution to create a fluid movement. Electrokinetic effects are the result of the combined movement, irregular charge distribution and screening at the solid liquid interface.

Electrokinetic effects can be classified in four cases :

- Electrophoresis : The movement of a charged surface plus attached material (i.e. dissolved or suspended material) relative to stationary liquid by an applied electric field.
- Electroosmosis : The movement of liquid relative to a stationary charged surface. (i.e. the complement of electrophoresis). The pressure

necessary to counterbalance electroosmotic flow is called electroosmotic pressure.

- Streaming Potential : The electric field created when liquid is made to flow along a stationary surface charged surface.
- Sedimentation potential : the electric field created when charged particles move relative to stationary fluid.

Electrokinetic pumping and particle manipulation, techniques are widely used to move liquid and particles at small length scales because they are implemented through surface forces which scale well when length scales are reduced. Electrokinetic techniques have the advantage of being easily integrated into micro fluidic systems when compared to external systems such as syringe pumps. They deliver a non pulsating flow and have the advantage of being non mechanical which reduces the chance of failure and allows long term study of fluid flow.

3.5.1. Electroosmosis principle:

When a polar liquid, like anything water based, and a solid are brought into contact, the surface of the solid will acquire an electric charge. The surface charges then influence the migration of charges within the liquid directly next to the wall. This results in strongly attracting ions from the liquid to the surface and forms a very thin layer called the Stern layer. This layer then influences the charge distribution deeper into the fluid creating a thicker layer of the same charge as in the Stern layer. Thermal agitation would contribute to even up the charge distribution as we move away from the Stern layer. This is call the diffuse layer. Together these two layers are called the electric double layer (EDL), as shown Figure 3-8. Although the charges at the wall are fixed, the diffuse layer can be mobile. In particular the diffuse layer has a net charge and can be moved with an electric field. Consequently the boundary between the Stern layer and the diffuse layer is called the shear surface because of the relative motion across it. The potential at the wall is called the wall potential ϕ_w and the potential at the shear surface is called the zeta potential ζ. Figure 3-8 displays the potential associated with gradient of charges (diffuse layer) and the screening at the interface (Stern layer).

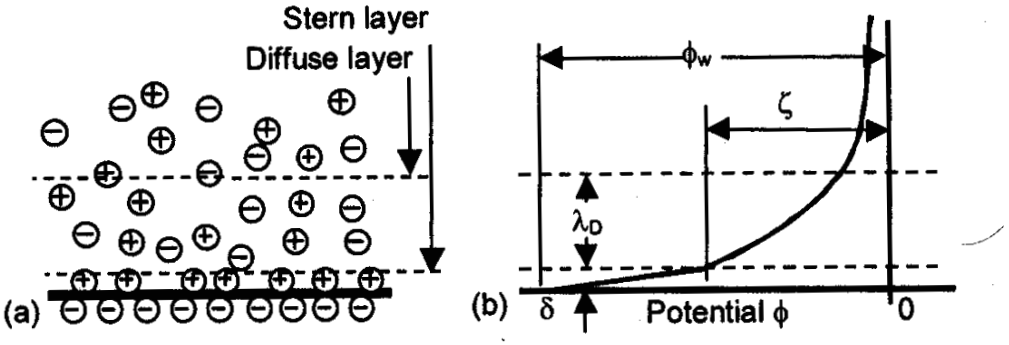

Figure 3-8 (a) Electrical Double Layer Electrical (EDL) configuration (b) Potential in the EDL

We can assume a Boltzman distribution of the charges :

$$c_{\pm} = c_0 \exp(\frac{\mathrm{m}\, zF\phi}{RT})\Big|_{\phi\to\phi_0}^{C\to C_0} \tag{25}$$

C the concentration (+ positive ion, - negative ion, electrolyte concentration), m the ion mass, z its ionic charge,K Boltzman constant, F the faraday number, T the temperature, ϕ the potential.

Combining this with Poisson's equations and ρ_E charge density is then

$$\rho_E = z c_0 \left[\exp(-\frac{zF\phi}{RT}) - \exp(\frac{zF\phi}{RT}) \right] = -2Fz c_0 \sinh(\frac{zF\phi}{RT}) . \tag{26}$$

Poisson's equation then becomes in one dimension

$$\nabla^2\phi = -\rho_E / \varepsilon = \frac{d^2\phi}{dx^2} = 2Fz c_0 / \varepsilon \sinh(\frac{zF\phi}{RT}) . \tag{27}$$

But we can note that for small potential $zF\phi$ << RT (with RT/F = 25.7 mV) we can simplify the Poisson 's equation to the first term of its Taylor series for the exponential.

We can find the potential as $\frac{d^2\phi}{dy} = \frac{\phi}{\lambda_D^2}$ where the Debye Length λ_D is

$$\lambda_D = \sqrt{\frac{\varepsilon KT}{2z^2F^2 c_0}}\,. \qquad (28)$$

If we consider the EDL to be relatively small the solution is then

$$\phi = \phi_w \exp(-\frac{y}{\lambda_D}), \qquad (29)$$

where ϕ_w is the potential at the wall.

The significance of the zeta potential is that its value can be related to the stability of colloidal dispersions. Colloids with high zeta potential (negative or positive) are electrically stabilized. Colloids with low zeta potentials tend to coagulate or flocculate as outlined in Table 3-1[1].

Zeta Potential [mV]	**Stablity behaviour of the colloid**
from 0 to ±5,	Rapid coagulation or flocculation
from ±10 to ±30	Incipient instability
from ±30 to ±40	Moderate stability
from ±40 to ±60	Good stability
more than ±61	Excellent stability

Table 3-1 : Stability behaviour for colloids as a function of their zeta potential

The zeta potential is widely used for quantification of the magnitude of the electrical charge at the double layer. However, the zeta potential is not equal to the Stern potential or electric surface potential in the double layer. Such assumptions of

[1] Summarised from various sources, including on-line materials (detailed references not available)

equality should be applied with caution. Nevertheless, the zeta potential is often the only available path for characterisation of double-layer properties.

This is of use for DC electroosmosis where the speed of the fluid in the EDL is directly proportional to the electric field and the charge density in the double layer. This is derived from the most known and widely used theory of electrophoresis, developed by Smoluchowski in 1903 [36] that describes the electrophoretic mobility μ_e,

$$\mu_e = \frac{\varepsilon\varepsilon_0\zeta}{\eta} \tag{30}$$

where ε is the dielectric constant of the dispersion medium, κ is the Debye parameter $\kappa = 1/\lambda_d$ (28), ε_0 is the permittivity of free space, η is dynamic viscosity of the dispersion medium (Pa.s). We derive from (30) the fluid velocity component over the surface. The fluid mobility is maximum at the electrically driven surface,

$$u_x = \frac{E_x\sigma_q}{\kappa\eta}. \tag{31}$$

If we apply a potential in a pipe the diffuse layer will tend to move according to its charge excess and drag the rest of the liquid accordingly (Figure 3-9). In an AC field one would expect the motion of the liquid to be nil over a period. Nevertheless for different geometry fluid flow is observed in AC too.

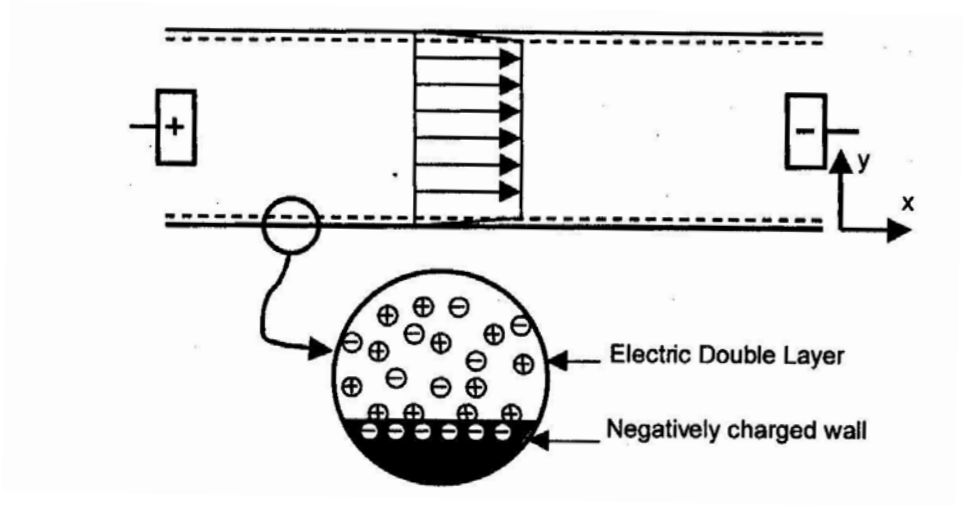

Figure 3-9 : Schematic of a DC electoosmosis fluid flow profile due to the presence of a tangential electric field on the negative ion in the diffuse layer of the EDL.

This system has been extensively used in separation for capillary electrophoresis. We will note the surface importance. Increasing the surface exposed to the liquid will increase the electroosmotic effect. We notice as well that the creation of charge excess is central in this effect and that such a system can require thousands of volts DC to work. This leads to a short-term life for pumping by destruction of the electrodes as well as electrolysis of the water and dissipation of energy that is not compatible with living cells.

Several ideas can be exploited from this. First, if we can produce charges temporarily we will be able to move the liquid as bulk and its suspension of particles. Secondly, porous materials should increase the surface-to-volume ratio so increasing the double-layer effect. This was proven with a bead filled micro pump [37-39] but never with a structured shape. Growing silicon as structured shape could enhance the effect and create effective systems with lower voltage. Using an AC signal and a suitable geometry could also allow a local movement of fluid. The fluid flow is due to the application of the electric field and the induced free charge in the double layer on the electrode. Solving this problem is not trivial and still subject to question, part of which is addressed in this thesis.

We have seen here how the theory can create interesting effect at micro scale, we have laid down the basic principle to simulate the DEP forces, fluid flow and the different relaxations. In order to profit from the effects mentioned in this chapter it is necessary to use micro size system we will introduce the material and method use to fabricate these devices in the next chapter. Prior to that we will outline the theory and design for an AC electroosmosis fluid movement.

3.6. AC Electroosmosis

Most of the recent analysis and experimental work on AC electroosmosis is by groups from the Universidad de Sevilla and the University of Glasgow (now University of Southampton). Some other authors have contributed to the idea of AC Electroosmosis.

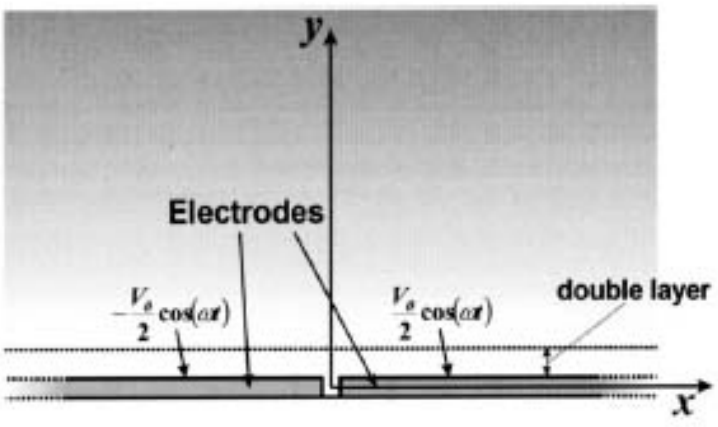

Figure 3-10 : **Symmetrical Electrodes Configuration**

Experiments with AC fields on coplanar electrodes (Figure 3-10) can generate local fluid motion. Understanding the polarization process of the electrodes is essential to understand this AC electroosmosis [40]. The polarization process governs all the necessary ingredients to create fluid flow. Since the electrodes are coplanar the field is non uniform, as is the polarization responsible for the potential at the outer edge of the EDL, and the charge accumulation in the diffuse layer, hence also the potential drop in the EDL. This results is a tangential electric field in the EDL, and resultant fluid flow.

The application of an AC field will create charges at the surface of the electrodes that will create the similar charge excess as in a diffuse layer. The fluid flow between the two electrodes creates roll-shape fluid structures above the electrode (see Figure 3-11). This is the result of the movement of charges under the influence of the electrical field. We note that the flow direction is not changing direction with each half period of the applied voltage because both the electrical field and the charges induced change sign.

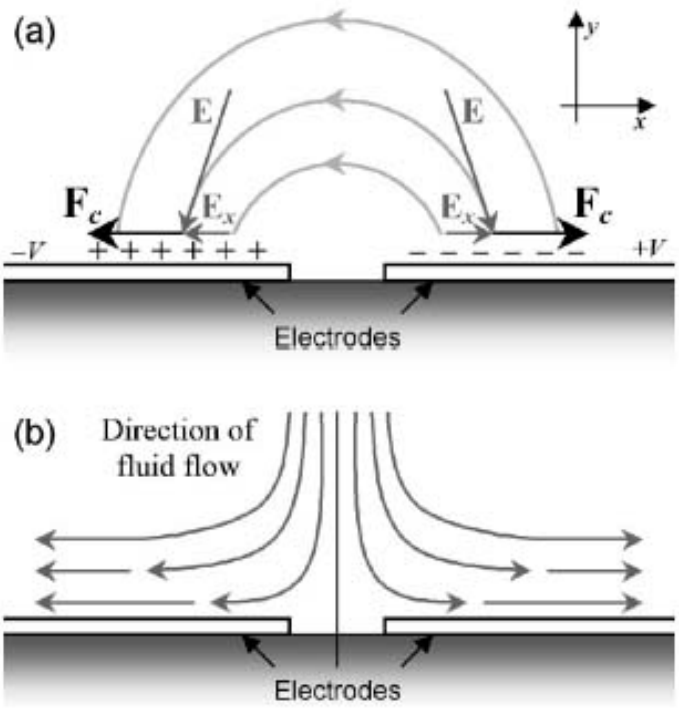

Figure 3-11 : (a) Repartition of the two electrical field components (b) fluid flow induced by the movement of charges in the EDL.

On Figure 3-11 *Fc* represents the average force the charges undergo during a period. It is the electrical field and it is its component parallel to the EDL.

Figure 3-11 (a) and (b) help to understand the interdependent phenomenon. The polarization gives rise to an electric field with a tangential component to the surface and exerts a force on the gradient of charges. These charges accelerate in the diffuse layer which in return drags the fluid around them (due to the polar nature of water). The AC field describes only one period of the sinusoidal signal. However during the second period the polarisation screening charges change sign and so charges in the diffuse layer and so is the direction of the field. Thus the fluid flow is in the same direction. The analysis of the fluid flow over the electrodes is available in ref [40].

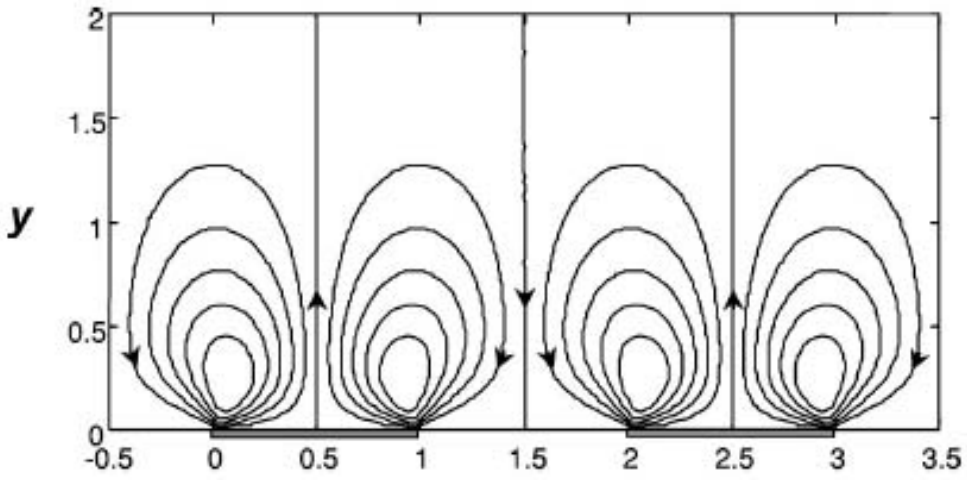

Figure 3-12 : Fig Fluid Flow on symmetrical electrodes

We observe a symmetrical flow due to the electrode symmetry as shown in Figure 3-12, but by breaking this symmetry we can produce a net flow that is the result of the preferential drag in one direction. If the system is now considered being an assembly of a wide and large electrodes separated by a narrow and a large gap Figure 3-13. It will produce a not nil global net flow going from the narrow electrode to the wide electrode. The electrical field is as well asymmetrical and the forces on the EDL are the key for the net flow.

In the DC situation we have seen the slip condition at the surface is governed by the Smoluchowski equation. It means that we can consider can consider a Couette Flow[2] above the electrode. Such a system can be open as well and we will have a free surface. Nevertheless due to the system dimension the viscosity dominates the fluid flow such that it can pinch a non mobile fluid zone and move it along.

[2] laminar flow of a viscous liquid in the space between two surfaces, one of which is moving relative to the other. The flow is driven by virtue of viscous drag force acting on the fluid.

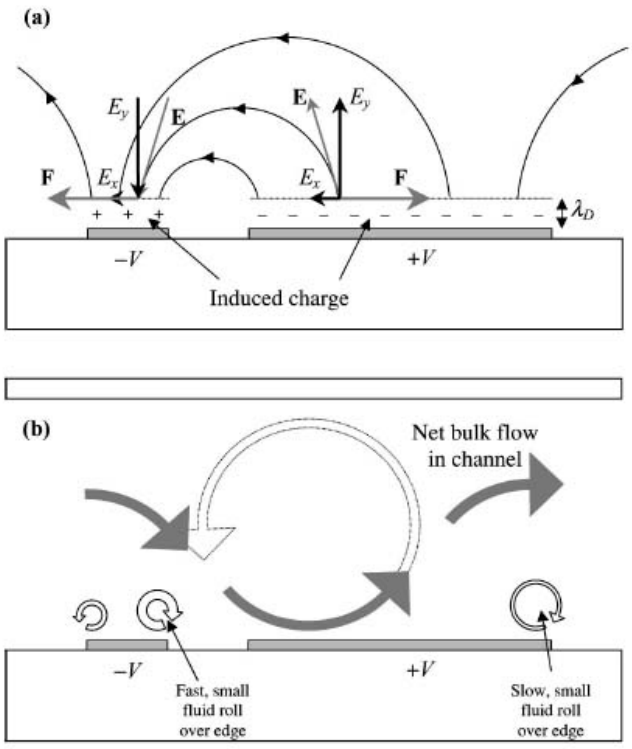

Figure 3-13 : (a) Electrical field on the asymmetrical electrode and forces applied in EDL (b) Net bulk flow resultant

The fluid velocity at surface of the electrode is similar as for DC electroomosis that is maximum immediately outside of the EDL. Gonzales, Green and Ramos [40] described in detail the calculation of the fluid velocity at surface of the electrode. although most of the fluid flow observed [41] and simulated [42] uses strong polarization above the Debye-Hückel approximation (i.e. low surface potential). Ajdari [43] studied a general geometric argument and forecasted bulk fluid flow if a series of asymmetric pair of electrode are designed. This was later proven by [44]. Figure 3-13 (a) displays the forces applied on the charges at two electrodes and (b) shows the typical fluid flow resulting of these forces. Several groups demonstrated the potential of AC electoosmosis pumping as depicted on Figure 3-14. In particular, we note the non uniformity of the electrical fields due to the loss of symmetry. It results in higher charge density at the edge of both electrodes on each side of the narrow gap, which contributes to increase the fluid flow at the surface.

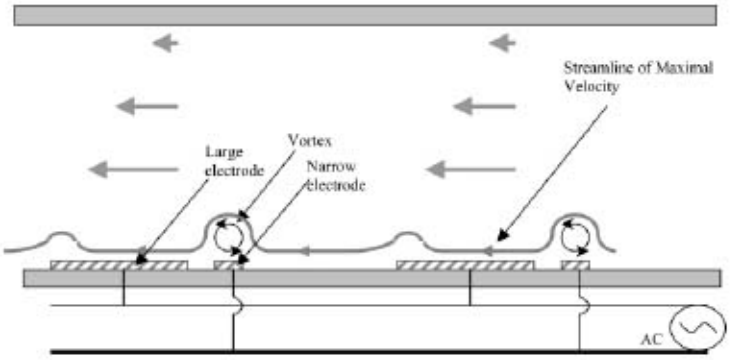

Figure 3-14 : Couette Flow for closed channel

The solution of such a problem both with symmetrical and asymmetrical electrodes is not trivial and the theoretical aspect requires a thorough investigation. The problem although could be decomposed in solving the electrical field first and then solving the fluidic problem.

In order to simplify the system we will consider ions with similar valence as well as same mobility, such as KCl. The electrodes considered are represented Figure 3-14, and we use the symmetry to break down the problem. The electrodes are assumed to be ideally polarisable. The media in use during our experiment can result in electrochemical interaction with the electrode. This would have to be taken into account if we want to change to more complex media. Nevertheless we will be interested only into the electrolyte response for the moment.

The equations considered are :

Poisson,

$$\nabla^2\phi = \frac{e(n_- - n_+)}{\varepsilon}\,; \tag{32}$$

and ion number conservation with n the concentration for each ion contribution (+/-).

$$\frac{\partial n_\pm}{\partial t} + \nabla.\mathrm{J}_\pm = 0\,, \tag{33}$$

with

$$\mathrm{J}_\pm = \mp n_\pm \mu \nabla\phi - D\nabla n_\pm + n_\pm \mathrm{u}\,. \tag{34}$$

The ionic flux J is made of three terms: electric drift , D the diffusion and drift due to the fluid motion and finally convection due to fluid motion. Under our condition the ion movement due to the electric field is considerable compared to fluid movement.

We assume that the signal applied as much as the fixed surface potential are assumed to be small. The applied potential is therefore

$$\phi = \begin{cases} \psi_0 + \frac{1}{2} V_0 \cos(\omega t) \text{ if } x > 0 \\ \psi_0 - \frac{1}{2} V_0 \cos(\omega t) \text{ if } x < 0 \end{cases}. \quad (35)$$

Once we have solved the potential we can superpose it to find the fluid motion. To find the fluid motion we need to solve the Navier-Stokes Equation and the incompressibility.

$$\nabla \bullet u = 0, \quad (36)$$

and

$$\rho_m \frac{du}{dt} = -\nabla p + \rho E + \eta \nabla^2 u. \quad (37)$$

We mentioned at the beginning that the dimension and fluid velocity was such that the Reynolds number was really low (about 10e-2) and for a Newtonian non compressible fluid we deduce the time average equations:

$$\frac{\partial u_x}{\partial x} + \frac{\partial u_y}{\partial y} = 0; \quad (38)$$

$$0 = -\frac{\partial p}{\partial x} - \left(\rho \frac{\partial \phi}{\partial x} \right) + \eta \left(\frac{\partial^2 u_x}{\partial x^2} + \frac{\partial^2 u_x}{\partial y^2} \right); \quad (39)$$

$$0 = -\frac{\partial p}{\partial y} - \left(\rho \frac{\partial \phi}{\partial y} \right) + \eta \left(\frac{\partial^2 u_y}{\partial x^2} + \frac{\partial^2 u_y}{\partial y^2} \right). \quad (40)$$

This results from the linear analysis described in Ref. [45] and the following approximations : (*i*) the bulk electrolyte is assumed to be charge neutral with uniform salt concentration, such that the ionic transport can be described as Ohmic current; (*ii*) the Debye layer is assumed to be in local equilibrium with the electrolyte immediately outside the layer, such that the charge distribution and potential variation in the Debye layer can be described by Gouy-Chapman theory; (*iii*) moreover, we assume that the thickness of the Debye layer is much smaller than the size of the

electrodes, and we neglect surface diffusion and migration of charge; (*iv*) the electrodes are assumed to be ideally polarizable so that no electrochemical reactions occur; (*v)* the bulk fluid motion is described by Stokes flow with a slip condition on the electrodes set by the electroosmotic flow induced in the Debye layer.

The fluid velocity at surface of the electrode is similar as for DC electroomosis that is maximum immediately outside of the EDL. Gonzales, Green, Ramos [40] described in detail the calculation of the fluid velocity at surface of the electrode. Most of the fluid flow observed [41] and simulated [42] uses strong polarization above the Debye-Hückel approximation (i.e. low surface potential (i) $V_0 << k_B T/e$ ~ 25 mV),

$$U = -\frac{\varepsilon}{4\eta}\Lambda\nabla_s\left(\left|\Delta V\right|^2\right), \tag{41}$$

where Λ is a dimensionless parameter representing the relative size of the electrical double layer and η the viscosity and ∇_s the surface del operator.

This expression is interesting because it allows us to separate the fluidic problem for the electrostatic problem and therefore give an 'easy' simulation base. Obviously all these approximations simplify the problem but have their limitations which are well described by [46]. Based on this approximation and the separation of the two problems several simulation was obtained with a finite element method (COMSOL) as described in Chapter 5.

3.6.1. Fluid Flow reversal[3]

Studer [47] used Platinum electrodes to investigate fluid flow in a circular pumping system to avoid the recirculation. They observed the flow was heading towards the other direction[1] for certain voltages and frequencies. Later on other groups observed the same [48] [49] as I have also [50].

This fluid flow reversal has been attributed by Faradaic charge injection [48]. It modifies the fluid flow rolls over the electrodes by transforming the potential and the number of charges in the EDL. It is currently well accepted but only Olesen and Ajdari [46] laid out the basic theoretical principle. They proved that Faradic current could be

[3] "Normal" direction of pumping is from the narrow electrode to the wide electrode.

the source of the fluid flow reversal. This theoretical paper nevertheless is still based on approximations like Debye-Hückel and equilibrium of the EDL with the bulk to neglect ion/mass transport current where we obtain mm/s speed over 20 micron sized electrodes which does not integrate the reality.

Nevertheless this micropump presents some inherent problem for the application envisaged. First of all, it does not create back pressure [51] which makes it difficult to integrate into a LOC to move fluid for a sizable reservoir where pressure difference creates recirculation over the electrode (Figure 3-15). It is largely dependent on the ionic content as shown by equation (30). Hence experimentally we observe little fluid flow for bulk conductivity above 100 mS/m (the diffuse layer becomes thinner: 9.6 nm for 1mM and 3 nm for 10mM of KCl, see eq (30)). This is a major hurdle since most of in vitro media have a high ionic content (0.1 M and above) [41]. Also Faradaic charge injection (due to the half electrochemical reactin Red->Ox+electron) are dependent of the ionic species and the metal in use since at higher voltage electrochemistry can have an important role. As we will see later, each metal has its own electrochemistry and therefore is subject to particular interaction with different ions like the highly pitting ion Cl^-.

Also, the asymmetric electrode produces an intense electric field; the colloidal species in solution are therefore affected by it and undergo a DEP force that either repels them or attracts them according to the electrical fluid characteristic of both the fluid and the colloids. Thus colloids can aggregate at critical places and therefore disturb the fluid flow and the field locally. Hence measuring the particle velocity is perturbing the fluid flow. In order to avoid this small fluorescent beads are used to characterize as they are less subject to DEP forces [17] due to their sizes (the smaller the bead is the less DEP force is exerted on the bead).

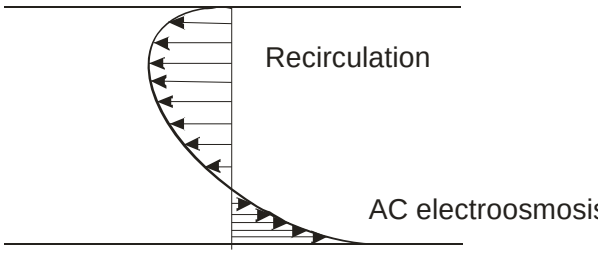

Figure 3-15 : Recirculation fluid due to a gradient of pressure on both side of the channel

3.6.2. Limitations

This system is frequency dependent. At high frequencies the double layer does not have time to form. The potential difference in the double layer and the charging of the EDL is nonexistent. Therefore no tangential field component exists and no movement is observed. At low frequency the potential across the suspending medium is nil so is the tangential field. No electroosmotic flow exists for both low and high frequency which result in an existing maximum flow. Several theoretical investigation of the fluid flow was done by [46] and [45] both find a calculated maximum fluid flow in the "normal direction". But in Studer [47] case and our case [50] the maximum fluid is obtain in reversal where this theory does not apply as mentioned earlier. Nonetheless, as there is little experimental work reported for this effect, it is worthwhile to fabricate and test the prototype pumping systems such as one reported in this thesis. The detail of the fabrication procedure follows.

Chapter IV

4. Materials and methods

The experimental work was carried out using microfabrication technology. We explored several methods in order to obtain the best system for its fluid integrity and its electrical behaviour. We also looked for inexpensive starting materials that would make a LOC a viable disposable tool. This chapter describes the diverse methods used to fabricate such devices and also other handling equipment and fabrication equipment.

4.1. Microfabrication overview

Macrofabrication is essentially very similar to the printing industry except that the materials deposited have variable physico-chemical properties and dimensions are scaled down by up to a factor of 1000. The fabrication cycle is subdivided by the industry into steps. Each of them represents an essential routine necessary in order to achieve the final product. Amongst these steps, four of them are crucial in the development: cleaning, lithography, deposition and etching, displayed in Figure 4-1.

4.2. Mask Making and lithography

The planar lithography process requires a mask – usually binary – that contains the pattern information for a particular process step. Mask making can be an expensive and complex process for devices that require high resolution (micron and submicron). Depending on the size of the structure needed, different design packages were used. Design using features smaller than 10 micron used L-Edit (Tanner Tools) or Wave Maker packages that allow the user to save in the GDSII format necessary for mask writer systems. For devices with 10-50 micron size, screen printing systems could be used using professional mask makers such as JD Phototools (in UK). Also local companies (e.g. Precision Lithographic) can achieve the necessary resolution with acetate transparencies.

4.3. Wafers and materials used

There are two main directions to fabrication, top down and bottom up. In both cases the starting material is essential. In our case the electrodes will be patterned on top of a flat wafer. Several materials were investigated as a substrate. The first chip was

designed on a 3 inch silicon wafer with a 1 micron layer of low stress silicon nitride at the surface. Grooves were etched on its surface by a series of dry and wet etches and electrodes were deposited on top of an other substrate and the two chips was to be bonded together. Unfortunately silicon is not transparent and could not be used to optically monitor the fluid and particle movement.

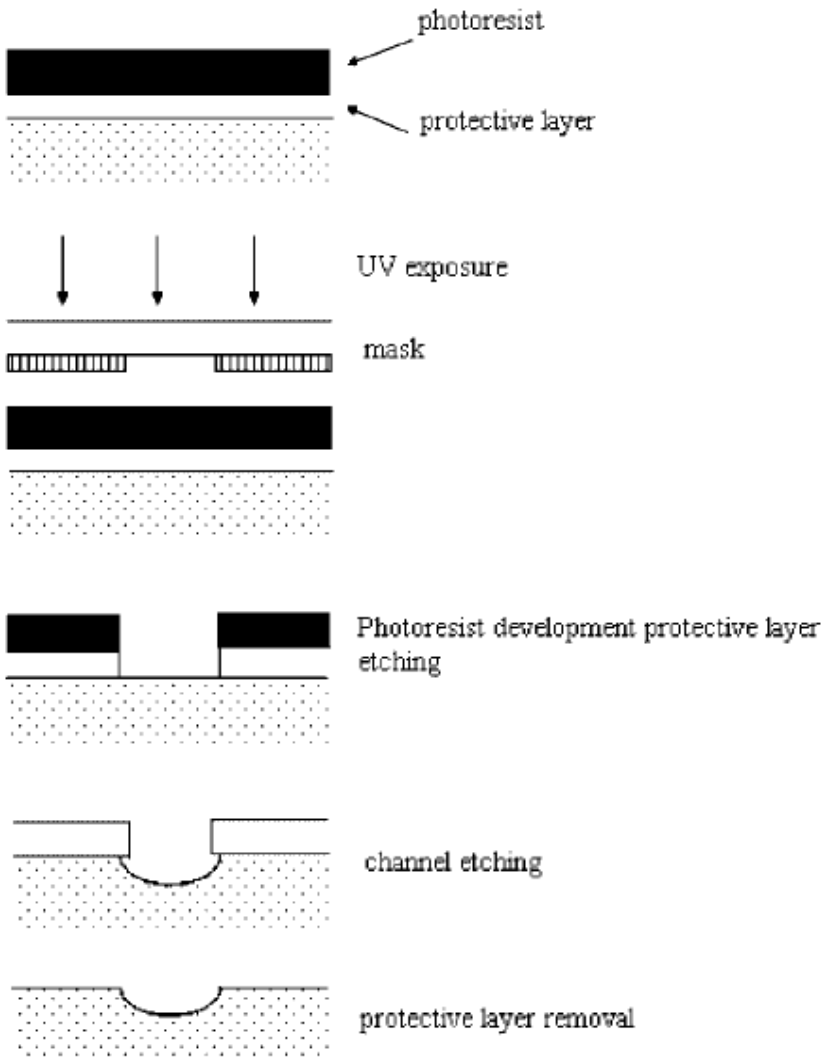

Figure 4-1 : Resist, deposition, exposure, development and etching micro fabrication process.

The major problem of such systems is the inability to use an inverted microscope to observe biological species as most biological labs use. We therefore used regularly pyrex wafers. This has the advantage of being transparent and also is to clean and can form solid bonds with Self Assembly Monolayers (SAMs). However pyrex or

borofloat is sometimes inconvenient especially when annealing is required. It can degas sodium which contaminates high temperature furnaces; also, it has a low softening point of around 800 °C.

Quartz is more expensive and in this case is used to replace pyrex because it can withstand high temperature. Other surfaces were used but transparency is an indispensable asset. Both quartz and pyrex are hard materials. For dicing such material a high speed saw was necessary and often broke due to the higher hardness of quartz. Large sample losses were encountered at the dicing stage. Since it was the last stage prior to use of the device it was not reliable enough to obtain a good yield and we often reverted to Pyrex.

4.3.1. Surface treatment and cleaning

The cleaning of the substrate prior to any other step is crucial to obtain a good surface state for the following steps which involve depositing sensitive materials. The optical patterning using a mask aligner needs the surface to be clear of particles like dust, or biological species, as they could interfere with the patterning process. As a consequence the cleaning step is thorough, as follows:

- Anti bacterial wash in DI (De-Ionized) water. Rinse with DI water.

- 3 solvent clean. Acetone/Methanol/Isopropanol

- 5-10 min in oxygen plasma at 500 W

- Dehydration in 195 deg Oven for 5 hours

4.4. Optical Patterning/ Lithography

In order to transfer the pattern onto the substrate we use spinable UV sensitive polymer know as resist. This resist have could be either negative tone or positive tone upon development. The mask could be either negative or positive of the pattern. Positive resists are normally easier to process and therefore the masks are made in conjunction with the required type of exposure.

4.4.1. Lift-off patterning

A lift-off technique as shown Figure 4-2 (a) is often used when repetitive patterns are used and when the removed material should be totally discarded. For instance in our case for patterning electrodes the gap between them is to be void of any conductors.

Once the substrate is cleaned the resist is spin coated, exposed and developed. The material, in our case a metal, is deposited over the patterned resist and then washed under acetone that will dissolve the resist and therefore lift off the undesired metal. Lift off is advantageous in order to define small patterns but the treatment of the resist could be complex as the feature sizes shrink. It can create trouble as sometimes some monolayer of polymer stays at the surface of the substrate and can be an inconvenient to subsequent patterning, like in the case of SAM or when the material cannot be etched or is difficult to etch. Lift off was used to pattern Platinum electrodes for this reason.

4.4.2. Wet/Dry etch patterning

The obvious alternative to lift off is to use the resist as a protective layer followed by the removal of the unwanted material. Etching is the process of removing material by either chemical or physical action, or both. The process is actually opposite to lift off (except for the cleaning step), as shown in Figure 4-2 (b). First it requires depositing the material to be patterned and above the resist is spin coated. Once the resist is patterned then the material exposed can be removed. There are several methods to remove material such as wet etch that uses an etchant in a liquid form that will attack the material or using low pressure dry etching where ions are accelerated and ablate the surface removing the material exposed to this plasma.

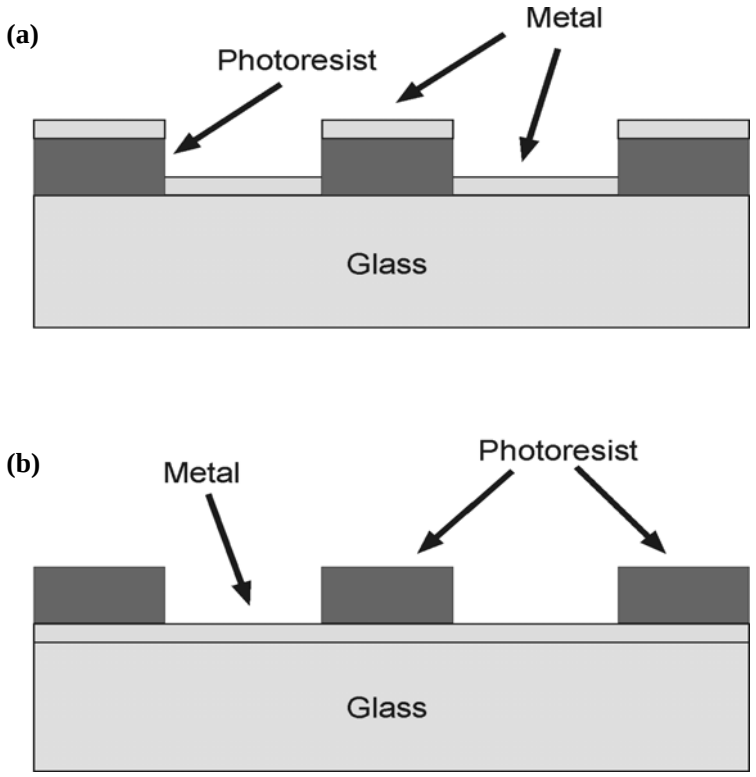

Figure 4-2: (a)Lift off (b) wet etch

Wet etching is isotropic and therefore results in an undercut pattern at edges. it is nevertheless a fast and parallel technique which often used in the industry. RIE, also called reactive ion etching, uses chemically active species that not only etch physically and also chemically the surface. The following wet etch recipies were used in this work :

- Titanium etch - 1 part hydrofluoric acid (HF) to 26 parts DI water. All work with HF was carried out using PTFE dishes/beakers as HF etches glass, although at a slower etch rate compared to Ti.
- Gold etch – 16% (w/v) of potassium iodide (KI) and 4% (w/v) of iodine (I_2) dissolved in water.

Non-focused Ion Beam Milling was also used; the system is a high density plasma generator that physically etches the surface of material by bombarding the target with high velocity ions. This system is highly anisotropic and gives sharp aspect ratio. It was used for fabricating electrode patterns in the Optical Research Centre (O.R.C.) in Southampton (U.K.).

4.4.3. UV exposure / mask aligner

Several different UV sources were used depending on the feature sizes. Whilst a simple UV lamp not collimated that can be used to expose 50 micron minimum feature-size patterns by flood exposures, higher resolution requires monochromatic collimated system delivered in our case by a Karl Suss MA 6 mask aligner. The system also has anti-vibration system necessary to keep the mask and the substrate together.

The different resists used are all UV sensitive. Depending on the tone of the resist the process is different. For the typical patterning of electrodes with wet etching we used S1813 or 1815 (Shipley Corporation). The resist is spun at 3000 rpm giving a thickness above a micron. The substrate is then baked at 95 °C for 2 min to remove the solvent. The resist is therefore ready to be exposed. When exposed the resist should normally be post baked and hard baked; although this can improve some pattern definition it also lengthens the process so these steps were not implemented for such an easy process.

In order to define electrodes by lift off we used S1813 with negative tone mask. The process is somewhat different from standard. The resist is spun and then baked as normal. But prior to exposure the substrate with the resist is then bathed in its developer (TMAH alkali—Tetramethylammonium hydroxide). This consequently hardens superficially the resist. The time for which the substrate is immersed into the developer is critical, indeed too much hardening and the surface is too hard and does not develop after exposure. 15 sec was found to be the best time for a 5 sec exposure (Figure 4-3 and Figure 4-4).

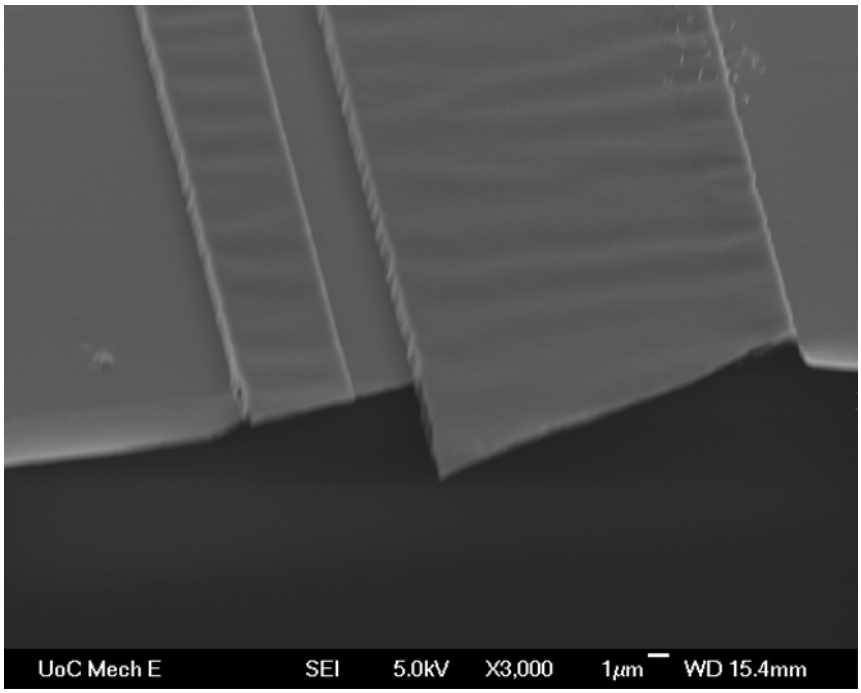

Figure 4-3 : SEM photo of lift-off method by using hardened resist surface.

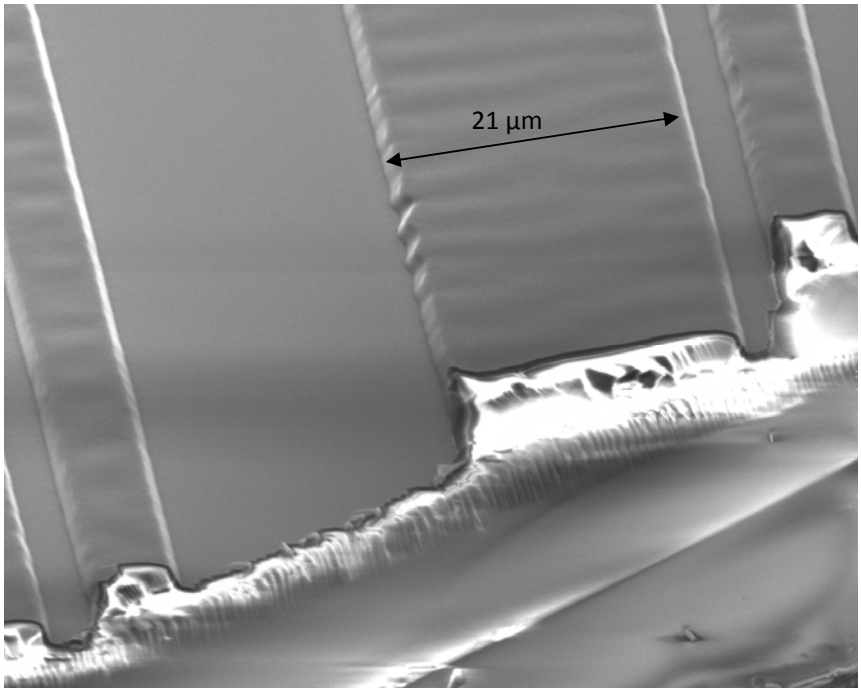

Figure 4-4 : SEM photo of lift-off method without resist treatment.

Another solution for lift off was to double-coat the substrate. The first layer is flood exposed but under exposed. The second layer is then mask exposed which causes the first layer to be overexposed. When the bi-layer is developed the bottom layer is

developed faster which results into the definition of an undercut that crucially helps the lift off step (Figure 4-5).

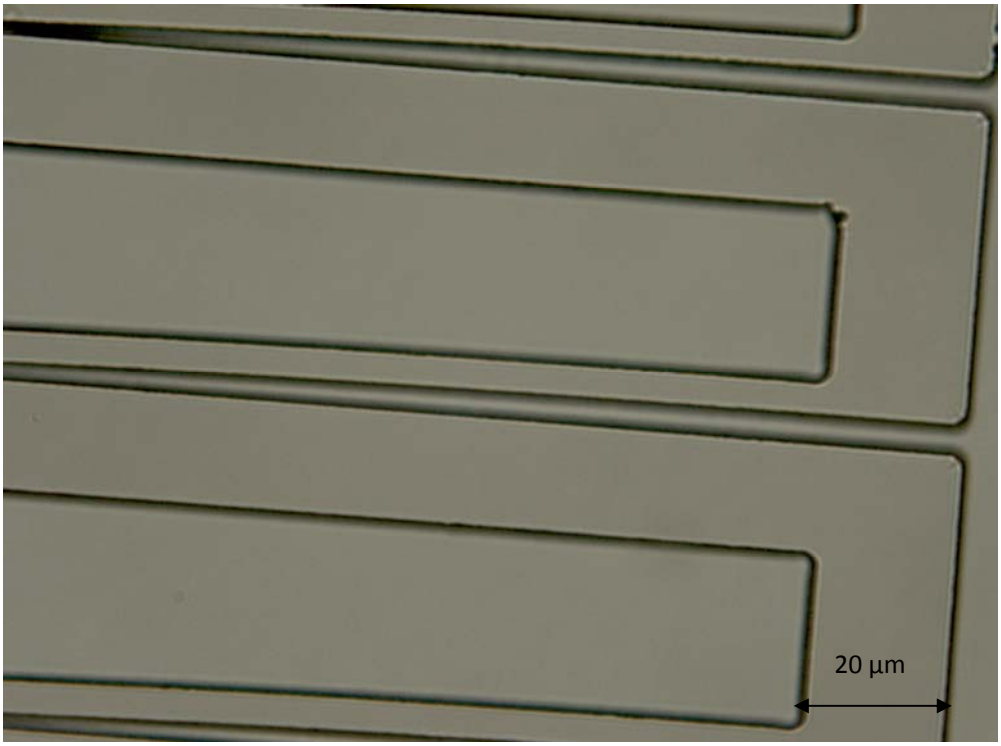

Figure 4-5 : Assymetric electrode developed by the two layer technique

4.4.4. Deposition

As we have seen earlier we will build up layer after layer to create the pattern necessary. In order to achieve this we need to deposit thin layers of material. Several methods exist and we will concentrate on explaining only the method relevant to our designs, namely evaporation (thermal) and sputtering (DC & RF).

We used two diverse, but similar in principle, methods of evaporation. Both are under vacuum which allows us to have a contaminant- free environment. Thermal evaporation is highly directional and convenient for lift off. It uses an electric resistance heater to melt the material and raise its vapour pressure to a useful range. Only material with a much higher vapour pressure than the heating element can be deposited without contamination. The evaporant material subsequently deposits on sample that is held in the same vacuum system and a thin film results.

As per its name the electron beam evaporator uses an electron beam to heat up a small amount material held in a crucible. This crucible is cool and only the material is heated up which results in a lower contamination of the layer condensed on the substrate. High temperature can be reached and materials such as Pt and Ti can be easily evaporated despite their high melting temperature.

Sputtering relies on a plasma (usually a noble gas, such as Argon) to knock material from a "target" a few atoms at a time. The target can be kept at a relatively low temperature, since the process is not one of evaporation, making this one of the most flexible deposition techniques. It is especially useful for compounds or mixtures, where different components would otherwise tend to evaporate at different rates. Note, sputtering's step coverage is more or less conformal.

In the case of most metals DC sputtering is used. The plasma created is sparked by the acceleration of electrons and the cascading effect that result from reaching the breakdown voltage dictated by the Paschen's Law. The ions present in the plasma are accelerated towards the target, causing sputtering.

In the case of insulating materials such as silicon oxide, RF plasmas are required to avoid surface charges that prevent the ablation of the target. Due to the AC periodic signal the surface is not charged and the heavier ions are accelerated to the target. The magnetron sputtering adds a magnetic field that increases the path length of the accelerated electrons. It results in an higher ionisation in the gas and a better rate of sputtering. In more complex target stoichiometry the system requires an added chemical reaction during deposition which is the work for SiO_2 and TiO_2 in our case, often O_2 gas is added into the excited plasma mixture.

In reactive sputtering, the deposited film is formed by chemical reaction between the target material and a gas which is introduced into the vacuum chamber. Oxide and nitride films are often fabricated using reactive sputtering. The composition of the film can be controlled by varying the relative pressures of the inert and reactive gases. Film stoichiometry is an important parameter for optimizing functional properties like the stress in SiN_x and the index of refraction of SiO_x. The transparent indium tin oxide conductor that is used in optoelectronics and solar cells is made by reactive sputtering.

4.4.5. Spin coating

In particular with electrowetting, insulating layers and hydrophobic layers need to be deposited. These layers were either deposited using the previous techniques such as reactive magnetron sputtering (in the case of the insulator) or using a more straightforward spin coat technique. Originally two approaches were used in the electrowetting experiments. Spin on glass was used as an insulator and Teflon AF for hydrophobic layer, and CYTOP from Asahi glass. Comparing the properties of amorphous Teflon, Cytop and Teflon AF, the Cytop product appears to bind better to the substrate than Teflon AF during the spin coating stage. Fluoroinert product from 3M, FC-75, was used to dilute AF Teflon.

The detailed process for spin on glass coating is the following

- SOG Coating:

  speed to 3000 rpm.

  Set spinning time to 20 seconds.

  dispense 3 cc of Futurex IC1-200 SiO_2 SOG on the wafer.

- Baking:

  Place wafer in 120°C oven for 30 minutes.

  Increase temperature of oven to 200°C and bake wafer for an additional 30 minutes.

- Annealing:

  Anneal wafer 400°C for 30 minutes.

Another baking step is required to obtain a true silicon dioxidelike film. This occurs around 800°C. This really high temperature is impracticable for our need since pyrex wafers soften at this temperature. Spin on glass was also seen to fracture on Quartz, probably due to differential expansion.

Cytop and Teflon AF were spun at 3000 rpm and baked on a hot plate for 2 min at 100 deg. The solvent is highly volatile and the layer is solid after spinning. There is little restructuring of Amorphous Teflon with temperature.

4.5. Post fabrication process

Contrary to most semi-conductor devices, most of MEMs fabrication involves some complex interfacing with mechanical subsystems. Indeed, these fabrication techniques involve 3 dimensional systems. In our case the need for manipulating fluid requires that we create a closed liquid handling system above the electrodes that we have just built. There are therefore two major complications, bonding & alignment.

First bonding since we need to close with a lid-like structure: we have to make sure that the seal created is tight. Indeed in order to prime the channels it is often necessary to apply great pressure that results in irreversible damage to the seal.

Second aligning, this in most of our cases was performed manually and by eye (about 100 micron resolution). Most of the systems did not required a better alignment. Although an EVG aligner bonder was used to create channels in polyimide most of other system was done by hand as this is faster. This is relevant for both AC electroosmosis and electrowetting.

4.6. Microfabrication of fluidics channels

We have seen the method to fabricate electrodes for electrowetting, AC electroomosis and DEP experiements. As such fluidic, channel features are larger therefore does not requires the same level of precision as the electrodes. Nevertheless the material are different and so are the methods

4.6.1. Materials used.

Polydimethylsiloxane (PDMS)

This is the most widely used silicon-based organic polymer, and is particularly known for its unusual rheological (or flow) properties. It is optically clear, and is generally considered to be inert, non-toxic and non-flammable. Thus an ideal candidate for fluid manipulation with biological compound. The chemical polymer formula is $(H_3C)_3[Si(CH_3)_2O]_nSi(CH_3)_3$.

The process used is by replicating a 3D master. A negative master is created either by the microfabrication technique explained earlier on or by using SU8 as mentioned later on. The PDMS is poured over with its curing agent as depicted in (Figure 4-6).

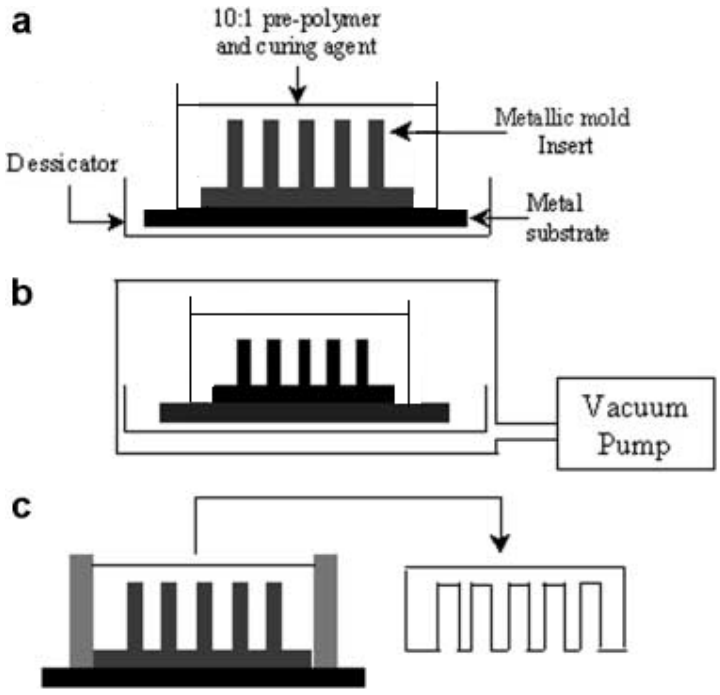

Figure 4-6: **PDMS replication (a) Mix of PDMS pre polymer and its curing agent at 10-1 (b) vacuum pumped to remove bubbles (c) curing at 80 degree c and peeling**

PDMS can be purchased as a two-part kit. The kit consists of a base and a cross-linking agent. The two parts are in a viscous liquid form until mixed and cross-linking occurs. The cross-linking procedure will occur without aid once the two parts are mixed. However, the procedure can be greatly accelerated with heat. The mixing ratios and curing procedures used during development determine the mechanical, chemical, and optical properties of the final solid.

The typical recipe is :

- Mix the PDMS base and curing agent in a 10:1 ratio measured by weight.
- De-gas the polymer in a desiccator for approximately 30 minutes. This removes any air bubbles resulting from the mixing process.
- Spin the polymer on a silicon wafer at 4000 rpm for 60 seconds. This spin recipe results in an approximate 2.5 µm layer.
- Cure the PDMS-coated wafer at 110° C for 1.5 hours to promote cross-linking. Also, store the wafer at room temperature for an additional 24 hours before use.

Polyimide.

Originally developed by Dupont, this is a resist that can be spin to thicknesses of around 15 microns and is photosensitive of negative tone. Multilayers can be spun. Traditionally polyimide was spun on wafers as a protective layer, patterned using positive resist on top and wet etched using TMAH developer. The ability to UV expose and pattern it makes it very interesting to build channels in double-side sandwiched systems. Indeed, whilst curing the polyimide, if in contact with another layer of polyimide, can create a robust seal can be created. It is similar to SU8 but is easier to remove and pattern. It also has a better wetability on surfaces such as SiO_2, TiO_2 and Silicon nitride.

The bonder aligner from EVG was used in Southampton to fabricate most of the AC electroosmosis devices. Polyimide from Fujifilm “Durimide” is an example of such polyimide application.

SU8.

SU8 is a negative tone photoresist with a high aspect ratio. It was used both as an insulator for electrowetting and to pattern channels in ac electroomosis. Many recipes exist but for thick SU8 the following procedure was used

- SU-8 was pipetted onto the slide and allowed to spread. The SU-8 coated slides were then placed on a horizontally level flat surface and left for 1-2 hours to obtain a bubble-free uniform layer.
- Samples were spun at 500rpm for 10 seconds; the speed was gradually increased to 2000rpm over 10 seconds, and held at 2000rpm for a further 15 seconds. The substrate was then left for 1-2 hours to remove any edge beading.

- Samples were soft-baked in an oven for 60 minutes at 90°C and allowed to cool slowly.
- Samples were exposed to light of 365nm through a chrome mask in three equal 100 second exposures, with 60 seconds between each exposure to allow cooling of the substrate; this was followed by a post-exposure bake for 15 minutes at 95°C.
- After gradual cooling the samples were developed sequentially in Microposit EC solvent (*Shipley*, UK), then 1:1 Microposit EC solvent:isopropyl alcohol (IPA) mixture, rinsed in IPA and dried under a stream of filtered air.

Several methods exist to bond SU8 with glass or with SU8 in order to create a lid. Most of them involve annealing treatment cycle with partially cured SU8 [52-54]. Manipulating SU8 for bonding is not as straightforward as many negative resists. It has a low yield largely dependent on humidity (it is so sensitive that we avoided samples when it rained outside).

Ordyl PCB Dry resist

Most of the systems and devices made for microfluidics/Bio-Mems systems needs are over the 10 micron size. Only the electrode and other optic or electronic structure need the use of a high precision system. Therefore the system can be printed onto acetate sheets (3000 dpi printer) that provide the transparency necessary for such a precision [55, 56].

The wafer used for prototyping and testing seals was microscope slides. The cleaning steps was similar to those described in 4.3.1; despite the poor surface quality the slide was sufficient to test the liquid handling using a syringe pump (Chapter 4).

The Ordyl PCB resist process is :

- The dry film resist is laminated at 115
- The channels are exposed by contact printing for about 60 sec. And then post-baked at 100°C.
- The resist is developed with sodium carbonate under sonification.
- Hard bake for chip bonding at 200°C. Hard baked dry film resist is transparent and therefore suitable for our application.

This process never required a high level of precision therefore development and baking was rough estimate based on optical assessment (Figure 4-7 and Figure 4-8) . If we use a chip to cover the system developed we can form an hybrid chip. The resist, during the hard baking process and with the pressure of a clamp, will adhere strongly to a second chip. It is then easy to produce using a press or a heavy weight thus obtaining a system with devices top and bottom of the channel.

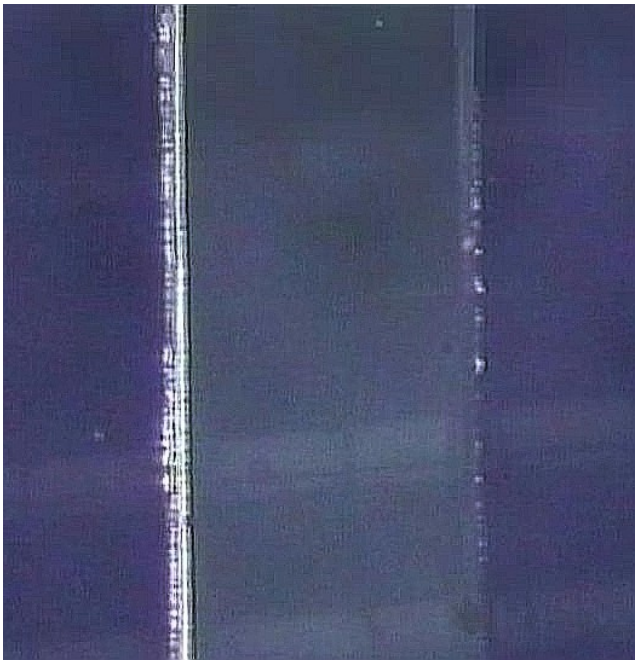

Figure 4-7 : Soft baked ordyl resist 1 mm channel

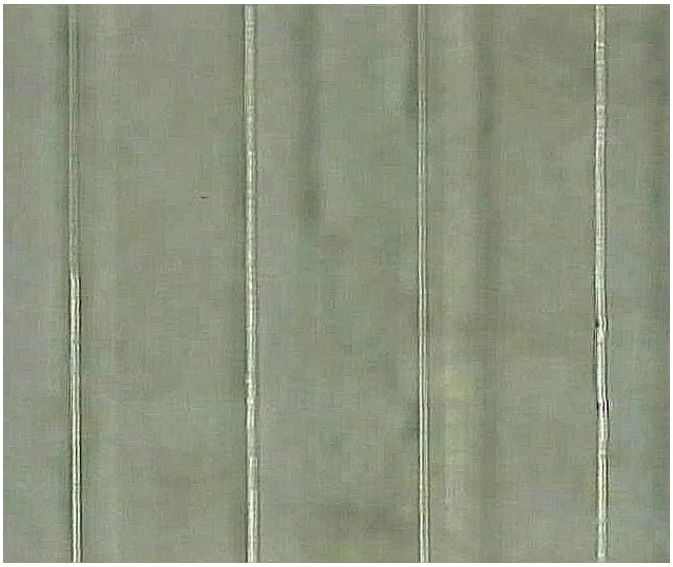

Figure 4-8 : Hard bake ordyl resist 1 mm channels.

The resist could also be used to cast PDMS, which yields for normal-size structures a reliable master without having to use a heavy tool such as DRIE. We experimented exposing the resist with the MA6 mask aligner, which gave better results on aspect ratio than the classical UV box. The dry resist comes in different varieties with some specifically applied for the Bio-MEMS field.

We have now explored all the materials and methods necessary to fabricate the devices. Most of the geometries studied come from the literature or are inspired by the literature. Prior to assessing the characteristics of these devices we need to simulate the overall theoretical principles and designs. The next chapter is dedicated to this purpose.

Chapter V :

5. Simulations

The previous chapters introduced the concept of microfluidics and microfabrication. The device that we propose to fabricate contains an active fluid micropump and a DEP trap to separate and isolate particles. We have seen in Chapter 4 the different techniques to fabricate channels and electrodes on glass and related materials. There are several issues that must be considered into the use of particles for AC electroosmosis; the first and foremost is the potential fouling of the electrodes by residual DEP. We therefore need to devise a strategy to use the fluid pumping and limit the fouling of the electrodes.

We also want to have preliminary experiments to assess the effectiveness of AC electroosmosis. Most of ACEO experiments to date involved electrodes laid on one side only of the channel; since the ACEO micropump does not produce sufficient back pressure [47, 51] we intend to increase the fluid flow laying electrodes on the bottom and the top of the channel [57] in order to improve the efficiency of the system. We propose to use a technique to pinch the fluid using viscous forces in order to manipulate the fluid that contains the particles.

5.1. AC Electroosmosis simulation preliminary

As we have seen in Chapter 3, simulating AC electroosmosis is not trivial, nevertheless the geometry we want to use both for pinching fluid and also to create fluid flow using both sides of the channel has not been observed before. Prior to creating the masks necessary for this endeavour we want to assess the basic feasibility which is observation of fluid rolling due to AC electroosmosis. Fluid pinching at the connection between the main channel and the ACEO micropumps are also to be modelled. DEP trapping forces for nDEP and pDEP (negative DEP and positive DEP) are also important to simulate.

This simulation exercise intends to observe the effect of electric field and how it disturbs the fluid flow on both side of the channel. Once the simulation is obtained we can study how to pinch a fluid from two reservoir using the shear stress created by a

moving fluid. Finally we will have a look at the positive and negative DEP force to attract or repel particles to segregate them on a DEP trap.

5.1.1. AC electrosmosis model.

The model investigated is adapted to the simulation package FEMLAB (COMSOL). We use the Debye Huckel approximation (see Chapter 2). This approximation is inappropriate above 25 mV_{rms} but a proper development of the instabilities resulting in the electrical double layer and the material electrochemical interaction is far from simple [40, 42, 46, 58]. We intend only to confirm the basic theory and observe the effect of two ACEO pumps on the top and bottom of the channel.

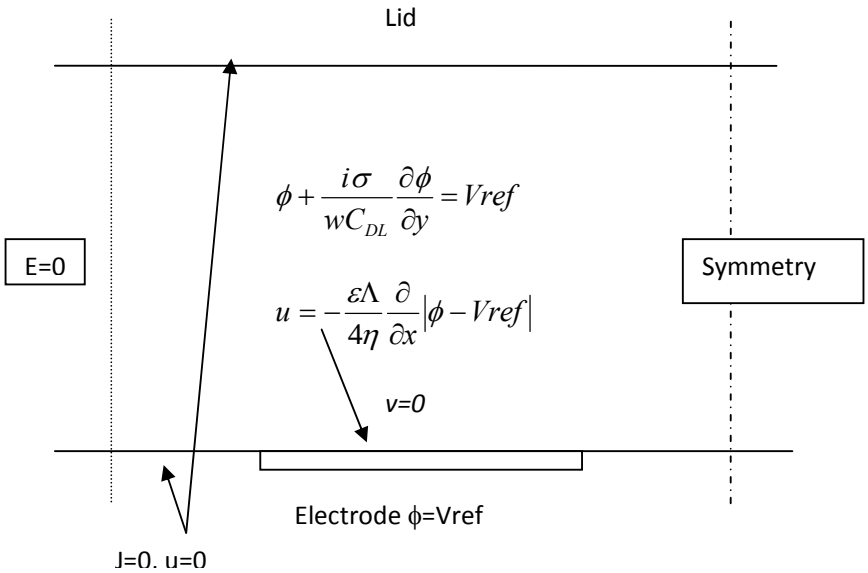

Figure 5-1 : Boundary condition for the electrode model.

We use for Figure 5-1 ϕ as the potential, C_{DL} the double layer capacitance and w the width.

Figure 5-1 displays the schematic of the model and boundary condition use to simulate symmetrical fluid flow activated by polarised electrodes. The details of the simulation was taken from [40-42, 58, 59]. In Figure 5-1 the boundary condition on the right side is representing the alternate electrode and therefore the fluid flow is symmetrical along the dashed line, so is the electric field. On the left side the electric

field is nil far from the electrode. In case of a simple electrode the fluid flow is nil far from the electrode and the left boundary is considered as a perfect insulator.

5.1.2. Boundary condition and meshing representation

We introduce in the boundary equations a thin layer representing the electrical double layer by some capacitance to which we refer to a phasor [42] such that we do not have to create a thin layer that will make the meshing impossible (the EDL is about 10 nm thick and the overall dimensions are 10s of microns).

In the approximation mentioned in Chapter 2 we can therefore separate the electrical problem from the fluidic problem. We first consider the electrodes ideally polarisable such that the discrete capacitance component does not exist.

The conductivity and the permittivity in the double layer is somewhat different than from the bulk. It is also due to the phenomenon of polarisation concentration [60] dependent of the frequency/material and electrochemical reaction. Several publications refer to a relative permittivity of 20 in the double layer for low concentration salt [16]. This is by neglecting any local electrochemistry. The conductivity is therefore increased dramatically as it will deplete completely of electrolyte the fluid surrounding the electrode. One approach for this was to use the phasor expression

$$Z_{DL} = \frac{A}{(i\omega)^{\beta}}. \quad (42)$$

For the double layer impedance the literature gives [16, 41, 42, 61] values for β between 0.6 and 0.8 where β=0 is a perfect resistor and β=1 is a perfect capacitor. Using a simple development we can express σ and ε are functions of β and A obtained from [42] but the result was giving unstable simulation as most of the fluid flow was concentrated at the edge of the electrode where the potential gradient is the highest.

This method gave good practical results but seems unfit for simulation due to lack of meshing resolution necessary for this problem; especially for higher electrolyte concentration the Smoluchowski equation is not valid and most of the flow is limited to the edge of the electrode [62]. Since the interest of the simulation is to observe the generic fluid flow as predicted by the low polarisation approximation the result in Figure 5-2 gives satisfactory information which show the extension of the fluid disturbance of

the size of the electrode. Therefore using such a system where both sides of the channel (top and bottom) contain asymmetrical electrode can be simulated.

5.2. Symmetrical electrode simulation

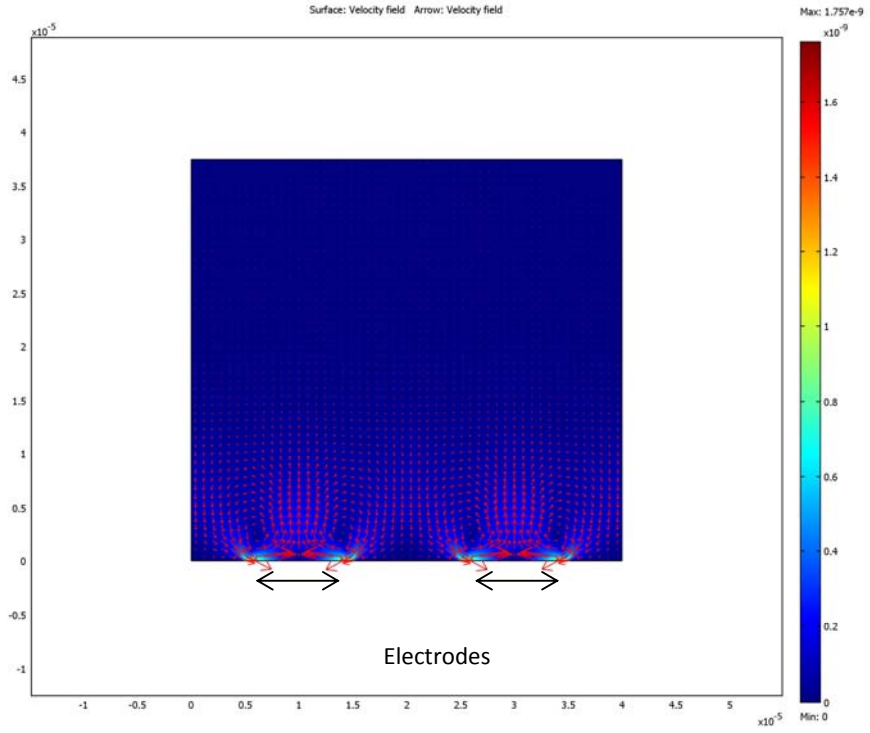

Figure 5-2 : 10 microns pair of electrodes polarised 1 Vpp in a limitless channel (above the electrode) display symmetric rolls on both edges of electrodes.

The simulation of Figure 5-2 shows lower fluid speed than expected by the original experimental work by Brown [44], but the direction is consistent with the theory [62]. We therefore need to observe if asymmetric electrodes create a bulk fluid flow. We can also increase the stability of the fluid flow by adding a set of electrodes system on the lid so that the fluid flow is symmetric around the centre of the channel. It will add stability to the particle in transit through the ACEO pump. The fluid rolls above the electrodes will act as slings for particles captured within the rolls. We can also superimpose (AM or FM) a higher frequency signal so that the we exert a negative DEP (ACEO is inexistent above 1 MHz see chapter 4). The simulations are similar with the previous system where the conductivity is 1e-4 $S.m^{-1}$ and the relative permittivity is about 80. The thickness of the electric double layer can be calculated by the Debye length (33) for the case of KCl,

$$\lambda_D = \sqrt{\frac{\varepsilon k_B T}{2 z^2 q^2 n_0}} = 1.764 \times 10^{-11} \sqrt{\frac{T}{C}} \,. \qquad (43)$$

C here is the concentration; nevertheless the conductivity σ is directly proportional to the concentration for a given Temperature. In the case of KCl for a conductivity of 1e-4 S.m^{-1} the Debye length is about 30 nm and for a conductivity about 1e-3 S.m^{-1} the Debye length is about 10 nm. The fluid flow collapses above 1e-2 S.m^{-1} because the electrical double layer is too thin to support fluid flow. At higher conductivities the diffuse part of the double layer is thin as a result a large percentage of the voltage is dropped across the Stern layer (See Chapter 2). Since the fluid velocity depends on the free charge in the diffuse layer, which in turn depends on the potential drop across the diffuse layer, the AC electroosmostic velocity decreases with increasing conductivity (see Chapter 6).

5.3. Asymmetrical solution one and two side : onset of net fluid flow

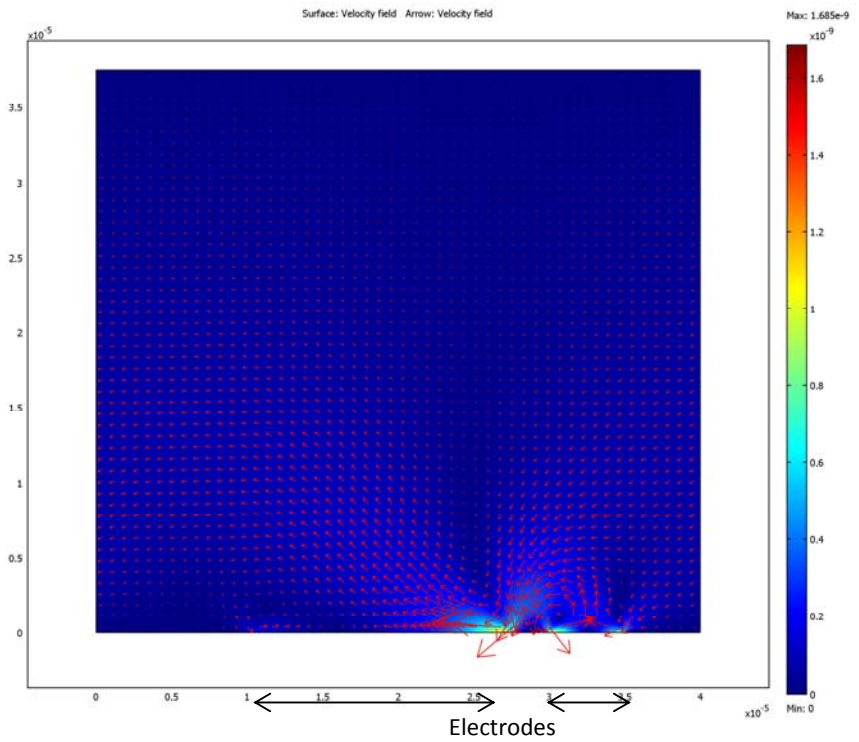

Figure 5-3 : Asymmetric electrode simulation 2 Vpp 500 Hz for 1e-4 S.m^{-1}. Colours show velocity magnitude (scale on right-hand side) and arrows indicate flow direction.

Figure 5-3 shows that an asymmetric array of electrode provides net fluid flow. It also within the approximation made displaying the expected strong roll above the thinner electrode where the potential gradient is the strongest. We observe also that the fluid speed is less on the upper part of the channel due to the non slip condition.

Figure 5-4 shows the existence of a stronger flow if an electrode is built up opposite to the bottom electrode like on Figure 5-3. The ACEO fluid flow is cumulative as described by [45] and [43]. It means that if U is the average bulk flow speed u_i is the contribution of each electrode pair then the total fluid flow is according to [63] the summation of the first term of discrete Fourier expression for the fluid so the net bulk fluid can be expressed as

$$\langle U \rangle = \sum_n u_i \,. \tag{44}$$

It is important to notice that the electrode surface is the active part of the ACEO, therefore the increase of surface to volume ratio will increase the magnitude of the flow which led us to lay electrodes on the lid as well. Also, having both sides of the channel active pushes particle at the centre of the channel and concentrate them within the maximum fluid sheath creating a quasi “plug flow” similar in profile to the DC capillary electroosmosis.

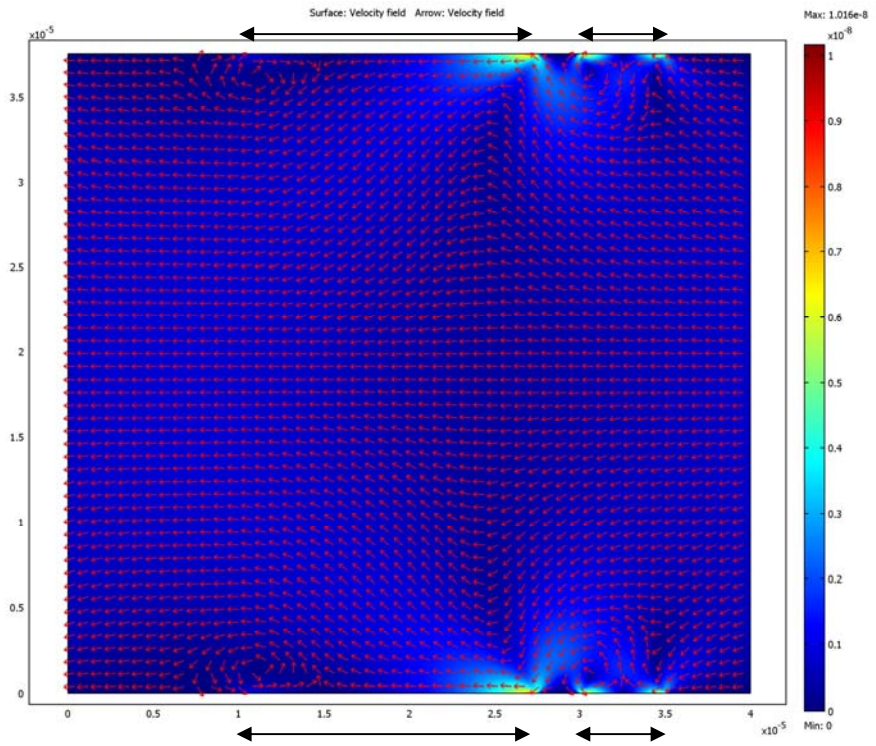

Figure 5-4 : Top and bottom electrode 2 Vpp 100 Hz 1e-4 S.m. Colours show velocity magnitude (scale on right-hand side) and arrows indicate flow direction. Electrode positions marked by black arrows.

As mentioned earlier, the aim of this exercise is too simulate the fluid flow over the electrodes in the case of electrodes on both side of the channel. Observing Figure 5-4, it can be seen that the fluid flow follows the theory described in Chapter 2, which forecasts the fluid flow direction from the narrow to the wide electrode.

These three simulations first proved the approximation in Chapter 2 that we can model by separating the Navier and Stokes fluidic problem and the Laplace problem. Nevertheless, while the simulation gives a good account of the fluid flow it is not performing as expected. The problem resides with the edges of the electrodes where the fluid speed is calculated according to the number of elements from the meshing. The potential gradient is high at the edges of the electrode which results in higher error locally (Figure 5-5). Also, the fluid is actively moving into a narrow sheath that is of the order of the Debye length. In order to simulate this it would require a higher computation system and also the approximations in Chapter 3 are not valid in this case. This simulation has been attempted by [46]; although the results are better, still several questions remain, especially with the influence of the material and its electrochemistry as we will see later in Chapter 6.

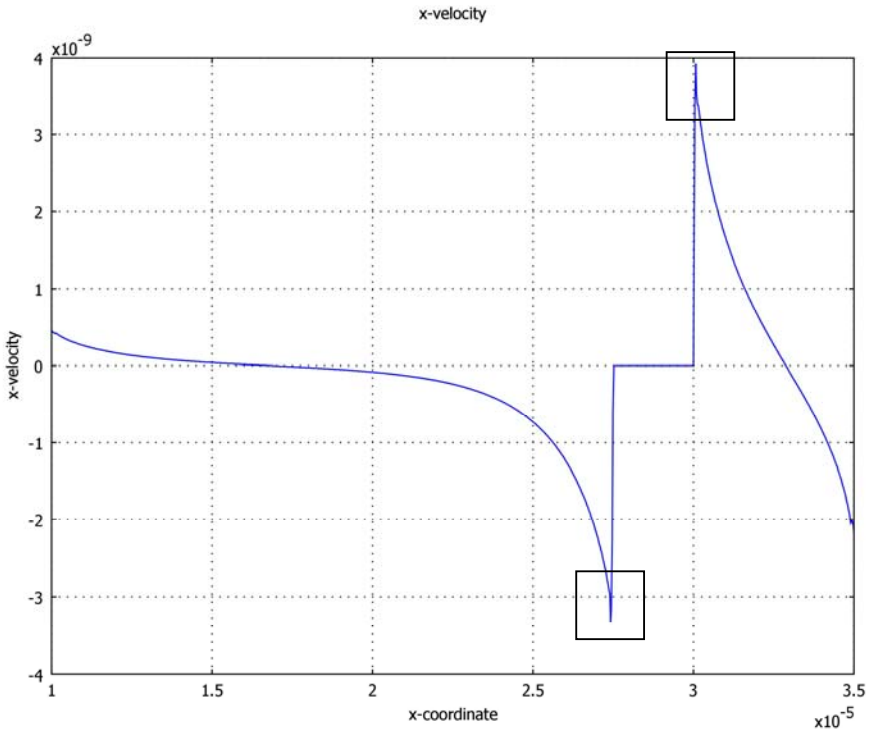

Figure 5-5: Fluid velocity on the surface of the electrodes of Figure 5-3.

From this we can build up channels with an active part for sorting and trapping the cells and use the ACEO pump on chip. Unfortunately, (as mentioned in Chapter 3) ACEO pump are viscous-drag driven therefore they do not generate strong enough backpressure as a normal peristaltic pump will do. We need to find a geometry to create a fluid flow in a channel.

5.4. Fluidic simulation to compensate lack of backpressure from ACEO pumping

The early experiment on ACEO to pump fluid was mainly to observe the fluid flow and characterise it. From the theoretical prediction by Ajdari, Ramos, Castellanos [16, 35, 42, 43, 45, 58, 59, 62-68] to the experimentalisation by Studer, Brown, Ramos, Garcia, Green and Morgan [41, 44, 49, 57], no device was fabricated as a demonstrator lab on chip. The ACEO pump is adapted to our design since we want to use electric field to trap particles. The circular pump built by Studer [47] to observe the fluid flow gave rise to the idea to have two pumps that will move the fluid in a common centre channel (Figure 5-6).

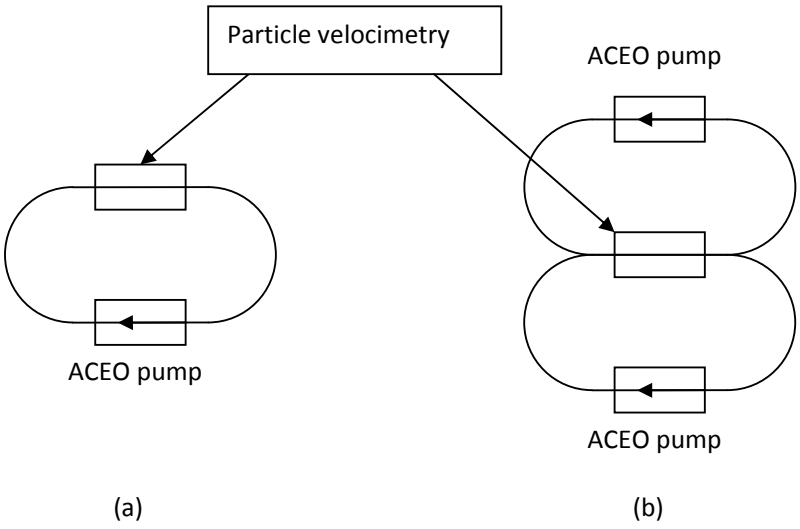

Figure 5-6 : **Circular system to compensate lack of back pressure.**

Several systems were investigated where the geometry and the place of injection change. Figure 5-7 displays chips after fabrication (blue colour is a plastic protection layer)

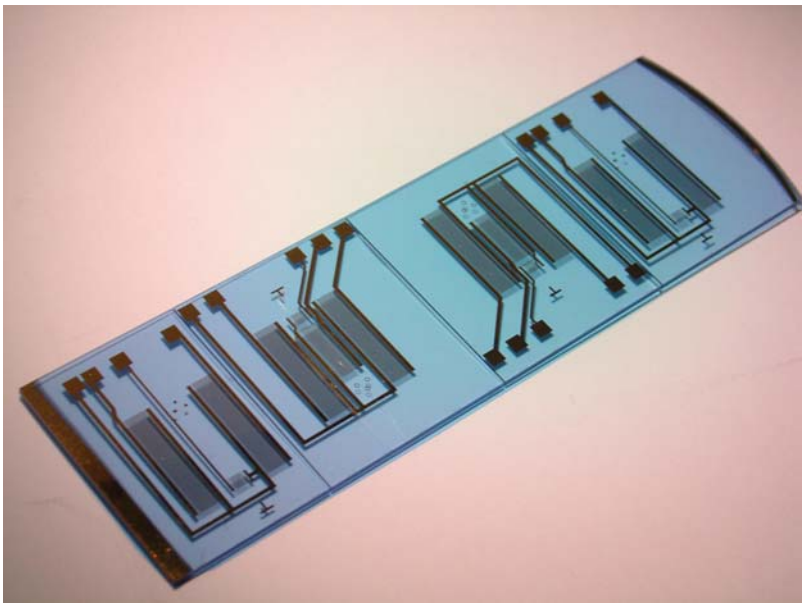

Figure 5-7 : Double ACEO pump with active DEP trap at the centre.

Figure 5-8 displays some of the masks used to create channels on top of the electrodes. These channels were fabricated using the techniques in Chapter 4, mainly using dry film resist which was easy to manipulate.

Initially, the system was only one side and the PDMS mould was obtained by soft lithography and replication. Since we wanted to be able to access the DEP trap using an AFM tip the idea was to obtain a lid that we can remove to obtain access to the cells trapped on the electrode. Two techniques were used: the first was to immerse the channel replica and the the chip into a KOH Eth 90%/DI H20 10%, which has the effect to activate silanol groups that bond strongly between the glass and PDMS (hydrogen bonds) but is reversible. The second technique [47] is to spin on the mould a low curing proportion PDMS layer (1/20) then lay a 1/5 cured layer on top, partially curing the first layer so that it remains sticky but cant flow. The first technique is easy to use but does not bond well over the electrode (weak bond between the PDMS and metals) which eventually leads to a leak at the priming stage. Also KOH degrades the electrode after repeated use. In the second technique, the uncured layer technique gives a better seal but is difficult to use and eventually degrades the substrate.

This method was not adapted and we abandoned the idea of accessing the cell from the top side. We developed the mask shown in Figure 5-8 to exploit the circular pumping scheme and the aim was to isolate the cell using fluid flow fractionation.

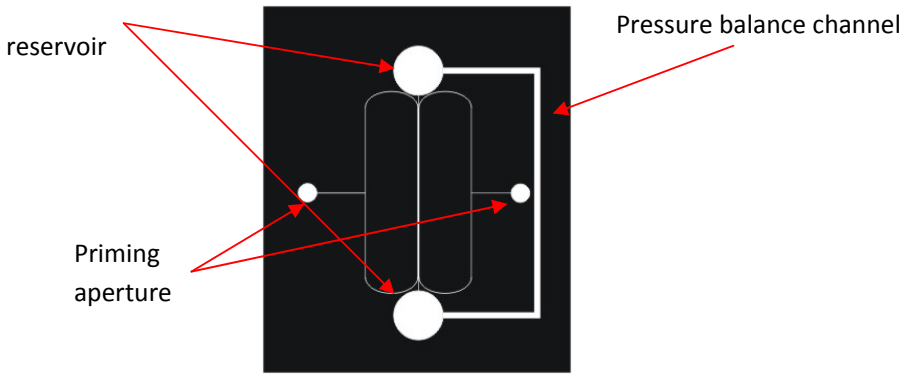

Figure 5-8 : Channel schematic and reservoir.

We simulated the fluid flow in the channel to observe the fluid pinching by viscous dragging in a similar manner than for dynamic focusing (Figure 5-9 and Figure

5-10). For the purpose of the simulation we considered the pumps as flow generators by assigning the boundary conditions $u = u_0$ as shown in Figure 5-9. Figure 5-10 shows that the inflow and outflow ports drag the liquid by viscous effect and generate a flow in the central channel, as desired.

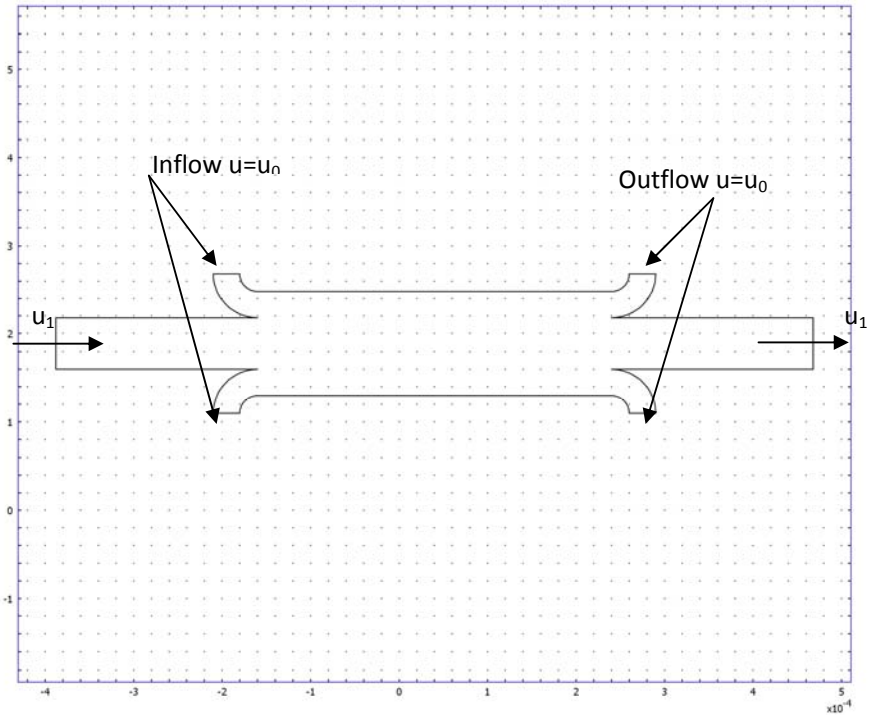

Figure 5-9 : Schematic of the central channel and the fluid flow condition.

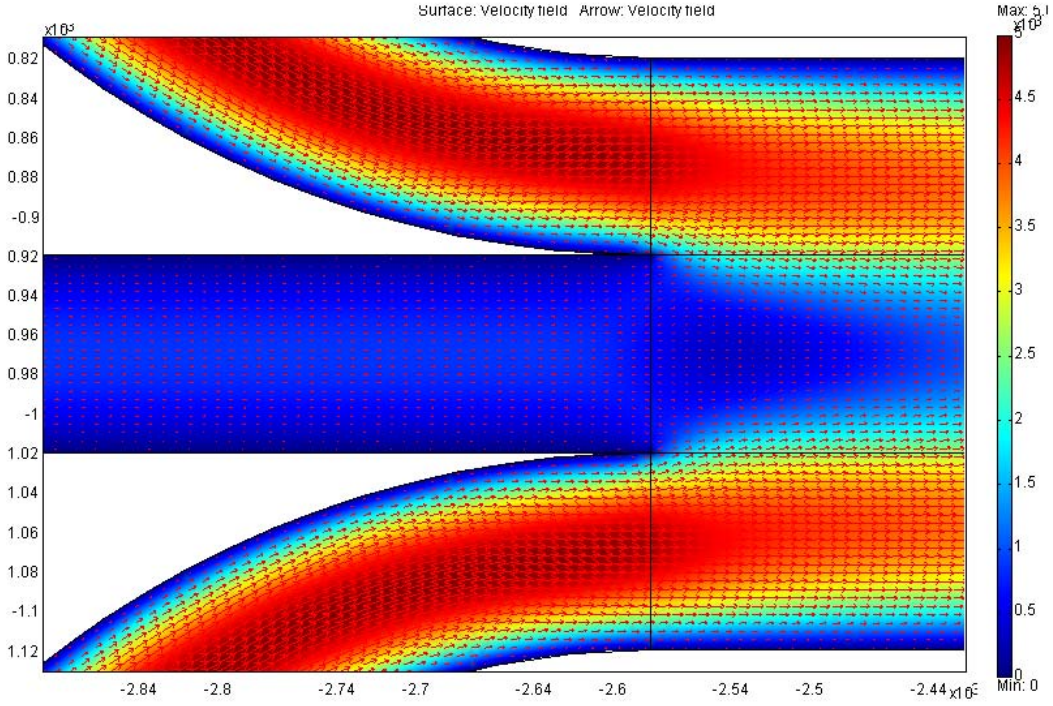

Figure 5-10 : Fluid pinching simulation of triple channel flow.

We therefore obtained the fluid flow by simulation which allowed us to create a viscous pumping device. These preliminary simulations allowed us to simulate diverse channel geometries and forecast the best fluid flow condition; the side channels deliver a stronger and smoother fluid flow if the channels are curved like Figure 5-9. This also creates a larger parabolic velocity profile which limits the pollution by diffusion of species from the central fluid flow to both sides.

5.5. DEP trapping

Since the design of the trapping system and DEP was largely inspired by [69] we will not expand on the trapping only to present the device and few properties. The trapping section is made of two independent sets of coplanar electrodes (Figure 5-11).

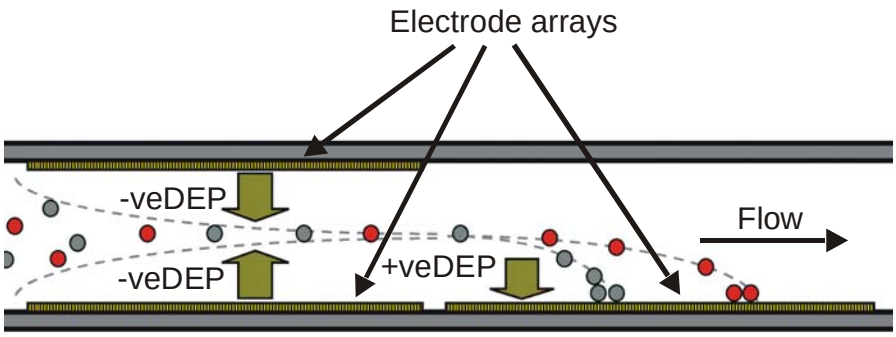

Figure 5-11 : **Particle Focusing electrodes and Particle trap[69]**

Both series of electrode are made of a repeat of electrodes (Figure 5-12). The focus electrodes are separated by 40 microns. Theoretically only a few electrodes are necessary to concentrate particles at the centre of the channel, nevertheless 20 to 40 pairs were fabricated. A simple rule of thumb indicates the extent of the DEP force being the gap distance so in our case 40 micron. Since the channel thickness is between 60-80 microns we obtained a good repulsion. The trap is based on the same principle but is longer.

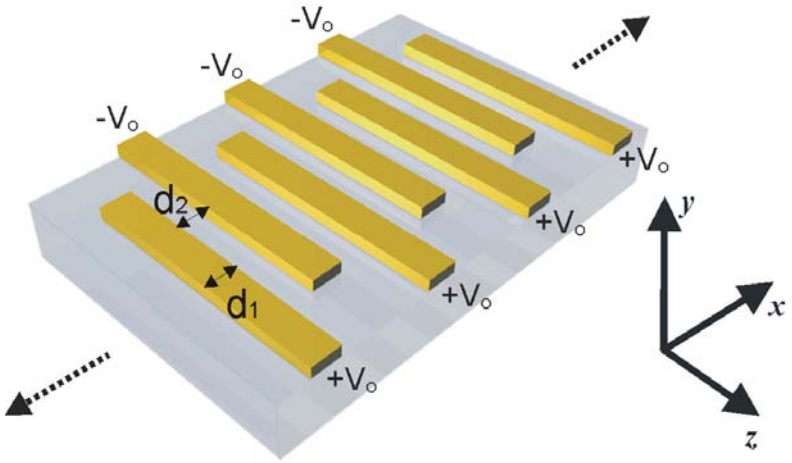

Figure 5-12 : Pairs of electrodes for DEP trap

We mentioned in Chapter 2 that particles with a more complex structure such as cells have a response in frequency where the DEP force can be either negative or

positive. The turn frequency is know as the crossover frequency [17, 70]. Particles can undergo a negative and the positive DEP force depending of the frequency used. We will note that beads in low electrolyte media due to their homogeneity have a negative DEP force all over the frequency band considered [71] (beads under 1 micron have positive DEP for hundreds of Hz). Cells nevertheless behave differently and have a region that will present a positive DEP. In our case PBCs have all different cross over frequency so we can separate blood cells simply. Figure 5-13 shows a simulation that predicts where a 5 micron particle will land if attracted for a fluid flow of 60 micron/s.

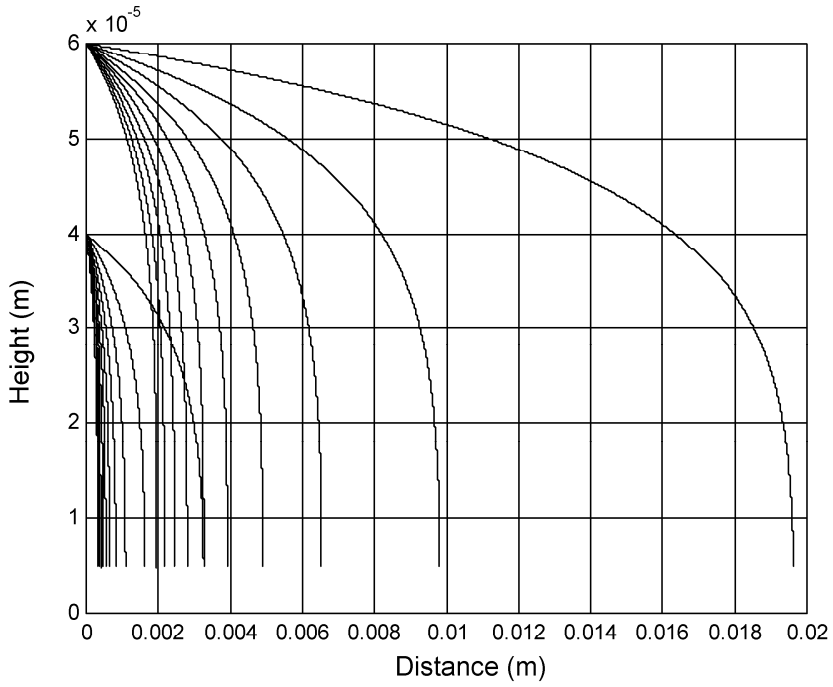

Figure 5-13 : Variation of the distance along the separation electrode array versus polarisability. Re[f_{CM}] varying between 0.1 and 1 and for two strarting positions 40µm and 60µm[69].

5.6. Conclusion

We have seen here the simulations that prove the feasibility of the project, however several hurdles are still to be overcome. The models are very simplistic and become extremely complex and the subject of a study itself if to be developed further. Based on this preliminary simulation we are now going to study experimentaly in detail the fluid flow of the ACEO micropump.

Chapter VI

6. AC electroosmosis devices

The previous chapters introduced the concept of lab-on-chip and its advantages. It also introduced the effects of electric fields on liquids and the creation of the electrical double layer which is necessary to activate fluid movement. We discussed also the pondemorotive force created by electric field on dielectrics. Thanks to the microfabrication technique we are able to shape electrode to take advantage of theoretical effect mentioned previously. These allow the channels for microfluid flow to be created as well. Simulation helped us to predict the potential fluid flow and therefore validate a model. We need to take fluid measurements in small channels to test this theory, but fluid flow measurements are difficult at the sizes involved. We also need to investigate and characterise the fluid flow depending on the voltage applied and the material used. Also we are investigating the capability of isolating cells and the surface of electrode by DEP forces.

6.1. Fluid flow measurement by particle velocimetry

6.1.1. System issues

For external connection use we first fabricated channels so that we can connect to the fluid reservoir using gripper fittings (Omnifit flangeless connection to tube system) to PTFE. The glass is drilled either by using a diamond mesh or sand blaster. The gripper fitting is then glued on the glass using 3M UV glue. The tube is then connected to the syringe pump (Figure 6-1).

In order to measure the fluid velocity within the channel we need to inject particles (fluorescent beads) inside the fluid that we can track using a microscope and a CCD camera. To calibrate the method we plugged a syringe pump to the gripper fitting that is used to access the reservoir for injecting fluid. Since we know the channel size and the syringe pump dispensing the flux, we can calculate the fluid velocity in the channel assuming a Poiseuille flow. The channel is fabricated using 4 mutli-layers of Ordyl150 that gives an overall thickness of 200 μm the width of the channel is 1 cm. The

micro syringe has a flow rate from 0.1 μL/h to 300 μL/h, and the calibration data is shown in Table 6-1.

Table 6-1 : Fluid flow calibration

Syringe pump fluid (μL/h)	0.5	50	80
Observed flow rate	0.44	42	75

We observed that for fluid speed under 20 micron/s and fluid speed over 700 micron/s the beads do not seem to travel as the same speed as calculated. We found a factor 0.9 between the bead fluid within this range. This correction factor changes with the size of the channel and the material used as the interaction with surface dominates in a laminar flow and it is difficult to know the exactly channel size due to shrinkage when the system is bonded together. Therefore we assume that the speed of the beads are the speed of the fluid and all fluid, measurements using particle velocimetry will use this imperfect approximation.

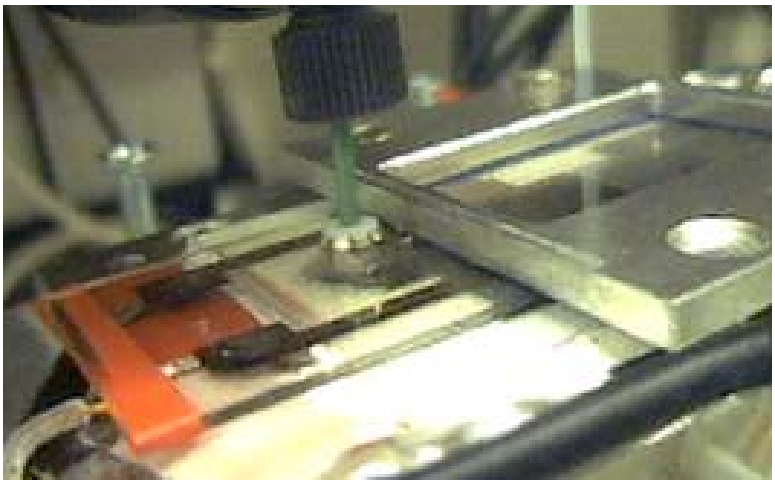

Figure 6-1: Gripper fitting glued on

In order to measure fluid flow we use particle velocimetry. This involves injecting fluorescent microbeads (Microprobe) in the liquid in use. As mentioned in Chapter 3, several methods were investigated to create channels to investigate the fluid flow above the electrode. We chose to use 500 nm beads to measure fluid flow. Smaller bead are less affected by the DEP forces [16] and therefore are good candidates as

tracking particles. We obtain satisfactory concentration for one µL at 1e+21 beads/cm^3 into 100 mL. We still observe trapping of beads at the edge of the electrodes, which can disturb the fluid flow by modifying the field lines at the edge of the electrode. This trapping can be reversed by applying a short pulse of high frequency (>200 kHz). It has for consequence to create a negative DEP force that repels the beads. Between each experiment the system is flushed with new solution and a short sine wave pulse is applied. We then proceed to measure the fluid flow.

6.1.2. Fluid Velocity Measurement

500 nm beads fluorescent at 513 nm were added to the electrolyte in use with concentration of one µL for a 100 mL. The fluid flow was recorded thanks using a acquisition camera taking 25 frames per sec attached to the customised observation microscope. The acquisition system is directly linked to a computer that records in digital format (Figure 6-2). The data files are uncompressed and large.

Figure 6-2 : The microscope with the camera at the centre left is the illumination system and right is the signal generator.

Adobe Premiere software allows us to analyse the films frame by frame. When a film is taken the time of any parameter change is noted (which allow a thorough post examination in Adobe Premiere). A 25 frames echo is then generated which gives a trace of the particle moving (Figure 6-3). A chip with apparent electrodes is recorded prior to the experiment. Since dimensions of the electrodes are known we can estimate

the frame size and by a simple measurement of the screen we can deduce the speed of the particles. The objective is a Nikon x20. The depth of focus is small, and in the order 50 microns (estimated from in/out of focus measurement on featured surface). Each measurement is an average of at least 5 to 10 other traces. The estimated error due to the pixel size and wrong focus is estimated at 5 %.

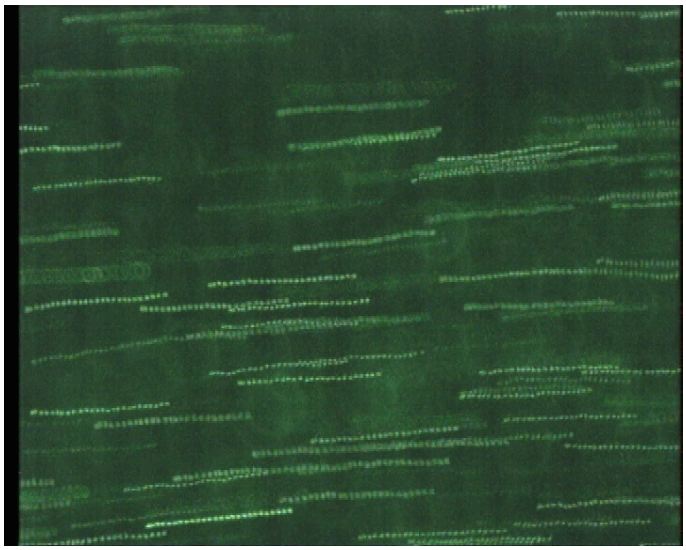

Figure 6-3 : Particle Velocity measurement by superimposing frames

6.1.3. System under test

The pumping system we tested using velocimetry is made of 4 individual ACEO pumps of 800 repeats of electrode pairs of 40 microns wide (2 gaps 13 µm and 5 µm + 2 electrodes width 21 µm and 5 µm). The layout is such that two pumps are facing each other, therefore creating a pump with no recirculation (Figure 6-4) as previously described and presented earlier in ref [57]. We will note that these authors never observed fluid reversal results, due to lower voltage, very resistive material (ITO) and higher electrolyte content in this experiment.

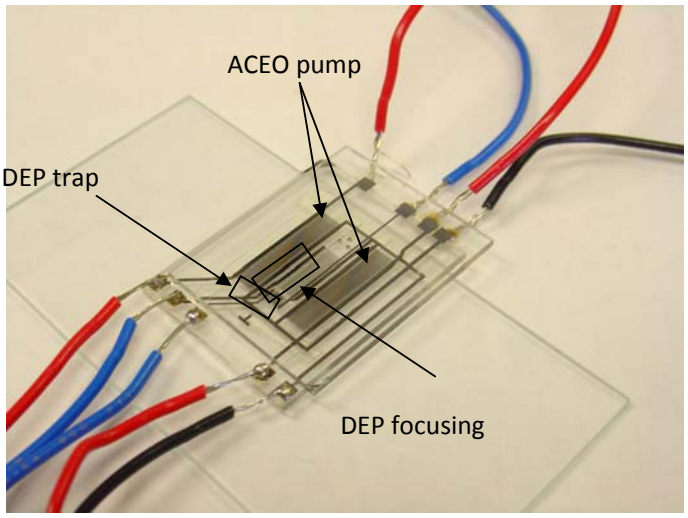

Figure 6-4 : Electrodes top and bottom and DEP trap assembled

6.1.4. Electrode degradation

The first flow measurements showed inconsistent and irreproducible results, and electrode degradation was observed. This effect was investigated using impedance spectroscopy in order to create reliable devices. Impedance spectroscopy, used in electrochemistry [60], is a way of characterising the kinetics of electrochemically activated reactions especially when surface driven like in our case. Some early experiments in Southampton using an alpha impedance analyser (H.P. 4192A impedance analyser) showed a decrease of the impedance value with cycling in frequency which was understood as being a slow destruction of the electrodes (Figure 6-5 and Figure 6-6). These electrodes were made of 20 nm of Ti and 100 nm of Gold. We observed as well that the electrode if used for pumping had irreproducible fluid flow velocity for a given medium conductivity, voltage and frequency of excitation. Later on these electrodes were observed by SEM and showed growth of material in the gap which is believed to be the short circuit observed in impedance spectroscopy (Figure 6-7). It is important to note that despite the AC polarisation electrochemistry will still happen.

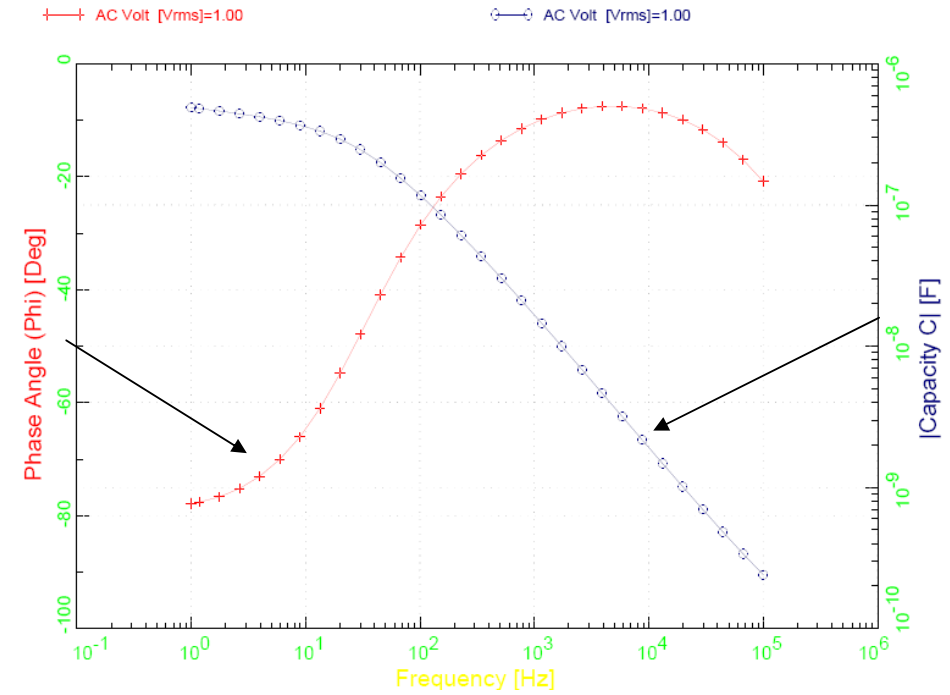

Figure 6-5 : **Impedance spectrometry using an alpha analyser. For gold electrode in 10mS/m at 1Vrms.**

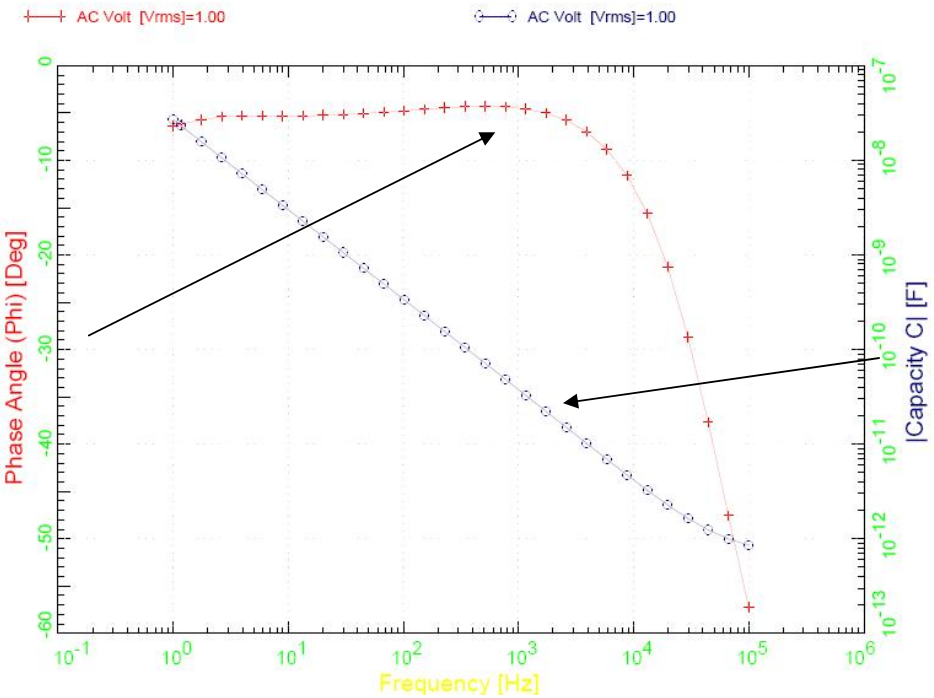

Figure 6-6 : **Impedance spectrometry using an alpha analyser. For gold electrode in 10mS/m at 1Vrms (after ACEO experiments stop to work).**

We observed here partial destruction of the electrode with some pitting and growth between them which explain the decrease of impedance that slowly leads to short circuiting and therefore the vanishing at low frequency of the EDL capacitance as shown in Figure 6-6, from the first test (Figure 6-5). It displays initially a capacitance due to the charging of the double layer and the linear total capacitance at higher frequency. Figure 6-6 shows a resistive system typical of a short circuit.

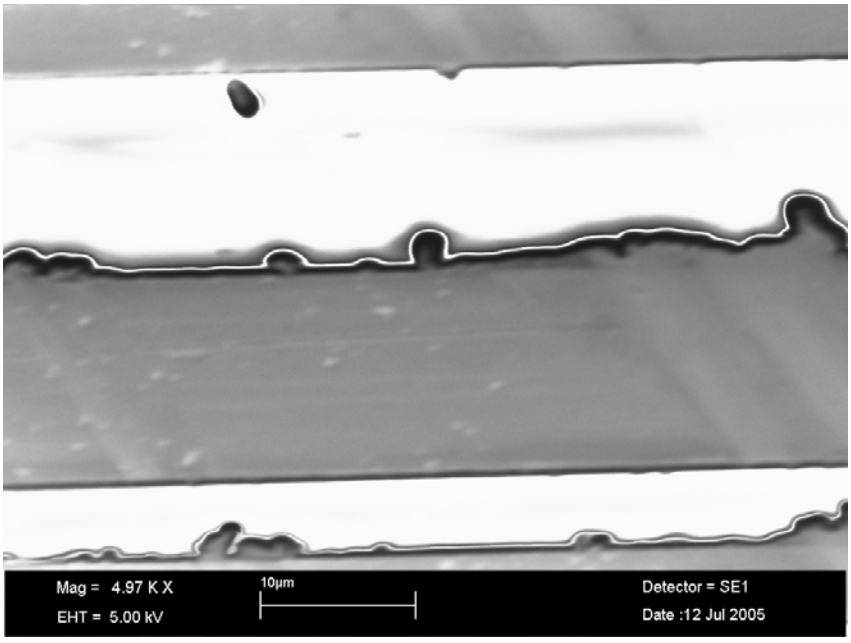

Figure 6-7 : Material formation in between electrodes.

Electrochemical reaction is occurring at the electrodes. On the other hand we also observed (but not recorded) a decreasing trend of velocity as we cycled around the kHz. The system is loaded with a 1mM KCl salt solution (about 10 mS/m depending the temperature). The signal was set and the potential is 3 Vrms. After (on average) a minute we observed a decrease of fluid velocity. It leads eventually no speed at all; as such, the ACEO pumping could not be systematically characterised in this system.

Consequently we decided to use different electrode to characterize the pumping scheme. Electrodes made of Titanium/Gold/Titanium 30nm/100nm/30nm were fabricated. The titanium is well known to create a thin layer of oxide known as a passivation layer; it was thought to protect the gold layer. Cycling the electrode in a low

concentration of KCl was then achieved. The electrodes were observed under the SEM and show a stable surface (Figure 6-8).

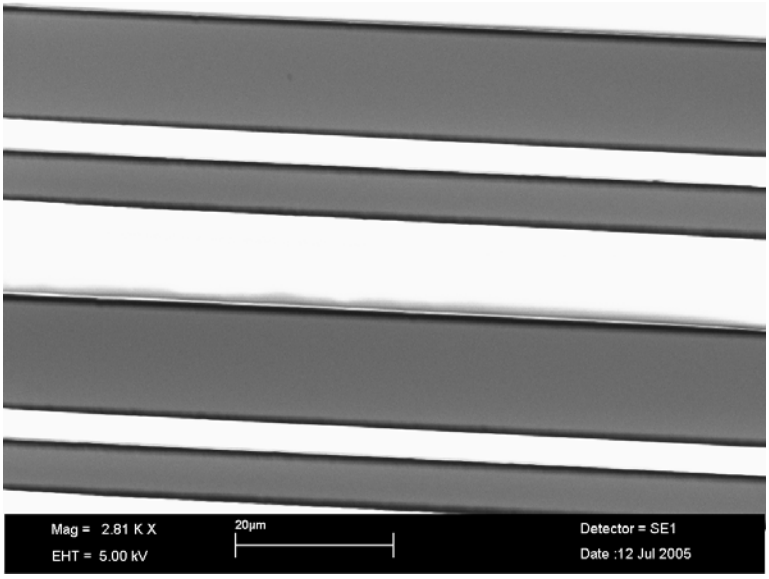

Figure 6-8 : Ti/Au/Ti after cycles (0.25 Vrms to 3 Vrms from 10 Hz at 100kHz) in 1 mM KCl

The result is obvious and no degradation occurs. However it does not mean that other electrochemical reactions do not happen. Titanium, for instance, oxidises easily in the presence of water. Although this layer is thin and fairly passive the voltage is important for any electrochemical reaction.

6.1.5. Fluid flow results

The results of the fluid flow for the Ti/Au/Ti electrodes are shown in Figure 6-9 and Figure 6-10 [50]. Since the arrays of electrodes are present on each side of the channel it is difficult to observe the fluid flow inside the pumping system, as compared with ref [57] that used ITO (transparent and resistive) electrodes. The thicknesses of the electrode of Ti/Au/Ti electrode are too large to be transparent. Therefore we observed the fluid flow in the central channel between the focusing electrode and the trapping array.

The mapping displayed in Figure 6-9 and Figure 6-10 shows clear fluid flow. The flow reversal exist, but at higher voltages and in the kHz region. We observe as well the pumping in reversal being stronger at low ionic content and slightly shifted towards the

lower frequencies. Each measurement was obtained with new liquid introduced in the device prior to polarizing the electrodes. We observe that sometime if the same liquid is used at a certain set of parameters (voltage, frequency) using the same liquid at a different set of parameters would be different than if we were using a new liquid. We conclude that the liquid must be changing to some extent (dissolution of metallic ion into the liquid), or the surface of the electrodes is changing, but refreshing the fluid for each measurement did provide reasonable consistency.

Figure 6-9 and Figure 6-10 display the mapping of the peak to peak voltage applied between electrodes pairs against the $\log_{10}$(frequency). They are the results of the summation of individual frequency mapping in fluid flow (10-12 plots using 20-30 point per plot each point an average speed calculated by measuring 5-10 traces) described in 6.1.2. Figure 6-9 shows low fluid flow (or none) for lower frequency which is consistent with the higher conductivity (Chapter 3). It also shows a zone of peaking fluid flow for higher frequency (10 kHz and 20 V_{PP}) and overall lower absolute fluid flow magnitude. Above the KHz a more linear trend appears that leads to reversal. This reversal effect is clearer in lower conductivity setting as shown in Figure 6-10.

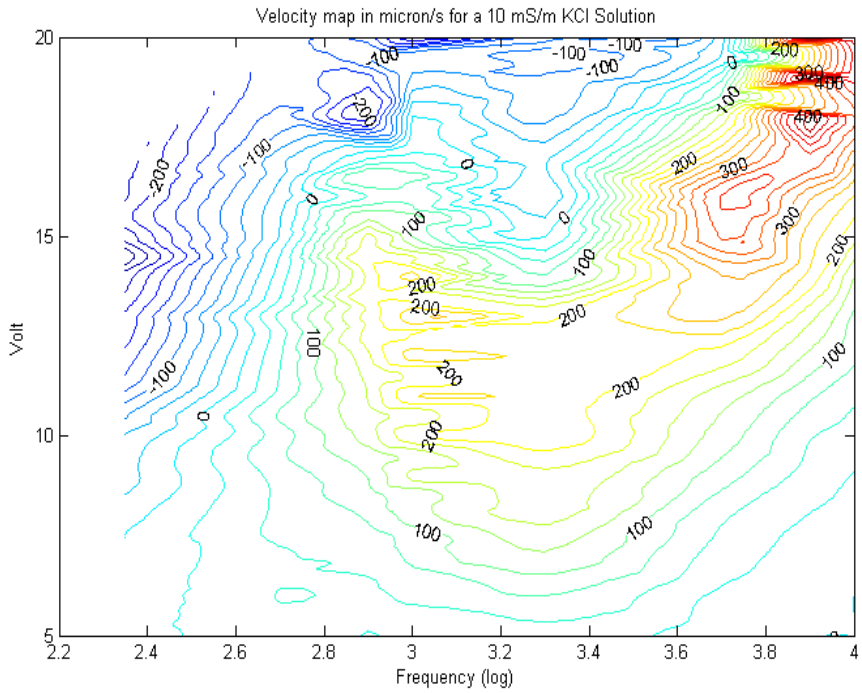

Figure 6-9 : Velocity map for a 10 mS/m KCl Solution taken at the middle of 150 micron channel by estimating the speed of 500 nm fluorescent beads.

We observe also transient behaviour if the electrodes are used for the first time. Although it is difficult to represent in writing, the film of the liquid motion is obvious. The electrodes are bathed into fresh liquid and polarized in this situation at 1 kHz for 1.5 mS/m; at first the fluid travels in the normal direction but after a few seconds the fluid slows down, becomes incoherent and swirls finally stopping and slowly starting to move in the opposite direction.

Figure 6-10 has more defined regions. The higher fluid flow at higher voltage reduces the ability to distinguish features at lower voltage but a similar trend in square voltage is observed under 10 V_{pp}. There is also a distinctive region of high fluid flow reversal that is similar to [47] and [49], also mentioned theoretically in [46]. We also notice that the absolute value of the fluid flow represents a function with a fluid flow maximum in kHz region which was anticipated on the early analysis of Ajdari, Green, and Ramos [41, 43, 59, 62]. Nevertheless we have seen the importance of the material and we can anticipate that the electrochemistry has a part to play in the overall fluid flow.

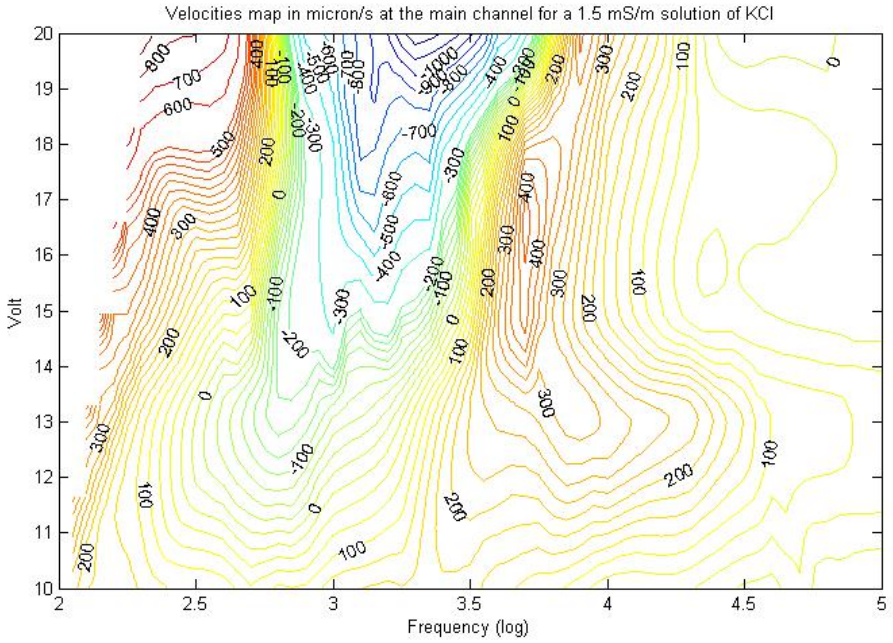

Figure 6-10 : Velocity map for a 1.5 mS/m KCl Solution taken at the middle of 150 micron channel by estimating the speed of 500 nm fluorescent beads.

Fluid flow was tested for a conductivity of KCl of 100 mS/m as well (results not shown); it displayed fluid velocity of less than 100 micron/s. Most of the electrodes are damaged due to the reduction water which has catastrophic consequence on microfabricated device. As previously forecast in Chapter 2, such high salt concentration results in low ACEO fluid movement and destruction of the electrodes. The maximum voltage reach was 10 V that resulted systematically in destroying the electrodes.

6.2. Electrochemistry

As we discuss earlier on, titanium can create an oxidation layer at its surface that passivates the Ti metal. We note on this Pourbaix diagram Figure 6-11 that at low pH there exists a domain where Ti^{n+} is soluble. We therefore have a situation where we can have dissolution of the titanium into the liquid. The titanium ions are larger than potassium and their degree of oxidation is higher which could result in an increase of the movement of fluid over one period of the AC signal.

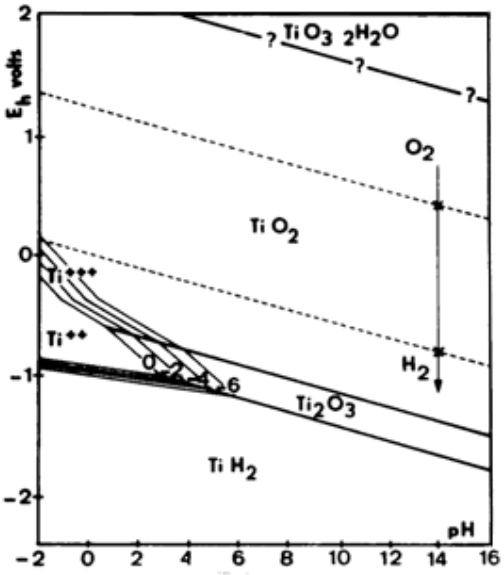

Figure 6-11 : Pourbaix diagram of Titanium metalic in water

The oxidation of Ti in titanium dioxide is the following

$$Ti+2H_2O->TiO_2+4H^++4e^- \quad (7)$$

Equation (7) is a proton pump which means that for each mole of Ti oxidized four moles of protons are released in the solution at the surface in the diffuse layer. This has two consequences: first and foremost it lowers the pH locally and in the bulk so that the Ti can enter a regime where it exists in solution; secondly, the protons can participate in the fluid flow. It is know as well [72] that other species coexist at lower pH like Ti(OH) and with Chloride $TiCl_4$. Therefore the electrochemistry is far from simple. Furthermore in low ionic content the pitting potential of TiO_2 is about 12-14 V which corresponds as well to the value where we begin to obtain fluid flow reversal [73].

6.2.1. Cyclic Voltametry

In order to understand further the Ti dissolution processes we investigated the electrochemistry of such a system. From this we wanted to observe if the Titanium dioxide electrochemistry changed if new fluid was inserted in a thin film condition (low volume). Although cyclic voltametry using a potentiostat is in DC, it gives valuable information of potential electrochemical reactions that could happen over the electrode during ACEO. We designed and micro-fabricated special electrodes to quantify this effect. Three materials were used : Ti, Au, Pt. We use platinum because is know to be neutral, although its oxide can be very thick and is a proton pump too. Contrary to

platinum, gold forms an oxide but is a monolayer thick. It is reduce almost completely at each cycle. The gold oxide reduction in the EDL has a destructive effect like observed in the presence of chloride (dissolution transport and redeposition).

Platinum is of interest because after discussion with P. Garcia of Sevilla University, [49] he observed in traveling wave and asymmetric array reversal changes in liquid flow and transient effect but in platinum. Therefore we hope to correlate the electrochemistry in titanium and in platinum.

We refer the reader to the analysis by [46] for charge injection. In this analysis Olesen observed theoretically that for the simple ox/red $M \rightarrow M^{+}+e^{-}$ reversal can occur. However the equation (41) involves something rather more complex and Olesen theory [46] does not account for the change of pH too.

For the electrochemistry experiments the main electrode (Figure 6-12) is 20*20 mm; the central part is deposited with Ti/Ag. The silver is then oxidized in a chloride solution and forms silver chloride to use as a reference. The rest of the electrode separated by 50 a micron gap is made of the material to be investigated (Ti,Pt,Au). In the case of titanium we are interested in the equivalent of our ACEO electrode so the layer is Ti/Au/Ti. An opposite layer of the same material is then assembled with a spacer of 150 micron which of similar thickness for our electrodes array-demonstrator. We also fabricate thin layer for bulk electrochemistry in high ionic content (> 0.1 M KCl) which is similar to normal electrochemical operation. We want to observe if some diffusion processes occurs at the electrode since the liquid in not degassed when used in ACEO (O_2 can play a role in the oxidation of the surfaces).

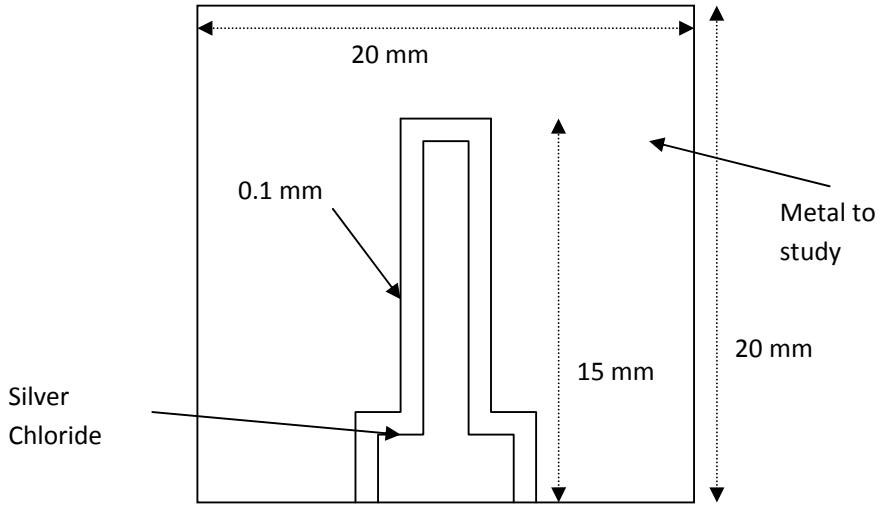

Figure 6-12 : Electrode principle for including Silver chloride electrode reference.

6.2.2. Titanium Irreversible passivation, oxidation and reduction.

Experiments were performed with a cycling rate of 100 mV/s with a silver chloride reference electrode. The KCl solution (0.1 mol/L) was prepared on the day of the experiment and was not degassed. The liquid was pipetted into the gap between the electrodes and entered the reaction chamber by capillary forces. With such concentration we should expect a ohmic behaviour but instead we observe an obvious oxidation that happen at the electrode surface (Figure 6-13). The Pourbaix diagram (Figure 6-11) shows the domain of existence of titanium dioxide. Since the overpotential (potential above the Nernst potential for a given reaction) accelerates the kinetics we can expect as we are cycling fast an oxidation drifted toward higher potential. We cycled several times and then after curve “current 10” we flushed fluid with new solution from the reservoir. Figure 6-14 shows a renewal of oxidation as the current is higher than previously obtained with curve 10 which indicates an increased oxidation and a change between the two solutions before and after 10 cycles.

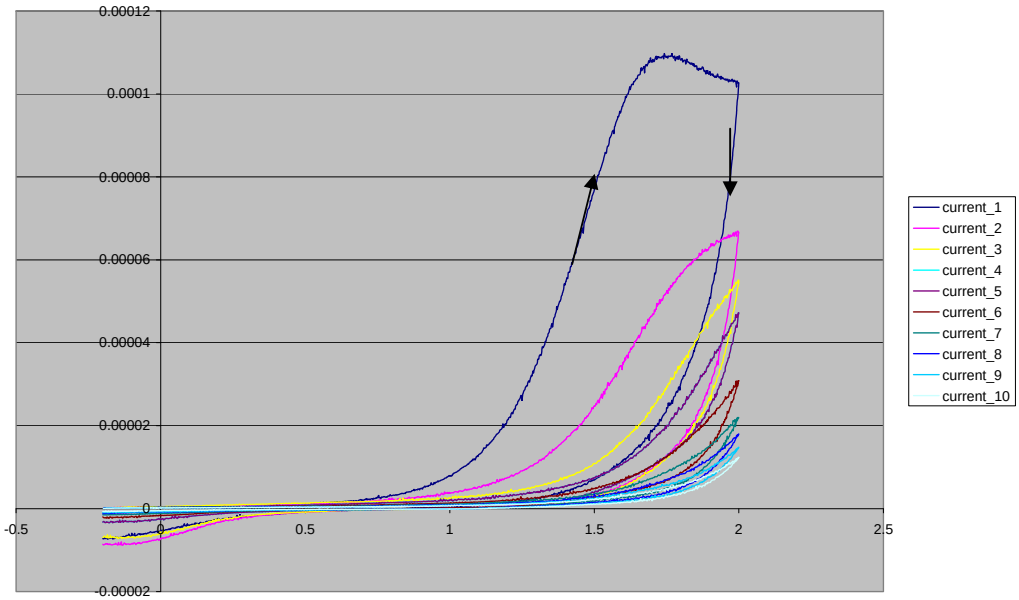

Figure 6-13 : Oxidation of Titanium in KCL 1e-3 mol/L (Scale A against V)

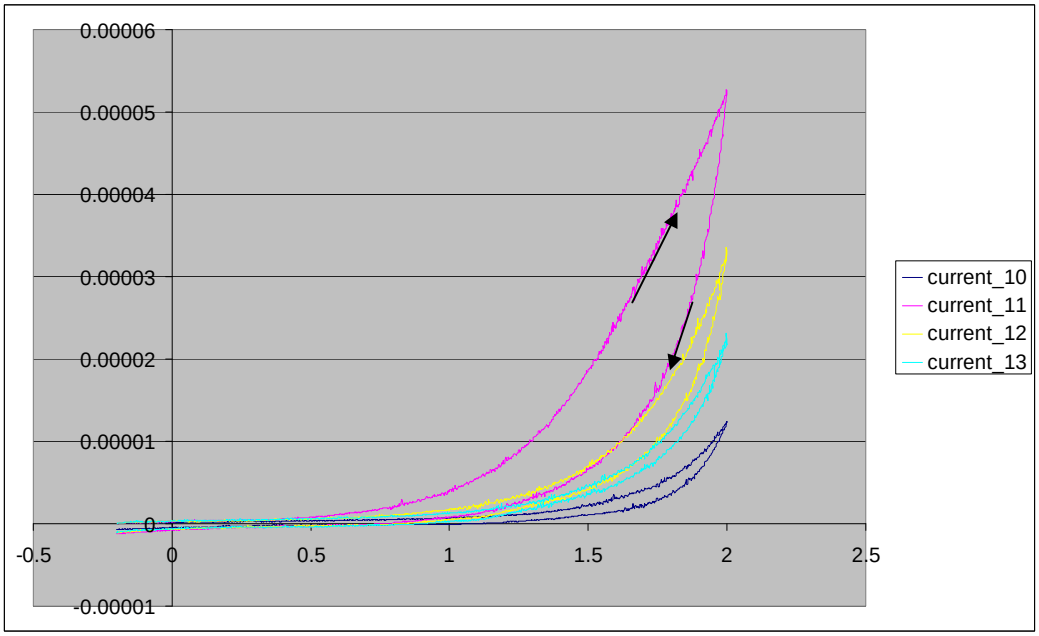

Figure 6-14 : Oxidation after flushing of Titanium in KCL 1e-3 mol/L 100 mV/s (Scale A against V).

The oxidation in bulk (large amount of liquid compared to the surface 0.1 mol/L) does not display such a behaviour with or without degasing (Figure 6-15). After an inititial oxidation the curves settle down to a simple ohmic behaviour.

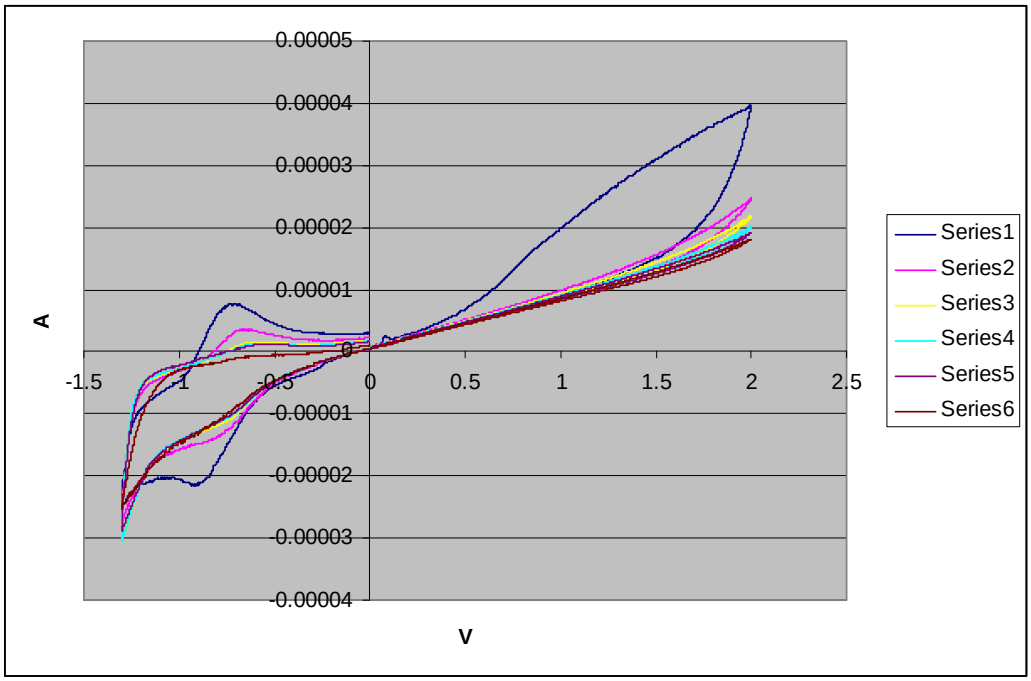

Figure 6-15 :Oxidation in bulk of Titanium 0.1 M 100mV/s

For the oxidation in bulk we observe the reduction of species as we cycle deeper to negative value (but not too low to avoid the hydrolysis of water into oxygen that damages irreversibly the electrode)

The hydrolysis of water in oxygen is generally responsible for the destruction of electrodes. We observe this destruction in the ACEO pump under 1 kHz at 20 Vpp (zone of high reversal flow). Therefore we can conclude that the other oxidation and reduction reactions are happening too. Since we drive the system at high frequency the different kinetics for these electrochemical reaction are harder to predict and impedance spectroscopy would be a better choice of investigation. However, whilst this was available during the initial studies at the University of Southampton, it was not available during later work when the author was back at the University of Canterbury.

6.2.3. Gold electrochemistry

We observe two peaks convoluted around 1 and 1.2 V then reduced (0.5 and 0.3 V); this is attributed to gold oxide formation. It is of a monolayer and its oxide is unstable which leads to gold in solution in its ion form Au^{3+}. Chloride and its pitting effect is expected to be present at higher potential. Figure 6-17 of Ti/Au/Ti displays a peak similar, so some gold is still unprotected by the Ti layer.

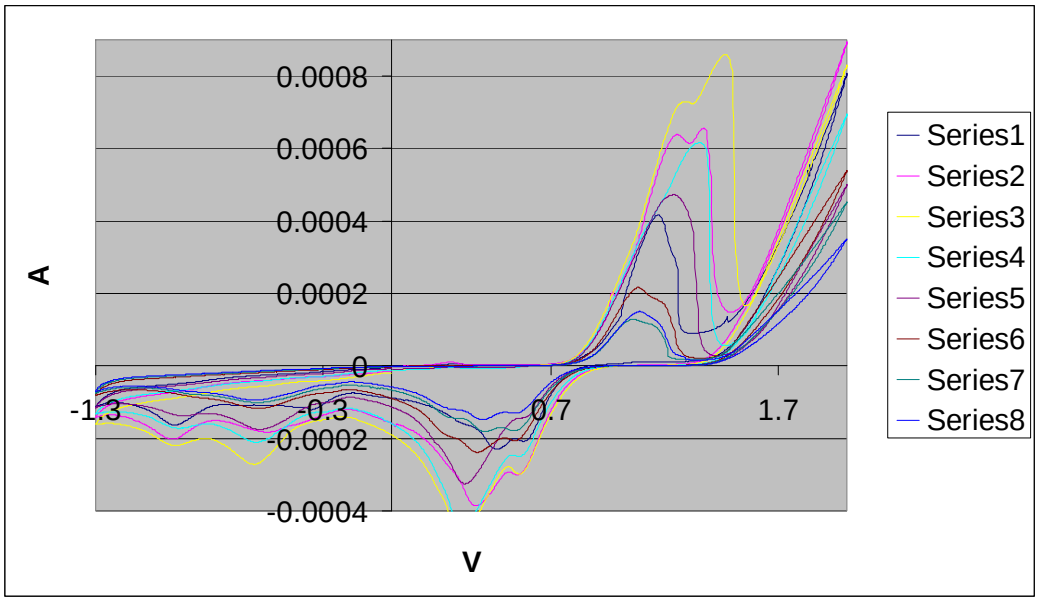

Figure 6-16: **The electrochemical cycle for Au. It shows a very intense peak at 1.0-1.2 V believed to be the gold oxide event Au_2O_3.**

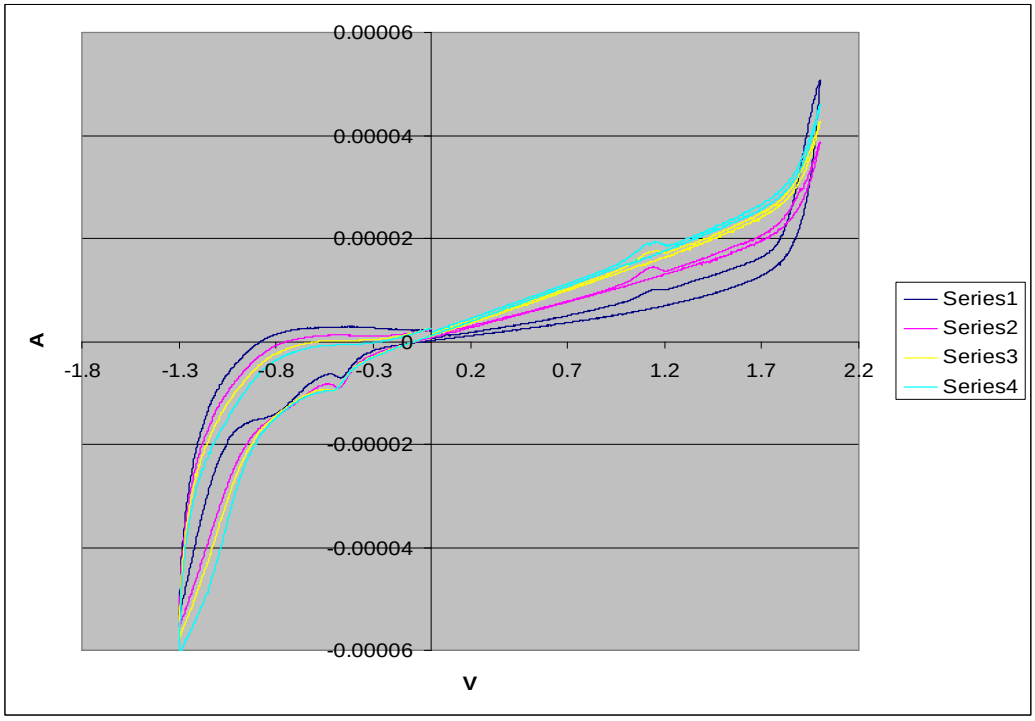

Figure 6-17 : Bulk cyclic voltametric for Ti/Au/Ti in KCL 0.1 M 100mV/s

6.2.4. Platinum electrochemistry

The platinum cyclic voltametry is somewhat different (Figure 6-18) but platinum is suffering as well of chloride pitting at higher voltages. The oxidation of platinum is also a proton pump and will lower the pH nevertheless. But the platinum oxide is thick and porous and keeps on growing (note the increase of oxidation and reduction after 5 cycles). We note as well the adsorption of hydrogen at lower potential (-0.3 V to -0.8 V).

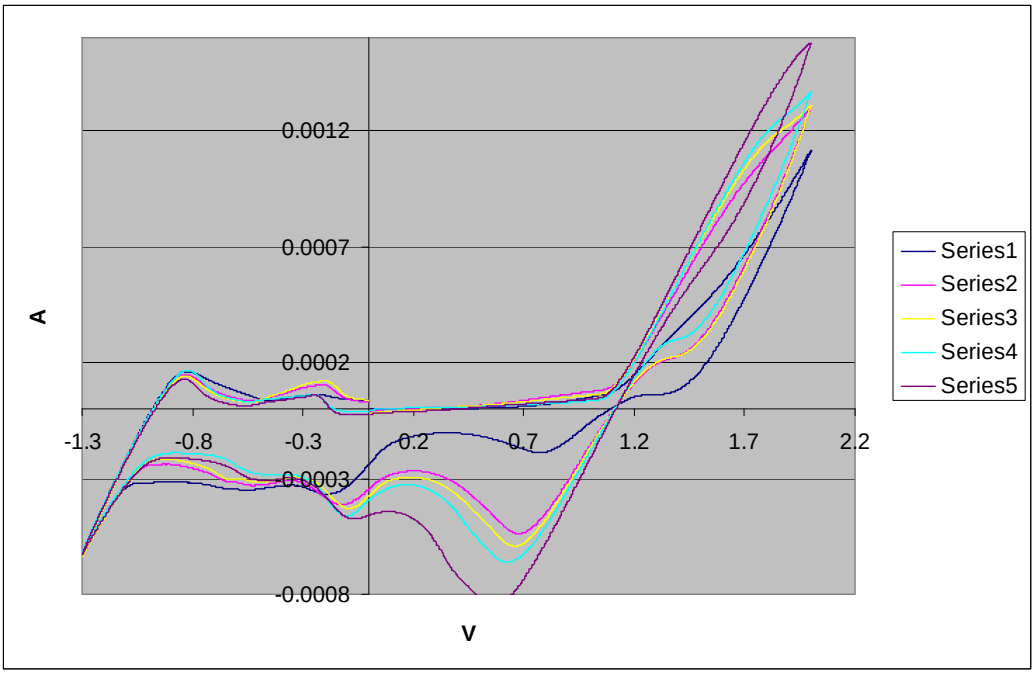

Figure 6-18 : Bulk cyclic voltametric for Pt in KCL 0.1 M 100mV/s

The cyclic voltametry for Pt in thin liquid film (1e-3 mol/L, Figure 6-19) does not show similar trend as in the bulk; the oxidation at 2V seems to reduce with the number of cycles contrary of what is observed in bulk which lead us to believe that a diffusion and depletion process ($PtCl_4$ maybe) is taking place.

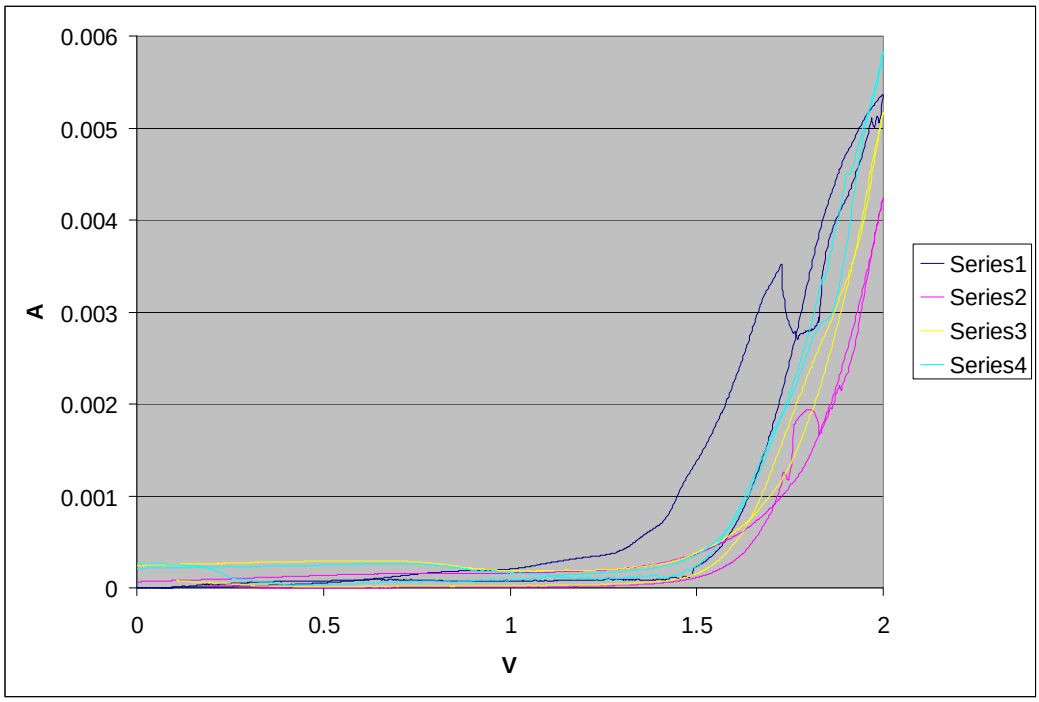

Figure 6-19 : Bulk cyclic voltametric for Pt in KCL 1e-3 in thin film M 100mV/s

6.2.5. Electrochemistry summary

We observed different cyclic voltametry between electrodes confining a small amount of liquid and a bulk situation where the voltaic cell contains a very large volume and therefore no depletion exists.

We found that removing fluid and renewing it in the thin film changed the voltametric cycle and increased the oxidation. Something is disappearing or being transformed into another chemical product less reactive. A XPS study by [74] showed the inclusion of phosphate when anodising titanium in PBS (Phosphate Buffer Saline). This would lead us to believe that a similar effect can happen with chloride and therefore contributing to lowering the chloride concentration. Also, the oxygen dissolved in the liquid might increase the oxidation process but it is a diffusion-driven process so slow maybe too slow for our frequency regime.

It is clear after looking at the gold electrochemistry that a large oxidation exists and therefore is not a good candidate. Nevertheless it might be that although the KCl as a medium is not appropriate. Chloride is very active and contributes to pitting. The original idea was to use KCl due to similar weight, size and electrophoretic mobility which was an asset for comparing with theoretical endeavour. Another ion should be

investigated like chloride perchlorate. But it is certain that the electrochemistry cannot be ignored and one would want to use an AC pump should investigate the electrolyte in conjunction with the material used for fabricating the electrode. We advance here the potentiality for changes in titanium during the cycles. We also observed a depletion of species which can relate to the Olesen argument on space charges [46] and the potential for an increase pumping ability at higher potential. Also, the growth of a passive oxide decreases the capacitance which is in parallel with the EDL capacitance; this is not happening immediately so can be responsible for transient behaviour in conjunction with the charge injection and lowering of the pH.

Monitoring the pH in situ in such a low volume would be an advantage. We calculate that if one monolayer of 10 mm^2 is transformed to TiO_2 then the pH will lower to 4. A pH buffer would be necessary to avoid this. Simply anodising the Ti prior to any experiment should help but still TiO_2 can be reduce and react with other species.

Several articles refer also to the pitting of TiO_2 by chloride in low concentration. This happens during the growth of Ti oxide by anodisation [75]. If the oxide exceeds a potential of 12-14 Volt film growth ceases and intense corrosion or pitting occurs at localised areas. This is troubling enough to observe that pumping reversal occurs at this voltage (Vpp) and above for certain frequencies.

The use of ACEO for biological study of cells is therefore limited by these effects but it could be used for different purposes and recently several group have investigated these [76, 77]; also, recently [64] used a symmetric array but deposited a insulator on one side of the electrode masking the creation of a vortex. The fluid looked like on a conveyor belt. ACEO could be use as well to transport fluid for cooling IC on chip as it will integrate an electronic and fluidic system together using the same micro fabrication technic.

6.3. DEP trapping and focusing electrodes

Although the DEP trapping system was embedded with the chip alongside the ACEO pumps it was used as a demonstrator since several other groups have obtain dielectrophoretic trapping. Most of the work was obtained on studying the ACEO effect nevertheless some trapping was obtained. The experiment used a cell suspension of PBMCs that showed strong trapping (Figure 6-20) and a banding effect (Figure 6-20 and

Figure 6-21). Also using fluorescence showed a better trapping for the THP-1 and PBMCs (Figure 6-21, these photos were obtained by Holmes [69]).

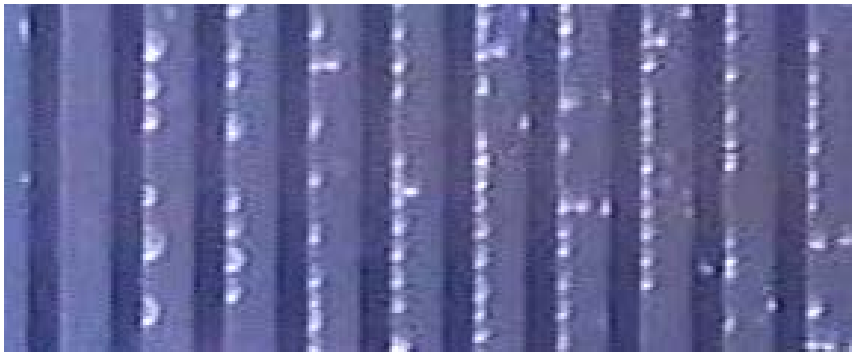

Figure 6-20 : PBMCs (Monocytes and then Lymphocyte) fractionation by size

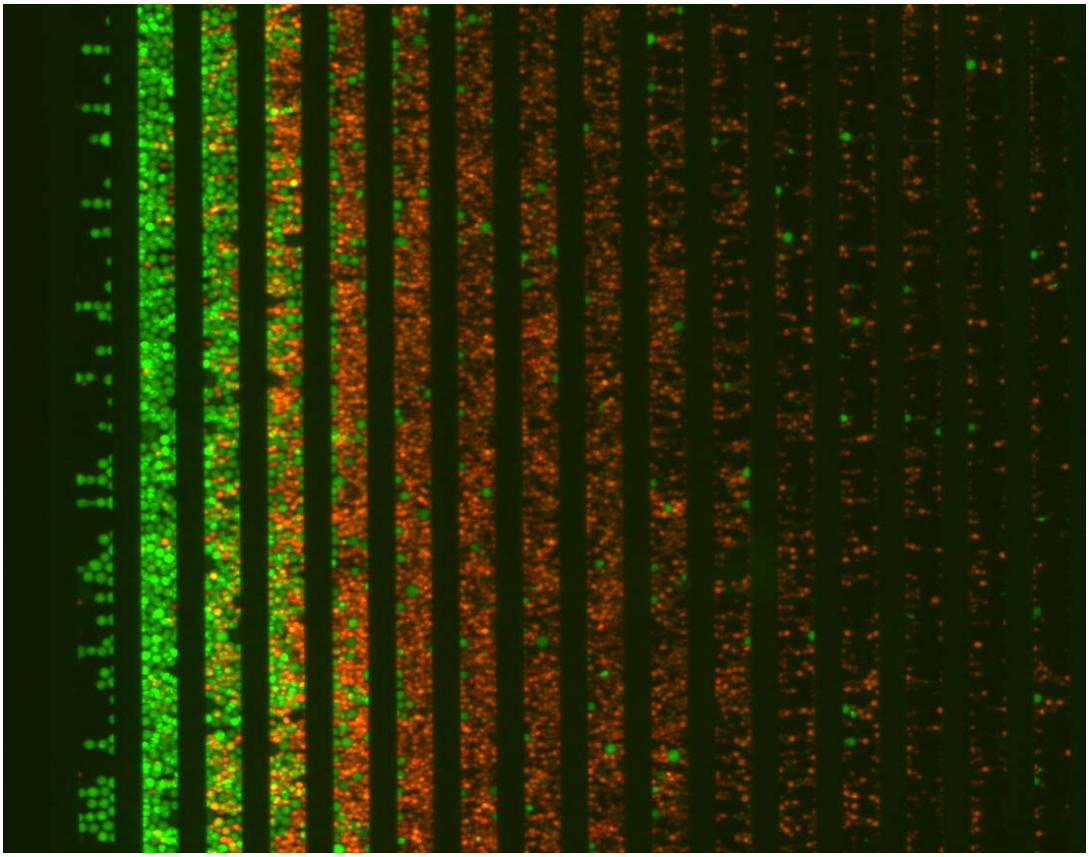

Figure 6-21 : Fluorescence image of THP-1 cells (green) and PBMCs (red) banding on a 40μm separation electrode array. Flow rate of 0.5mlhr^{-1}, applied peak voltage of 1.5V at 150kHz.[69]

6.4. Conclusion

We proved the existence of fluid flow reversal in an ACEO pump at a range of frequencies for a given concentration of electrolyte. We showed that the fluid flow speed is highly dependent on the electrolyte concentration, which in turn varies with temperature. We proved the feasibility of circular pumping by using ingenious channel and electrodes design. We observed the surface modification due to electrochemistry happening at the titanium dioxide interface. We showed the inherent drawback in using gold for a KCl medium. Finally we showed the inability of using ACEO-based micropumping for displacing cells due to all the reasons above.

Displacing particles and isolating them was approach on the notion that the fluid is contained within a vessel and that the vessel contains the microfabricated devices that allow the separation and fractionation of the particles. Another way would be use the liquid as the vessel itself where we would control the shape through contact forces and electrical forces. Essentially we use again the conception of diverging electrical field interacting with matter as the Maxwell stress tensor express.

Electrowetting on dielectric (EWOD) or also sometimes called liquid dielectrophoretic actuation (LDEP) presents the ability to control droplets on highly hydrophobic surfaces. The next chapter will be dedicated to this matter.

Chapter VII

7. Digital microfluidic and "electrowetting devices"

We have seen earlier a method that uses ion movement within the fluid as the motor of a micropump. This system presents some inherent problem such as the limited range of conductivity which forbids its use for biological purposes. Although trapping cells and their separation using DEP fluid flow fractionation was shown.

Electrowetting on dielectric (EWOD) is a method where we control the fluid via the dielectric properties of the liquid but also the modification of surface forces which dominate fluid characteristics at this size [78]. The liquid is kept in microdroplets which are the vessel for cell assays. The theoretical analysis of the origin of the forces involve in the modification of the fluid shape and the substrate surface is apparent wettability is still under scrutiny. Although it is essential to have an understanding of the effect involved we refer the reader to the following publications for deeper understanding of the ideas [79-82]. The approach here uses the electromechanical theory expressed by Jones et al; we refer to EWOD as the low frequency case of the solution of the Maxwell stress tensor. The Liquid Dielectrophoresis (LDEP) is the high frequency alternative. It can be represented by the electric field acting on single charge effect at low frequency and its reciprocal at high frequency acting on dipole rather than single charges (Chapter 2).

7.1. Electric field interaction with surface forces.

Microfabricated parallel electrodes energized with an AC field are used to manipulate small amount of liquid as well as creating droplets. This liquid electro-actuation scheme can be use for applications such as LOC where each droplet is itself such a micro-lab. The system is made of vapor deposited metal on borosilicate glass then micro patterned on the 10 micron scale. A dielectric is then deposited as an interface between the electrode and the conductive aqueous media. A second layer of dielectric can be deposited for surface treatment such as contact angle control (Figure 7-1).

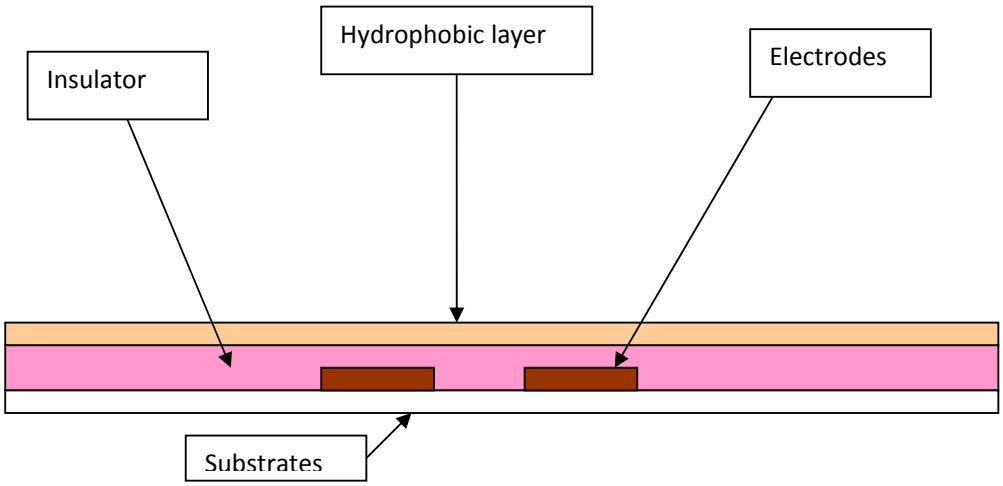

Figure 7-1 : **Cross section of tri electrode configuration**

7.2. LDEP on coplanar electrodes

Liquid DEP actuation does not necessarily need a lid and can operate with an open end. This simplifies its operation and its fabrication (where two-chip bonding is not necessary). Previous study shows the possibility of using this electrode scheme in conjunction with particle DEP in order to isolate and manipulate particles of different size or dielectric constant such as a dispersion of electric beads. Liquid dielectrics also responds to non-uniform electric field by moving towards the region of higher electric field gradient. We use this liquid DEP actuation technique to form droplets of deionised liquid (water and oil) across micropatterned coplanar electrode (Figure 7-1) coated by a spinable dielectric. This structure can produce an array of single droplets from a parent one through the creation of a rivulet by the action of the electric ponderomotive force.

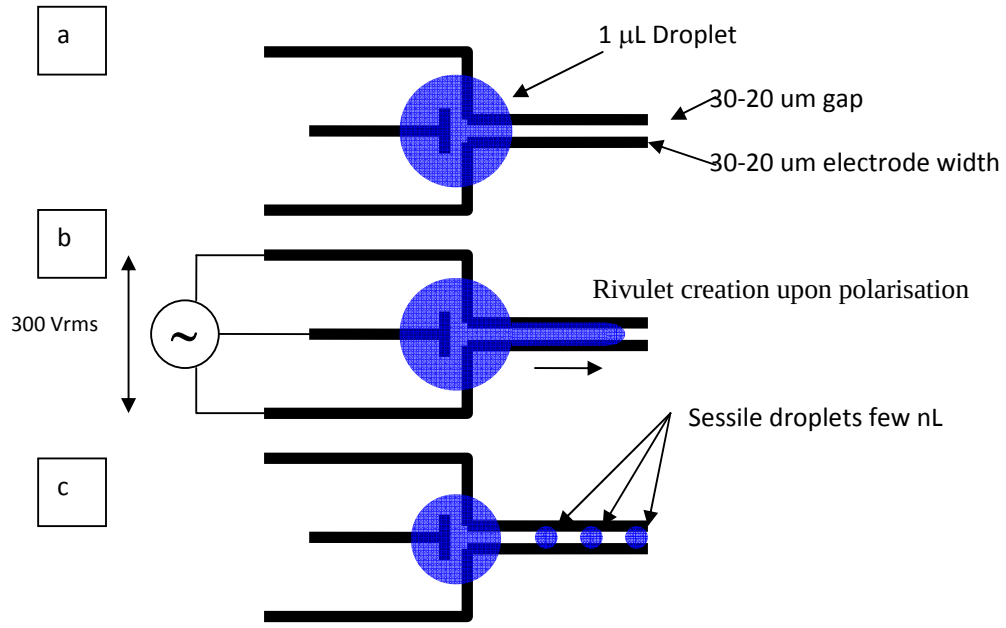

Figure 7-2 : a) Tri electrode system after priming b) potential apply across electrode midpoint kept to the ground c) sessile droplet created following the voltage cut off.

Once the voltage is applied on the electrode a new hydrostatic equilibrium must be found and a finger of liquid is formed above the electrode (rivulet). Releasing the polarization, the capillary forces will take over by breaking the finger into smaller droplets. The droplet spacing is controlled by the fastest growing instability predicted by Raylegh's classical theory for hydrodynamic instability and the volume are partly controlled by the geometry of such pair of electrode (width and gap: 2w+g) [80, 83, 84].

7.2.1. Pellat experiments

Pellat's classic experience of the DEP rise of liquid depicts well such a phenomena and demonstrates the difference of DEP actuation with Electro HydroDynamic (EHD) phenomenon (Figure 7-3). The liquid rises between the electrodes to the point where a new hydrostatic equilibrium is reached. Two conductive electrodes are brought into a liquid of permittivity *k*. the distance between electrode *D* is filled by the liquid once the voltage *V* is applied and reach the height of rise $H_{DEP,}$

$$H_{DEP} = \varepsilon_0(K-1)E^2/2*\rho*g \quad (45)$$

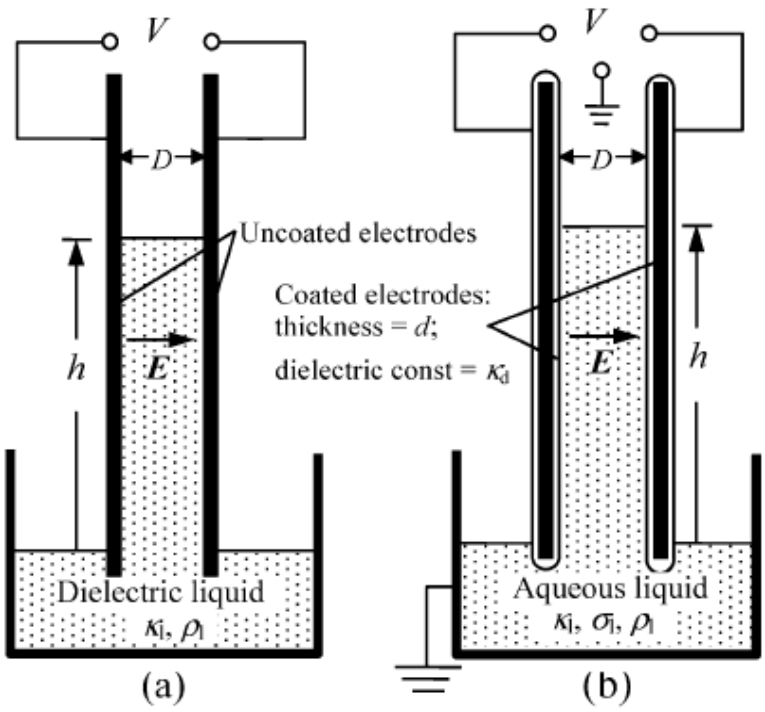

Figure 7-3 : (a) Original Pellat Experiment (b) modified Pellat experiment

The modified Pellat experiment uses a dielectric-coated electrode, which allows one to use conductive fluid and therefore drive the electrode with higher voltages.

Liquid DEP is often confused with electrowetting but also part of a similar electromechanical phenomenon. Electrowetting is characterised by a change in the contact angle of a sessile droplet of conductive liquid placed on electrodes covered by a dielectric. The contact area increases as the contact angle increases resulting in a decrease of interfacial stress between the solid and the liquid. The droplet is therefore spreading, appearing to be on a more hydrophilic surface. Electrowetting uses DC or low AC voltage strength. To exploit this system aqueous liquid is introduced between two plates, one of which is grounded, to take advantage on the disequilibrium of contact angle between two sides of the droplet.

7.2.2. Application of LDEP/EWOD to particle trapping

Jones et al, proved the feasibility on different electrode geometry to subdivide µL droplets into sub families of smaller droplets. Mixers were achieved as well. Therefore analytical chemistry on small droplets can be achieved. Prof Jones used time in Southampton University to develop trapping of particles such as beads and cells on electrodes using DEP forces as well similar to the technique he developed in Rochester

[85-86]. The DEP liquid actuation is used to transport the particle over shaped electrodes for DEP trapping.

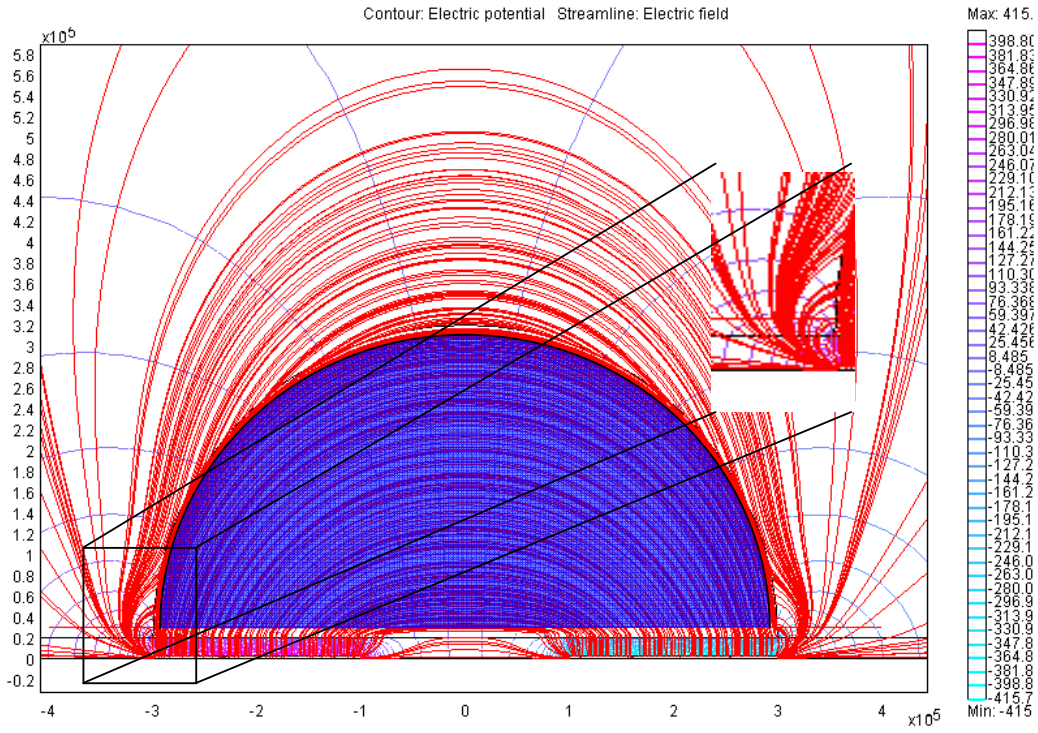

Figure 7-4 : Simulation of Field Line created by a 300 Vrms 100 kHz Potential across microfabricated 20 micron Electrodes (-30 micron to -10 and +10 to 20 micron

The frontier between these two expressions of the same phenomenon could be expressed by considering a circuit equivalent for the droplet and the dielectric in which the water would be a resistor in parallel with a capacitor in series with the capacitor of the dielectric. Hence there exists a cut off frequency mainly ruled by the conductivity of the water. For a low frequency the water behaves like a conductor and most of the field lines are nil inside the droplet. Most of the voltage drop happens in the dielectric and the forces are applied on free charges which lead to an electrowetting effect (called EWOD). On the other hand at higher frequencies the voltage is dropped according to the capacitance and the field act on the dipole as for dielectrophoretic effect. Figure 7-4 shows the field lines (red) and the Potential (blue) for 300 Vrms at 100 kHz on a 60 µm diameter water droplet. We can notice the divergence of the field around the triple line which gives rise to a strong force at the triple line also visible in the cross-section graphs (Figure 7-5 and Figure 7-6).

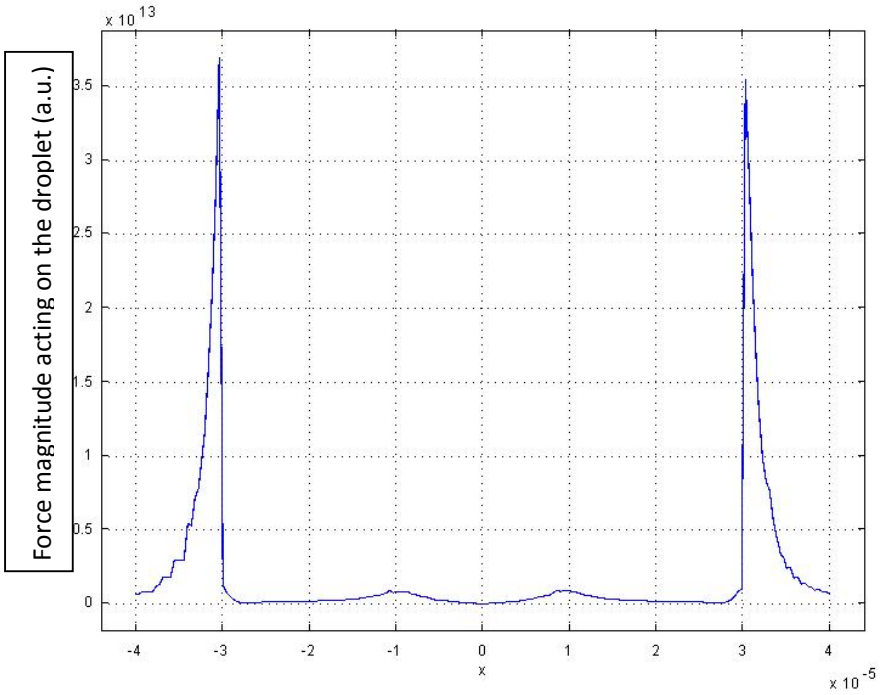

Figure 7-5 : Numerical simulation of the DEP force magnitude at 1 micron above the dielectric layer and across the droplet.

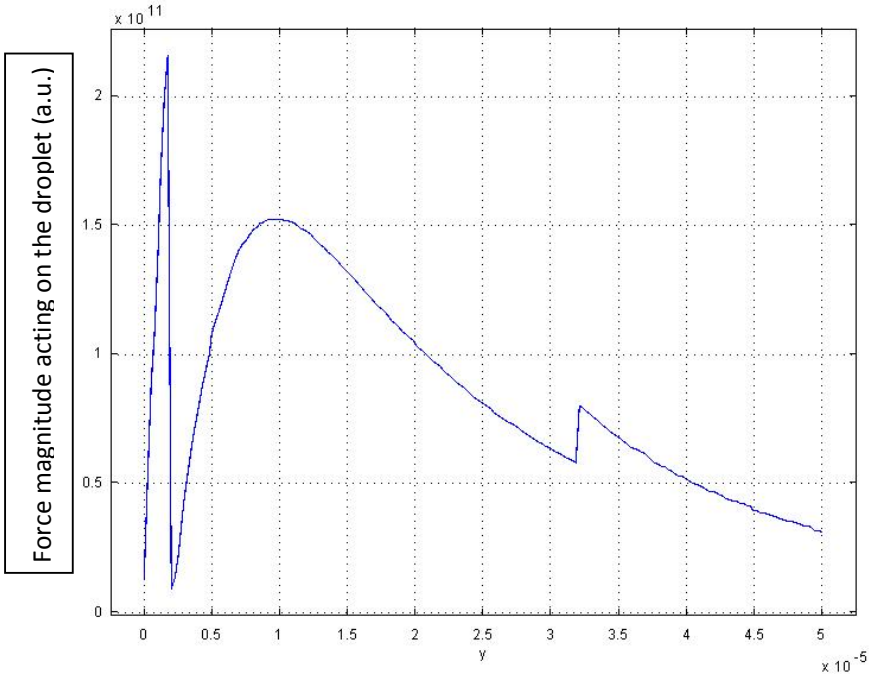

Figure 7-6 : Numerical simulation of the DEP force magnitude across the dielectric and perpendicular to its surface, across the droplet.

The actuation effect is closely related to the divergence of the electric field at the interface between materials. Namely, this is at the triple line of the droplet edge where three phases met. The Maxwell stress tensor represents the electric tensor of forces applied there. It is important to note the more divergent the tensor is the stronger the forces are on the interface with the droplet which is the case if a hydrophobic condition exist.

7.3. Microfabrication of electrodes and surface modification.

7.3.1. Material and process

The methods used for microfabrication is essentially the same as in Chapter 4, nevertheless we include here the particularity involved with surface treatment and modification.

The devices are made by deposition of metal on borosilicate wafers. The metal is a 'sandwich' of Ti/Au/Ti of respectively 30/100/30 nm. The metal is then patterned by photolithography using S1813 positive tone resist. Once developed the metal is etched using Ti etchant and Au etchant, successively. Alternatively ion beam milling can be used as well. Two designs were achieved for combining electrowetting and DEP trapping, which are shown in Figures 7-7 and 7-8. Figure 7-8 shows the 'bump' pattern with DEP structure to promote particle trapping. The two right electrodes and the gap are use to dispense the dropets from a mother drop. Each other pair are used only for particle DEP but are polarized as well for DEP actuation.

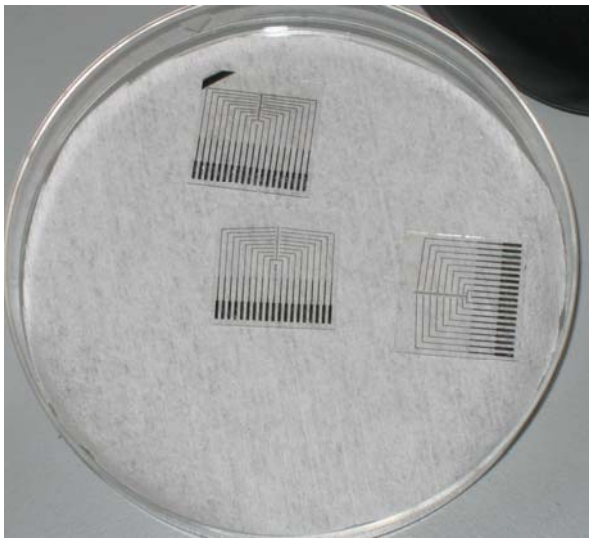

Figure 7-7: Sample 20*20 mm

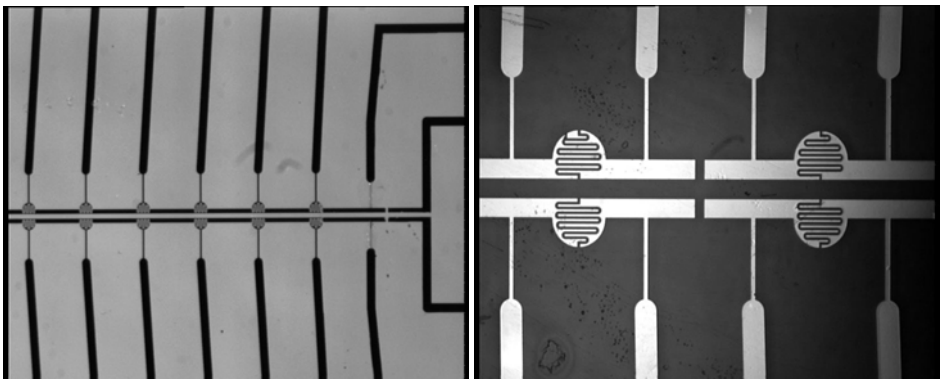

(a) (b)

Figure 7-8 : Electrode design and DEP particle structure.

7.3.2. Deposition of dielectrics and surface treatment in Southampton

Aqueous media have a relative low conductivity nevertheless enough to create hydrolysis and therefore destroy the electrode. Hence dielectrics are necessary to separate the liquid from the electrode. At high voltage we would need high permittivity dielectric in the thinnest film possible.

Spin on glass IC201 from Futurex, (SOG), was used as a dielectric. It is spun on the electrode at 3000 rpm then baked successively at 100 °C then 200 °C on a hot plate to drive the solvent out and promote crosslinking. We note that a further bake is possible at 350 °C under nitrogen. This is to drive out the ethoxil group and free the surface of silanol groups.

Nevertheless, experiments showed a bake a 200 °C was sufficient to obtain DEP actuation. SOG planarises the surface and is used primarily by the semiconductor industry for such a purpose. 3000 rpm spin for 60 sec gives a 200 nm thickness. Other dielectrics such as SU8 resist was also used and gave results as well but was not thoroughly investigated in this study.

AF Teflon from Dupont is then spun above the dielectric to give a hydrophobic surface of the dielectric (see contact angle measurement). It gives a surface made of amorphous Teflon. It can be diluted into its fluoroinert solvent (FC 75) to thin it a decrease the thickness whilst spinning it at the same speed.

AF Teflon does not have a good adhesion and, despite being neutral to most solvents, if dipped into acetone the layer will be easily lifted off (Figure 7-9). Using an adhesion promoter is advised. Another product of the same type called CYTOP (available from Asahi Glass Co) has better adhesion and swells less upon solvent wash.

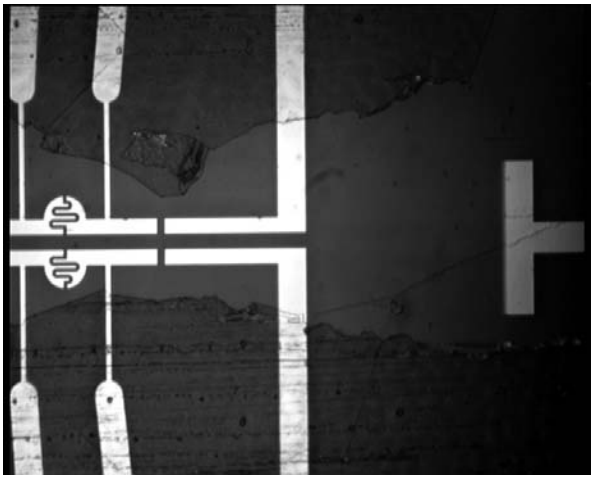

Figure 7-9 : AF Teflon lift off

7.3.3. Surface Treatment and contact angle measurement

Trichloro (1H,1H, 2H,2H- perfluorooctyl) Silane. (TPS) and 3-(2-Aminoethylamino)propyltrimethoxysilane (APTS) were used to treat surface to make it hydrophobic or hydrophilic. Also, these silanes can be used as surface adhesion promoters for AF Teflon. In order to create a good adhesion surface for silane the glass samples were cleaned with the 3 solvents and fuming nitric acid. Then they were dipped into a solution at 90 % eth and saturated in KOH. This insures silanol function groups bind with silane and increases the covering of the surface. Oxygen plasma ashing will have the same effect.

Two methods exist to coat the surface with silane :

- First by diluting silane in Eth. Water acts by polymerizing silane so Eth chromatography grade is necessary. The sample is then dipped into the solution overnight. The optimum time is about 13 hours. After this multilayer appears (the contact angle peaks at 13 hours).
- Second by evaporation. The sample is placed into a desiccator and drops of silane are place next to the sample to coat. Once the vacuum is reached the

chamber is sealed and left overnight. Results of contact angle measurement are available in Figure 7-10 and Table 7-1

Contact angle was measured using a professional goniometer with 1 µL droplets in an enclosed system. Contact angle is reported and various technic was used to measured it. Figure 7-10 displays two contact angles (extreme hydrophobic and hydrophilic respectively) available by surface treatment as described earlier. Contact angle values for different surface treatments are available in Table 7-1.

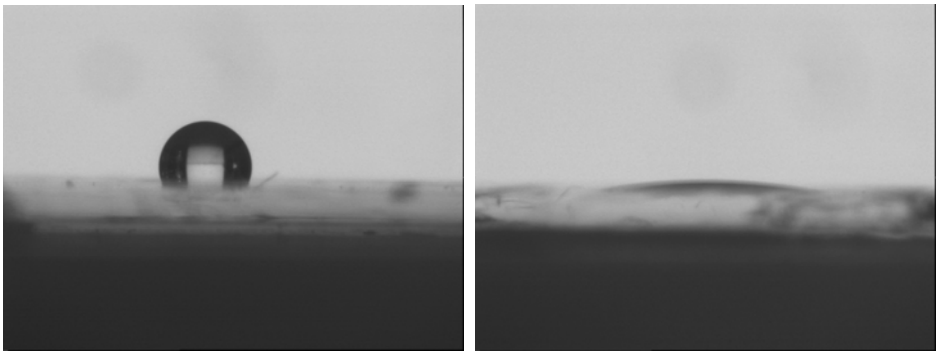

Figure 7-10 : Left AF Teflon 1 µL Droplet Right KOH+eth treated glass overnight

Table 7-1 : Contact angle measurement for a variety of material and surface treatments

Material	Contact angle (deg)
AF Teflon on SOG bake on Hot plate at 200 for 60 sec	114.5
Glass test sample prepared in KOH/eth and exposed to APTS in eth for 13 hours	19.6
Glass on KOH overnight	10.6
SOG before 400 bake	62.8
SOG after 400 deg bake	55.5
TPS before bake	82.3
Overnight TPS after bake	83.5
Pyrex glass froM electrode without sog	77.7

7.3.4. DEP Actuation System

The electrodes for the test system are made of 19 pads (Figure 7-7) and a standard substrate holder was fabricated. A signal generator is amplified[4] to obtain about 350 V maximum. Such a system is for DEP actuation and a separate signal generator is used to produce particle DEP at a higher frequency. Each pair of electrodes must be individually addressable and a switch box was made for this purpose.

Designs

The design used for electromechanical actuation of droplets by an AC field is made of three gold evaporated coplanar electrodes. Two electrodes carry HV signal (180° out of phase). The third is grounded in order to act as an anchor for the droplet. The electrode mask pattern was made using local printing company with size variation with the gap and the electrode size around the 30 micron mark.

This is the simplest design possible and a good test platform. The goal for this test platform is to evaluate insulators deposited on top of the electrodes as well as the thinnest possible hydrophobic layer (an insulator itself). The electrodes are 20 nm of NiCr and 40 nm of Au. Platinum was also investigated as a conductive layer since the pad used for contact slides into a substrate holder and after repeated experiment might wear off. Pt is stronger to abrasion and therefore better.

An example of sessile droplet formation is presented in Figure 7-11 for 300 V_{rms} pulsed excitation on a Teflon-coated SOG hydrophobic surface. In this case 5 droplets have formed along a 1-cm long parallel-electrode pair, each containing approximately 2 nl of fluid.

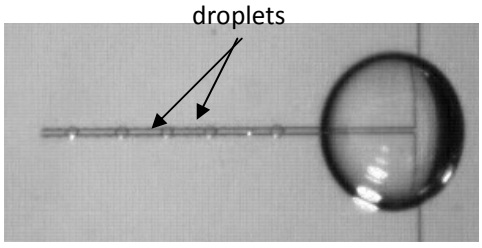

Figure 7-11: Formation of sessile droplets on straight electrode using 300 Vrms and DI water on PYREX cover with SOG and Teflon AF.

[4] A custom amplifier/transformer combination was designed and built for this purpose, as no suitable high-voltage and high-frequency amplifiers were available at the University of Canterbury.

The following series of photos (Figure 7-12) shows the finger of liquid being pulled from the droplet and when the polarization is removed the droplet forming. This sample used a double layer of spin on glass and a double coating of Teflon and excitation was at 250 V_{rms}. You can note the structure on each bump to allow DEP particle trapping, and several designs with different sizes were successfully tested.

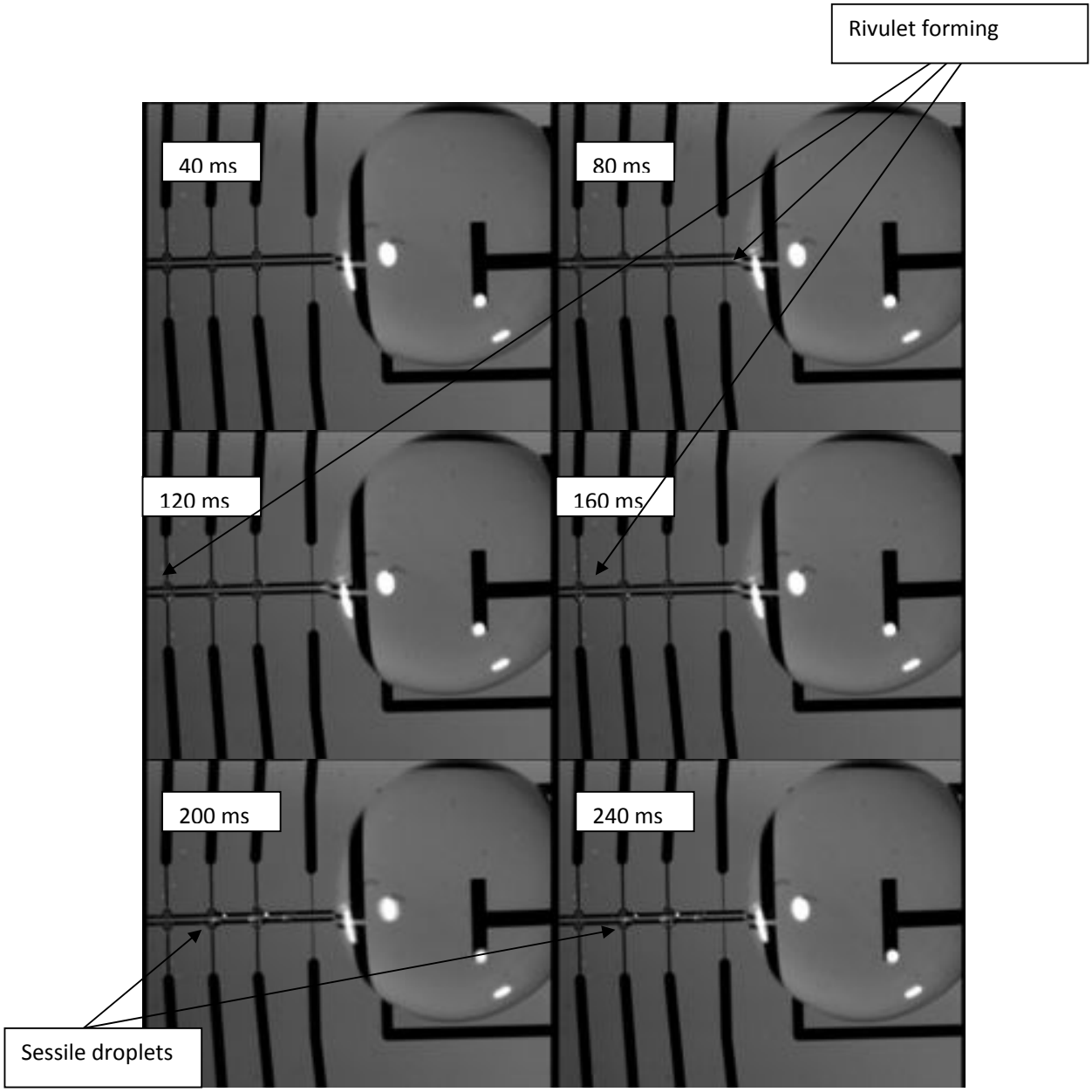

Figure 7-12 : Formation of droplet on liquid DEP Electrodes. Droplet dispenser for DEP TRAP

We can observe the finger of DI water pulled, and when the polarization is stopped the droplets form at the bumps as described before. Nevertheless, it seems the

finger is not extending completely, and as such some major problems occur with the dispensing of the rivulet before the droplet formation can occur. In many cases the rivulet extension was inhibited much earlier in the process, and higher and higher voltages were required to get reasonable extension for droplet formation. As a consequence, dielectric breakdown would often occur before successful droplet formation could be obtained. This breakdown is an irreversible process, and was not reproducible (even for samples prepared under nominally identical conditions) and so an investigation of the dielectric breakdown phenomenon itself was undertaken.

Improving the dielectric breakdown.

The preliminary experience showed a high rate of failure and almost constant destruction of the electrodes irrespective of the electrode size as we will discuss later. The droplet seems boiling, but it is unclear if it is due to heating as a result of the intense voltage applied or due to ohmic conduction. It shows total destruction of the electrode and melting of the gold. We observe also the destruction of the electrodes does not occur (depending on the dielectric material) without the droplet. This tends to indicate the presence of water is responsible for the break down.

The dielectric permittivity of DI water is 80. It contributes to concentrating the field into the dielectric layer which in turn can reach its dielectric breakdown limit. Also, the Pyrex wafer is not good heat conductor which can result in heating tremendously the dielectric and the hydrophobic layer which in turn can peel off, opening pores and letting water permeate through.

As a consequence, other insulators were investigated like PR and SU8, which are easily spun on; but unfortunately all these samples showed dielectric breakdown too. Also, the substrate was changed to use a silicon/silicon nitride wafer which is better at dissipating heat. Silicon dioxide was sputtered on long deposition time (4 hours). It also had the breakdown problem. Silicon dioxide is notorious to embed pin holes, which can be the mechanism responsible for the breakdown. Also, only 300 nm was deposited which can be too thin and therefore longer deposition could be necessary with annealing step to repair the defects. The advantage of using silicon dioxide is to be able to use SAMs such as trichlorooctoperfluorosilane that covalent bind to the surface of silicon dioxide

Nevertheless, no samples showed any actuation without breakdown (with or without droplet creation). It occurs above 290 V_{rms} which is too high for the dielectric to cope. It seems as well that the rivulets/droplets move by a ratchet movement, which indicates that they propagate until they encounter a pinning point, making it harder to move [89] and therefore requiring a higher field to overcome the problem. A surface analysis by AFM showed a wave like structure that is believed to be coming from the spinning of the Teflon like material (Figure 7-13). This structure can be an obstacle to the formation of the rivulet.

1

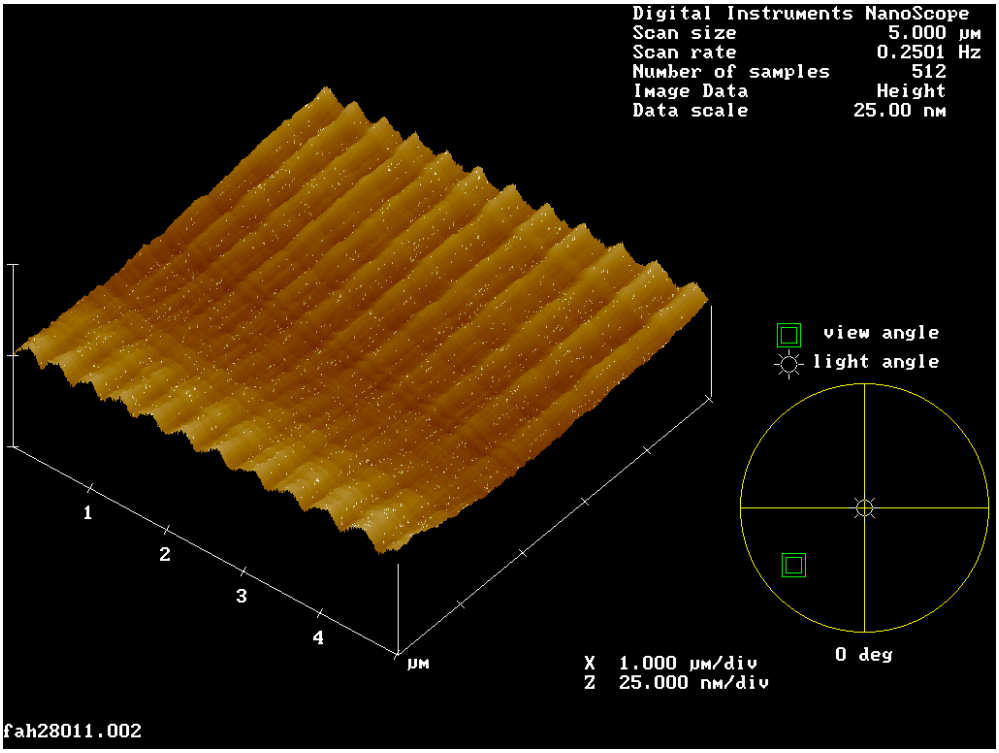

Figure 7-13 : AFM picture of a Teflon surface after spin coating. Surface pining the advance of the rivulet

Also, the permittivity of SiO_2 is low (4.7) which results in a higher field concentration which in return could lead to local dielectric breakdown and cracking allowing liquid to permeate. TiO_2 on its rutile (tetrahedral) phase has a permittivity of 80 which would match the permittivity of the water. It's been reported also that high permittivity sandwich between two other layer improves the dielectric breakdown of the system [80, 90].

Table 7-2 display values of dielectric breakdown with or without the parent droplet left on the tri-electrode zone. Some of these system obtain actuation but without a

satisfying reproductive pattern. The values obtained are the lowest value observed. We observe that the sandwich of $SiO_2/TiO_2/SiO_2$ offers the highest breakdown as suggested by [90] (here in thin film where the ref is in bulk) the total thickness of the sandwich system is believe to be around a micron.

Table 7-2 : Breakdown values for diverse material and surface treatment

Material	Breakdown without droplet (Vrms)	Breakdown with droplet (Vrms)	Actuation
Teflon	250	250	no
SOG+Teflon	none *	260	no
SOG+APTS	none *	260	yes
SU8	none *	240	no
PR	250	230	no
SiO_2/teflon	none *	250	no
TiO_2/teflon	none *	250	yes
$SiO_2/TiO_2/SiO_2$/teflon	none *	270	yes

Some preliminary deposition was achieved to test the TiO_2 structure and permittivity. Deposition parameters such as the oxygen mass flow rate during deposition were recorded. The layer so deposited between two Pt electrodes was then analysed in AC to characterise its capacitance and therefore find its permittivity. Surface profilometer measurements gave a 500 nm thickness for 4 hours deposition with 120 W/10 sccm of Ar/ x sccm of oxygen by sputerring. The increase of oxygen during deposition gives a better relative permittivity as shown in Table 7-3.

Table 7-3 : Relative permittivity by calculating a capacitance

Oxygen mass flow (x) (sccm)	ε_r
3	15
6	21
9	23
12	31
15	33

The relative permittivity is calculated assuming a planar capacitor. The results are approximate since it is difficult to measure the exact area used and to exclude the fringing field. The trend show an increase in the relative permittivity without reaching the rutile form which as a relative permittivity of 80. We assume this is a mixed form and the ε_r measured is the result of several crystalline form. The literature advises an annealing under O_2 for several hours at 1000 °C. The Pyrex substrate will never subsist under such a temperature and therefore other substrates are required like quartz.

To conclude, actuation occurs but at too high voltage which result in the destruction of thin film electrode and dielectrics layers. More effort is necessary to comprehend the mechanism of the layers' destruction.

Geometrical and other effects.

Of the two geometries developed the geometry Figure 7-8 seemed to obtain the best result although it is certain that the dielectric used showed weakness and experiments proved the occurrence of pinholes and dielectric breakdown. The destruction of the electrodes occured between 200 V_{rms} and 300 V_{rms}. Several other factors can explain the destruction. The SOG is a sol gel, therefore the removal of solvent by baking can leave pores and pinholes. Furthermore at the 200 °C bake the cross linking is partial. A droplet of copper sulfate was deposited on the surface of a 200 nm layer of SOG and a 200 nm layer of AF Teflon on top. Nucleation of copper was observed (when copper sulfate was added to the droplet) above the Spin on glass which

leads to believe on presence of pin holes in the dielectric and pores in the teflon layer (Figure 7-14 and Figure 7-15).

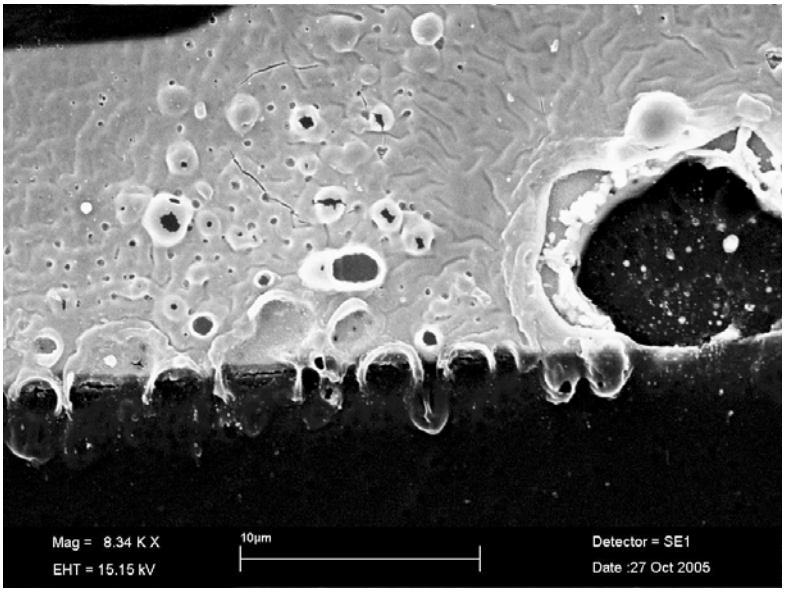

Figure 7-14: Electrode after dielectric breakdown (pinhole). Layer of AF Teflon, SOG, Metal

The voltage applied is high about 300 V_{rms}. The Dielectric breakdown for the SOG is 3 MV/cm. The SOG is also used for planarizing the surface, hence since we have 160 nm of metal on top of the surface and we are spinning 200 nm of SOG we should have only 40 nm of SOG on the surface above the electrode. With a simulation we found the potential drop of about 90 V between the electrode and the interface SOG water. These results give a field above the breakdown voltage.

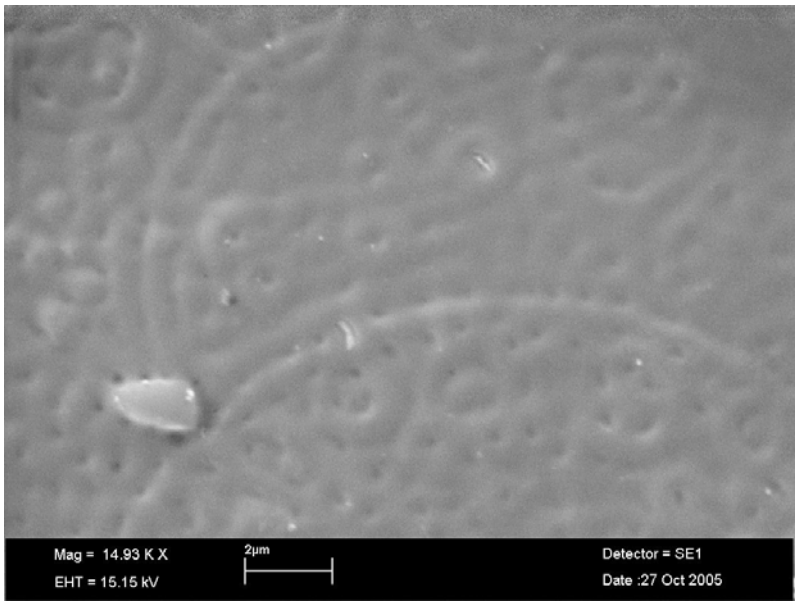

Figure 7-15 : Pores in the AF Teflon

Other dielectrics such as SU8 and S1813 were investigated but seem to result in the same problem. Bubbles formed whilst the resist are baked on the hot plate that lead to short circuiting the system and destruction of the electrodes (Figure 7-16).

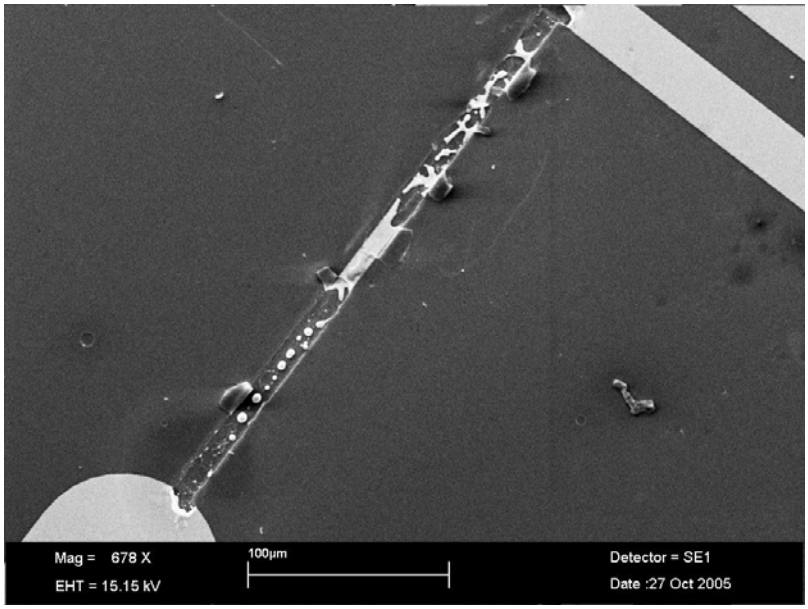

Figure 7-16 : Bubble after baking leads to electrode damage

Nevertheless a careful dielectric survey would yield some result on the reason of such destruction. Figure 7-15 shows clearly the roughness of the AF Teflon surface. This

could have an effect on the movement of the liquid on itself and hysteresis effect can occur. Hysteresis can lead to increase the force necessary to pull the liquid finger which in return would need an increase of voltage. The increase of voltage might be enough to reach breakdown on the SOG and therefore the catastrophic results. Annealing AF Teflon at 330°C would allow the surface to reflow and potentially decrease the roughness, although this was not attempted.

DEP trapping with DEP liquid actuation.

We obtained some DEP actuation as proved by Figure 7-12 but unfortunately not enough repeatable to do consecutive liquid actuation and particle DEP. Nevertheless, particle DEP was achieved separately with yeast cells in 1 mM of Mannitol on the surface of the electrode which open the potential for distribution of droplet that contain cell followed by DEP trapping. We can imagine then other protocols of testing on such an isolated cell. Several experiments were achieved to observe the patterning of hydrophobic and hydrophilic surfaces. The most obvious was by observing water on the hydrophilic pattern. Attempting to functionalize the surface with linking amine to fluorescene or green fluorescent protein unfortunately did not work

7.4. Summary

We showed the use of a comprehensive series of tools for digitial microfluidics. Although the success is all relative, this is the preliminary work necessary to obtain a dedicated digital fluidic system. More work is necessary especially on the material side.

Digital microfluidics displays a real potential to operate with minute amounts of liquids. Already nanolitre droplets are available using LDEP actuation [91]. Several groups have obtained the movement of individual droplets with high salt concentration using EWOD technique. All the requirements necessary for merging the two techniques are available and some aspects of its use were described here.

Chapter VIII

8. The present and the future…

8.1. Conclusion on work achieved

Two electric-field fluidic working systems were undertaken to manipulate fluids and colloids These are two radically different approaches but all based on macrofabricated devices. Both systems wered designed to trap cells and displace liquid which was achieved in both cases. The DEP chromatograph separated by size PBMCs and show the separation of THP1 and PBMCs. Digital microfluidic sytems showed trapping of yeast cells [92].

Several fabrication method were investigated including SU8, dry film resist, PR, polyimide and the bonding of such system was also described. It show that dry film resist is ideal for rapid prototyping but SU8 and polyimide have the best profiles.

ACEO was characterized on the system constructed and shows the reversal as observed by different group cited through this thesis. Nevertheless the characteristic of this reversal in magnitude is dependent of the electrode repeat and geometry therefore difficult to compare with other work. On the other hand the frequency dependence is probably less affected by the geometry as it is related to its material intrinsic electrochemical properties. All material shows reversal at lower frequency and it seems to be subjected strong electrochemical reaction.

Electrochemically we found strong evidence of a correlation between the fluid flow reversal and the oxido-reduction that the metal is going through. Also we related the oxidation of virgin electrodes to transient effect on first time used. The regain of oxidation when the media is re-introduce showed the modification of the electrolyte content of the liquid in low volume systems, which is the case our chip.

Simulation was undertaken and the basic fluid movement is found and in agreement with the theoretical model. It is nevertheless very simple and lacks a proper theoretical investigation.

This study has proven the feasibility of encompassing a DEP trap with a double sided circular micropump. It also shows the repetitive occurrence of the phenomenom called fluid flow reversal attributed the faradaic charge injection in electrical double layer induced by the screening of the polarized electrodes. It also show the influence of diverse material on the fluid flow reversal.

On the other hand digital microfluidic offer a solution for single cell analysis but the material use and their assembly still remains a challenge. The use of electrical fields remains highly interesting for colloidal manipulation because of its scalability and its measurable effect in both frequency and amplitude.

The liquid DEP actuation had shown the difficulty of bringing together fluid and electricity at the micron scale. The material preparation and selection is paramount in the success of the digital fluidic system required.

We observed droplet creation at under 300 V_{rms} but in very erratic way. Several factors contributed to the failure of consistent droplet creation. First, the voltage used is close to the dielectric breakdown. The presence of a liquid droplet bends the field line such that voltage drop could be locally above the critical dielectric breakdown. Also, polymeric resists have pores created under excitation which could lead to the permeation of water and dielectric breakdown. Since the system is dynamic some transient fields might exist that also disturb locally the insulator. We observe the improvement by using sandwich dioxide system which seems to be the only way so far to reduce the excitation voltage.

The digital microfluidic demonstrate the ability of using droplets as a vessel for colloid manipulation and expose the challenge of integrating high voltage microfabricated devices prior to dielectric breakdown.

8.2. Future Work

The area of microfluidic is still young and this thesis asks more questions than it solves. On the two directions undertaken several work as to be done on the material consideration. Especially because these systems are used in an environment very different than the classic MEMs system.

The understanding of the fluid reversal is more a theoretical question that has little application, but since this system is easily fabricated it is worth while investigating. Material like Pt and other more inert system should be a focus for investigation of the electrochemical conditions. Also higher salt concentration and diverse geometries could find application in other fields than biology.

Already some labs combine traditional EWOD with LDEP, which is the way forward for subdividing sessile droplets and moving then [93]. Digital microfluidics offers more potential in the biological assay, and lowering the excitation voltage is paramount in the manipulation of colloids such biological cells. The cells lyse for even short pulses (commercially 240 V) therefore if any cell manipulation is undertaken the voltage should be such that electroporation does not occur. This could be achieved by increasing the capacitance with higher permittivity such as titanium oxides, tantalum oxides or PZT. This could be sandwiched in high-low permittivity system such as the dielectric breakdown is much lower than the actuation potential. Strong covalently bonded SAM at the surface would be the necessary thin hydrophobic interface with the droplets.

Obtaining reliable digital droplet systems has the potential to operate minuscule amounts of liquid for biological assays. In turn, it would guarantee a faster treatment of routine assays with a tremendous reduction of expensive reagents.

References

1. Moore, G.E., *Cramming more components onto integrated circuits.* Electronics Magazine. April 19, 1965. pp 110-114
2. Terry, S.C., J.H. Jerman, and J.B. Angell, *Gas-Chromatographic Air Analyzer Fabricated on a Silicon-Wafer.* IEEE Transactions on Electron Devices, 1979. **26**(12): p. 1880-1886.
3. Pimbley, W.T., *Drop Formation from a Liquid Jet - Linear One-Dimensional Analysis Considered as a Boundary-Value Problem.* IBM Journal of Research and Development, 1976. **20**(2): p. 148-156.
4. Collins, F.S., M. Morgan, and A. Patrinos, *The human genome project: Lessons from large-scale biology.* Science, 2003. **300**(5617): p. 286-290.
5. Pennisi, E., *The human genome.* Science, 2001. **291**(5507): p. 1177-1180.
6. Thomson, J., *DNA chips detect disease.* Green Chemistry, 2007. **9**(9): p. T68-T68.
7. Khanna, V.K., *Existing and emerging detection technologies for DNA (Deoxyribonucleic Acid) finger printing, sequencing, bio- and analytical chips: A multidisciplinary development unifying molecular biology, chemical and electronics engineering.* Biotechnology Advances, 2007. **25**(1): p. 85-98.
8. Morgan, H., et al., *Single cell dielectric spectroscopy.* Journal of Physics D-Applied Physics, 2007. **40**(1): p. 61-70.
9. Luke, S. and K. Kaul, *Detection of breast cancer cells in blood using immunomagnetic bead selection and reverse transcription polymerase chain reaction.* Molecular Diagnosis, 1998. **3**(3): p. 149-155.
10. Z'graggen, K., et al., *Biological implications of tumor cells in blood and bone marrow of pancreatic cancer patients.* Surgery, 2001. **129**(5): p. 537-546.
11. Deisseroth, A., *Use of Retroviral Markers to Identify Efficacy of Purging and Origin of Relapse Following Autologous Bone-Marrow and Peripheral-Blood Cell Transplantation in Indolent-B Cell Neoplasms (Follicular Non-Hodgkins-Lymphoma or Chronic Lymphocytic-Leukemia (Cll) Patients).* Human Gene Therapy, 1993. **4**(6): p. 821-834.
12. Desai, J.P., A. Pillarisetti, and A.D. Brooks, *Engineering approaches to biomanipulation.* Annual Review of Biomedical Engineering, 2007. **9**: p. 35-53.
13. Muys, J., et al., *Biochip: Cellular analysis by atomic force microscopy using dielectrophoretic manipulation.* Japanese Journal of Applied Physics Part 1-

Regular Papers Brief Communications & Review Papers, 2005. **44**(7B): p. 5717-5723.

14. Auroux, P.A., et al., *Micro total analysis systems. 2. Analytical standard operations and applications.* Analytical Chemistry, 2002. **74**(12): p. 2637-2652.
15. Evans, J.J., F.L. Pragg, and D.R. Mason, *Release of luteinizing hormone from the anterior pituitary gland in vitro can be concurrently regulated by at least three peptides: Gonadotropin-releasing hormone, oxytocin and neuropeptide Y.* Neuroendocrinology, 2001. **73**(6): p. 408-416.
16. Morgan, H., Green, N, *AC electrokinetics*. 2000. RESEARCH STUDIES PRESS; 1st edition (June 15, 2002). **ISBN-10:** 0863802559
17. Jones, T.B., *Electromechanics of particles*, ed. C.U. press. 1995, New York City.
18. Alberts,B. Lewis, J. Raff, M. Roberts, K. *Molecular biology of the cell.* 4th edition. Garland science, NY (October 2005).
19. Schwan, H.P. and C.F. Kay, *The Conductivity of Living Tissues.* Annals of the New York Academy of Sciences, 1957. **65**(6): p. 1007-1013.
20. Schwan, H.P. and C.F. Kay, *Capacitive Properties of Body Tissues.* Circulation Research, 1957. **5**(4): p. 439-443.
21. Schwan, H.P. and E.L. Carstensen, *Dielectric Properties of the Membrane of Lysed Erythrocytes.* Science, 1957. **125**(3255): p. 985-986.
22. Christodoulides, N., et al., *Lab-on-a-chip methods for point-of-care measurements of salivary biomarkers of periodontitis.* Oral-Based Diagnostics, 2007. **1098**: p. 411-428.
23. Weigum, S.E., et al., *Cell-based sensor for analysis of EGFR biomarker expression in oral cancer.* Lab on a Chip, 2007. **7**(8): p. 995-1003.
24. Coulter, W.H., Proceedings of the national electronic conference, 1956. **12**: p. 1034.
25. Winslow, T., *how do researcher use markers to identify stem cells.* stem cells information. **http://stemcells.nih.gov/info/scireport/appendixE.asp**.
26. Baker, R.J., et al., *Expression of breast cancer resistance protein in malignant cells from patients with leukaemia.* Leukemia, 2003. **17**(3): p. 662-662.
27. Carlson, C.L., et al., *Primary leptomeningeal lymphoma of the lumbar spine.* Clinical Imaging, 2003. **27**(6): p. 389-393.
28. Mainou-Fowler, T., S.J. Proctor, and P.R.A. Taylor, *Interleukin 4 production by peripheral blood lymphocytes in patients with classical Hodgkin lymphoma.* Leukemia Research, 2004. **28**(2): p. 159-166.

29. Kinter, A.L., et al., *CD25(+) CD4(+) regulatory T cells from the peripheral blood of asymptomatic HIV-infected individuals regulate CD4(+) and CD8(+) HIV-specific T cell immune responses in vitro and are associated with favorable clinical markers of disease status.* Journal of Experimental Medicine, 2004. **200**(3): p. 331-343.
30. F.F. Mandy, *Guidelines for performing single-platform absolute CD4+ T-cell determinations with CD45 gating for persons infected with human immunodeficiency virus.* MMWR, Recomm. Rep, 2003. **1**(52 (2003)).
31. Hanahan, D.J., J.E. Ekholm, and M.G. Luthra, *Is Lipid Lost during Preparation of Erythrocyte-Membranes.* Biochimica Et Biophysica Acta, 1974. **363**(2): p. 283-286.
32. Pohl, H.A., *The Motion and Precipitation of Suspensoids in Divergent Electric Fields.* Journal of Applied Physics, 1951. **22**(7): p. 869-871.
33. Maxwell, J.C., A *treatise on electricity and magnetism.* Clarendon Press, 1881. **1**.
34. Debye, P., *Polar Molecules.* Dover, 1947.
35. Castellanos, A., et al., *Electrohydrodynamics in microelectrode structures.* Electrostatics 2003, 2004(178): p. 175-180.
36. Smoluchowski, M.v., Bull. Int. Acad. Sci., 1903(184).
37. Zhang, L.H., et al., *In-capillary solid-phase extraction-capillary electrophoresis for the determination of chlorophenols in water.* Electrophoresis, 2006. **27**(16): p. 3224-3232.
38. Zeng, S.L., et al., *Fabrication and characterization of electroosmotic micropumps.* Sensors and Actuators B-Chemical, 2001. **79**(2-3): p. 107-114.
39. Jinno, K. and H. Sawada, *Open-tubular capillary electrochromatography (Review).* Bunseki Kagaku, 1999. **48**(11): p. 957-971.
40. Gonzalez, A., et al., *Fluid flow induced by nonuniform ac electric fields in electrolytes on microelectrodes. II. A linear double-layer analysis.* Physical Review E, 2000. **61**(4): p. 4019-4028.
41. Green, N.G., et al., *Fluid flow induced by nonuniform ac electric fields in electrolytes on microelectrodes. I. Experimental measurements.* Physical Review E, 2000. **61**(4): p. 4011-4018.
42. Green, N.G., et al., *Fluid flow induced by nonuniform ac electric fields in electrolytes on microelectrodes. III. Observation of streamlines and numerical simulation.* Physical Review E, 2002. **66**(2).

43. Ajdari, A., *Pumping liquids using asymmetric electrode arrays.* Physical Review E, 2000. **61**(1): p. R45-R48.

44. Brown, A.B.D., C.G. Smith, and A.R. Rennie, *Pumping of water with ac electric fields applied to asymmetric pairs of microelectrodes.* Physical Review E, 2001. **6302**(2).

45. Ramos, A., et al., *Pumping of liquids with ac voltages applied to asymmetric pairs of microelectrodes.* Physical Review E, 2003. **67**(5): art. no. 056302.

46. Olesen, L.H., H. Bruus, and A. Ajdari, *ac electrokinetic micropumps: The effect of geometrical confinement, Faradaic current injection, and nonlinear surface capacitance.* Physical Review E, 2006. **73**(5): art. no. 056313

47. Studer, V., et al., *An integrated AC electrokinetic pump in a microfluidic loop for fast and tunable flow control.* Analyst, 2004. **129**(10): p. 944-949.

48. Lastochkin, D., et al., *Electrokinetic micropump and micromixer design based on ac faradaic polarization.* Journal of Applied Physics, 2004. **96**(3): p. 1730-1733.

49. Garcia-Sanchez, P., et al., *Experiments on AC electrokinetic pumping of liquids using arrays of microelectrodes.* IEEE Transactions on Dielectrics and Electrical Insulation, 2006. **13**(3): p. 670-677.

50. L'Hostis, F. *Solid state AC electroosmosis micro pump : a demonstrator for cell and nanoparticle trapping*. in *ICONN 2006*. 2006.

51. Studer, V., et al., *Fabrication of microfluidic devices for AC electrokinetic fluid pumping.* Microelectronic Engineering, 2002. **61-2**: p. 915-920.

52. Iliescu, C., *Microfluidics in glass: Technologies and applications.* Informacije Midem-Journal of Microelectronics Electronic Components and Materials, 2006. **36**(4): p. 204-211.

53. Gracias, A., et al., *Novel microfabrication approach of embedded SU8 (TM) fluidic networks for cell transport on chips.* Journal of Microlithography Microfabrication and Microsystems, 2006. **5**(2): art. no. 021602.

54. Ruano-Lopez, J.M., et al., *A new SU-8 process to integrate buried waveguides and sealed microchannels for a Lab-on-a-Chip.* Sensors and Actuators B-Chemical, 2006. **114**(1): p. 542-551.

55. Vulto, P., et al., *Microfluidic channel fabrication in dry film resist for production and prototyping of hybrid chips.* Lab on a Chip, 2005. **5**(2): p. 158-162.

56. Sandison, M.E. and H. Morgan, *Rapid fabrication of polymer microfluidic systems for the production of artificial lipid bilayers.* Journal of Micromechanics and Microengineering, 2005. **15**(7): p. S139-S144.
57. Mpholo, M., C.G. Smith, and A.B.D. Brown, *Low voltage plug flow pumping using anisotropic electrode arrays.* Sensors and Actuators B-Chemical, 2003. **92**(3): p. 262-268.
58. Ramos, A., et al., *Pumping of liquids with traveling-wave electroosmosis.* Journal of Applied Physics, 2005. **97**(8): p. -.
59. Ramos, A., et al., *Pumping of electrolytes using arrays of asymmetric pairs of microelectrodes subjected to ac voltages.* Electrostatics 2003, 2004(178): p. 187-192.
60. Bard, A.J., *Electromechanical method : Fundamental and applications*. 2000.
61. Bard, A.J., *Photoelectrochemistry.* Science, 1980. **207**(4427): p. 139-144.
62. Ramos, A., et al., Fluid flow driven by a.c. electric fields in microelectrodes. Electrostatics 1999, 1999. 163: p. 137-140.
63. Morgan, H., et al., The dielectrophoretic and travelling wave forces generated by interdigitated electrode arrays: analytical solution using Fourier series. Journal of Physics D-Applied Physics, 2001. 34(10): p. 1553-1561.
64. Bazant, M.Z. and Y.X. Ben, Theoretical prediction of fast 3D AC electro-osmotic pumps. Lab on a Chip, 2006. 6(11): p. 1455-1461.
65. Castellanos, A., et al., Electrohydrodynamics and dielectrophoresis in microsystems: scaling laws. Journal of Physics D-Applied Physics, 2003. 36(20): p. 2584-2597.
66. Green, N.G., A. Ramos, and H. Morgan, Ac electrokinetics: a survey of sub-micrometre particle dynamics. Journal of Physics D-Applied Physics, 2000. 33(6): p. 632-641.
67. Ramos, A., et al., Comment on "Theoretical model of electrode polarization and AC electroosmotic fluid flow in planar electrode arrays". Journal of Colloid and Interface Science, 2001. 243(1): p. 265-266.
68. Ramos, A., et al., Ac electrokinetics: a review of forces in microelectrode structures. Journal of Physics D-Applied Physics, 1998. 31(18): p. 2338-2353.
69. Holmes, D., N.G. Green, and H. Morgan, Microdevices for dielectrophoretic flow-through cell separation. Ieee Engineering in Medicine and Biology Magazine, 2003. 22(6): p. 85-90.

70. Jones, T.B., Invited Plenary Lecture presented at 2003 Institute of Physics Congress, March, 2003, Edinburgh, Scotland, UK. J. Electrostatics 2004 (178): p. 1-10.
71. Ermolina, I. and H. Morgan, The electrokinetic properties of latex particles: comparison of electrophoresis and dielectrophoresis. Journal of Colloid and Interface Science, 2005. 285(1): p. 419-428.
72. D. M. Brunette, P.T., M. Textor, P. Thomsen, Titanium in medicine. 2001: Springer.
73. Uhlig, H. H. *Corrosion and corrosion control*. Wiley-Interscience; 3rd edition (January 4, 1985) 1971, Cambridge.
74. Marino, C.E.B., et al., XPS characterization of anodic titanium oxide films grown in phosphate buffer solutions. Thin Solid Films, 2004. 468(1-2): p. 109-112.
75. Shreir, L.L. and A. Weinraub, The Anodic Polarisation of Lead-Platinum Bi-Electrodes. Chemistry & Industry, 1958(41): p. 1326-1327.
76. Bown, M.R. and C.D. Meinhart, AC electroosmotic flow in a DNA concentrator. Microfluidics and Nanofluidics, 2006. 2(6): p. 513-523.
77. Wu, J., Y.X. Ben, and H.C. Chang, Particle detection by electrical impedance spectroscopy with asymmetric-polarization AC electroosmotic trapping. Microfluidics and Nanofluidics, 2005. 1(2): p. 161-167.
78. Melcher, a.R., A tutorial on induced electrohydrodynamic forces. 2000 (Massachussets Institute of Technology Lecture).
79. Cooney, C.G., et al., Electrowetting droplet microfluidics on a single planar surface. Microfluidics and Nanofluidics, 2006. 2(5): p. 435-446.
80. Moon, H., et al., Low voltage electrowetting-on-dielectric. Journal of Applied Physics, 2002. 92(7): p. 4080-4087.
81. Mugele, F. and J.C. Baret, Electrowetting: From basics to applications. Journal of Physics-Condensed Matter, 2005. 17(28): p. R705-R774.
82. Jones, T.B., An electromechanical interpretation of electrowetting. Journal of Micromechanics and Microengineering, 2005. 15(6): p. 1184-1187.
83. Vallet, M., B. Berge, and L. Vovelle, Electrowetting of water and aqueous solutions on poly(ethylene terephthalate) insulating films. Polymer, 1996. 37(12): p. 2465-2470.

84. Vallet, M., M. Vallade, and B. Berge, Limiting phenomena for the spreading of water on polymer films by electrowetting. European Physical Journal B, 1999. 11(4): p. 583-591.
85. Ahmed, R. and T.B. Jones, Dispensing picoliter droplets on substrates using dielectrophoresis. Journal of Electrostatics, 2006. 64(7-9): p. 543-549.
86. Ahmed, R., et al., Dispensing picoliter droplets using dielectrophoretic (DEP) microactuation. Microscale Thermophysical Engineering, 2004. 8(3): p. 271-283.
87. Dubois, P., et al., Ionic liquid droplet as e-microreactor. Analytical Chemistry, 2006. 78(14): p. 4909-4917.
88. Velev, O.D., B.G. Prevo, and K.H. Bhatt, On-chip manipulation of free droplets. Nature, 2003. 426(6966): p. 515-516.
89. Berthier, J., et al., Actuation potentials and capillary forces in electrowetting based microsysterns. Sensors and Actuators a-Physical, 2007. 134(2): p. 471-479.
90. Lebedev, S.M., et al., Influence of high-permittivity barriers on PD activity in three-layer dielectrics. Journal of Physics D-Applied Physics, 2004. 37(22): p. 3155-3159.
91. Jones, T.B., et al., Dielectrophoretic liquid actuation and nanodroplet formation. Journal of Applied Physics, 2001. 89(2): p. 1441-1448.
92. L'Hostis, F., 2nd year Progress report, in Electronic and Computer Engineering. 2005, Canterbury: Christchurch.
93. Yen Chen Lin, Kai Cheng Chuang and Shih Kang Fan`, Nanoliter droplet creation by EWOD and LDEP. 2006 (The 10th International Conference on Miniaturized Systems for Chemistry and Life Sciences (μTAS2006)).